QATAR UNIVERSITY

COLLEGE OF ENGINEERING

OPTIMIZING PILOT-SCALE PERFORMANCE OF SUPERHYDROPHOBIC MEMBRANES BY DIRECT-CONTACT MEMBRANE DISTILLATION

BY

HANEEN WADI ABDELRAZEQ

A Dissertation Submitted to

the College of Engineering

in Partial Fulfillment of the Requirements for the Degree of

Doctor of Philosophy in Chemical Engineering

June 2023

COMMITTEE PAGE

The members of the Committee approve the Dissertation of
Haneen Abdelrazeq defended on 02/05/2023.

_____
Dr. Majeda Khraisheh
Supervisor

_____
Dr. Mohammad Hassan
Co-Supervisor

_____
Dr. Ramazan Kahraman
Committee Member

_____
Dr. Nidal Hilal
External Examiner

Approved:

_____
Khalid Kamal Naji, Dean, College of Engineering

ABSTRACT

ABDELRAZEQ, HANEEN W., Doctorate : June : [2023], Doctorate of Philosophy in Chemical Engineering

Title:_OPTIMIZING PILOT-SCALE PERFORMANCE OF SUPERHYDROPHOBIC MEMBRANES BY DIRECT-CONTACT MEMBRANE DISTILLATION.

Supervisor of Dissertation: MAJEDA, KHRAISHEH.

Membrane technology is a promising approach that offers effective solutions for treating saline wastewater, not only to meet the discharge standard, but also to offer the opportunities for water reuse. This study highlights the unique features and limitations of membrane processes for treating saline wastewater and identifies the existing research gaps areas for improvement in produced water treatment based on related literature in direct contact membrane distillation (DCMD). This research is aligned with the latest innovative wastewater technologies and play a significant role in investigating the impact of synthetic brine on electropsun polystyrene and commercial polyethylene membranes using a bench-scale set-up, a high-tech DCMD pilot module, as well as optimization and numerical predictions using Python. The effect of varying brine concentrations on the desalination performance, the energetic performance and the long-term impact of membrane fouling provides insights that are difficult to achieve through conventional bench-scale systems. Based on experimental results, an optimized iterative method was used to reduce the error between the estimated and actual surface membrane temperature to predict the temperature accurately in each experiment. The research findings highlight the effect of porosity on the efficiency of the pilot unit with emphasis on thermal and evaporation efficiency.

DEDICATION

This dissertation is dedicated to my greatest blessings: Eyas, Eyan, Eyam, and Eyad.

ACKNOWLEDGMENTS

I am deeply thankful to all those who have supported me during my doctoral journey and contributed to the completion of this dissertation.

To begin, my deepest appreciation goes to my supervisor, Dr. Majeda Khraisheh, for her guidance, encouragement, and endless support throughout my PhD studies. Her expertise and extensive knowledge in the field have been invaluable in shaping the direction and scope of this dissertation. I would also like to express my appreciation to my co-supervisor, Dr. Mohammad Hassan, for his insightful comments and suggestions, which have greatly contributed to the significance of this work.

I am grateful to the professional support of staff and academic members in the Department of Chemical Engineering at Qatar University, Mr. Saeed Gad, Mr. Sivaprasad, and Dr. Ahmed ElKhatat, for being very supportive in providing me with all the resources and support I needed in my research work.

I am lovingly grateful to my family for their constant encouragement. They have always been there to celebrate my achievements and lift me up during challenging times.

An extraordinary thanks to my husband, Omar, for his love, patience and understanding. It would have been impossible to finish my studies without his support over the past five years.

I would like to give a shout-out to my friends for their friendship and support. Roba, Hania, Malak, Hafsa, Alanoud, Wamda, Fatima, Afnan, Mona, Sifani, Tasneem, Sumaya, and all my other amazing colleagues and lab mates. Cheers to everyone who has been there for me emotionally in good and bad times.

I am also grateful for the endless support received from the Center for Advanced Materials

(CAM, QU) and Central Laboratory Unit (CLU, QU) for their professional assistance in the characterization and analysis of the samples used in my research.

Finally, I would like to thank the Qatar National Research Fund (A Member of The Qatar Foundation) for providing the funding [GSRA5-1-0524-18068] that made the completion of my PhD dissertation possible.

TABLE OF CONTENTS

LIST OF TABLES

LIST OF FIGURES

CHAPTER 1: INTRODUCTION

1.1 Background

Produced water (PW) in Qatar associated with the oil and gas exploitation is estimated at about 490 million m^3, which is more than half the annual demand of fresh water coming from desalination plants. This fact provides a good opportunity to using treated process water and produced water for industrial and agricultural activities. Treated water can be used for non-human usage including farm irrigation, Landscaping, construction field, road works and flashing for salinity [1]. Water produced in the oil and gas industry is the largest waste stream in the current era due to the growing demand for petroleum and by-products and the need for more extraction [2]. This type of wastewater includes a mixture of both organic and inorganic materials which their physical properties vary based on location, geologic structures, extraction procedures, and the fluid used for hydraulic fracturing [3]. Besides, a massive amount of PW is salty water brought up along with oil or gas, since they are trapped inside oil wells rock [4–10]. However, any necessary purification process may encounter many barriers including the costs of treatment methods or risky procedures/materials for the environment [11].

Based on the fact that water desalination technologies is in great demand in the Middle East, statistics have shown water production capacities of 38.8 million cubic meter per day [12,13]. Desalination has become a necessary part of the global resolutions that tackles the issue of water scarcity [14]. Studies have shown that there is a growing demand for the purification of high-level concentrations of wastewater (saline brine), especially that which is generated from existing desalination plants and to reduce its harmful environmental consequences to the minimum [15] [16]. Brine is usually disposed of as a waste product

without proper pre-treatment protocols. However, taking into consideration the massive amounts of wastewater generated from the oil and gas industries, the focus on mature and fully developed innovative membrane technologies must be fully considered in terms of desalination performance with emphasis on energy efficiency.

Over the past decade, over 650 research publications were made on DCMD for use in desalination applications. Figure 1 illustrates the total number of research publications specifically focusing on either wastewater or produced water treatment using DCMD technologies over the last ten years. It is evident that there has been a substantial growth in the number of publications. This growth can be attributed to increased water-driven research activities around the world.

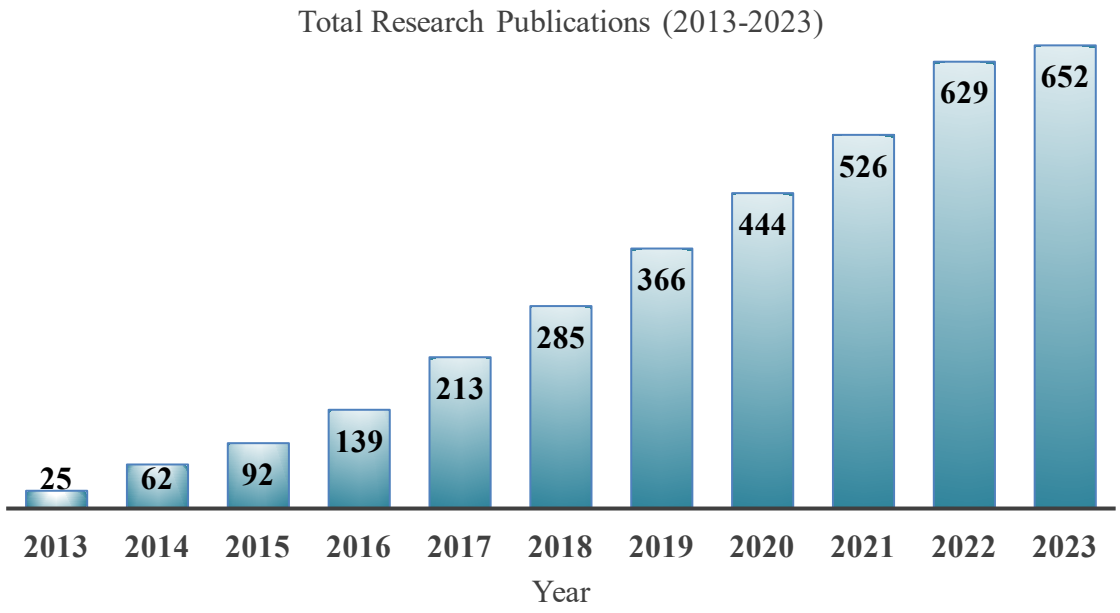

Figure 1. Growth of research publications in DCMD technologies for use in either produced water treatment or desalination applications over the last 10 years (Data taken from Scopus database, accessed on 15-Mar-2023).

1.2 Objectives

In industrial scale desalination systems, The DCMD process works on the basis of utilizing abundant waste heat from other industrial processes. This leads to the creation of low-cost and highly efficient desalination processes. Nevertheless, deep knowledge regarding large-scale performance of fabricated hydrophobic membranes was rarely reported in literature. From this point arises the significance of this study; focusing on a larger-scale approach to obtain optimal performance for desalinating synthetic brine; mimicking real industrial produced water.

In parallel to the unique MD approach applied via the direct contact membrane distillation bench system, this work also delivered an innovative approach to applying direct contact membrane distillation (DCMD) on a larger scale. This procedure is highly beneficial in terms of examining the fouling and wettability behavior of the fabricated membranes and obtaining more efficient data in higher running process desalination times in compared with available commercial ones. Hence, the following objectives were addressed throughout this study:

1. Design and synthesize electrospun polystyrene membranes with controlled morphology and optimized properties to enhance the DCMD performance.
2. Evaluate the desalination performance of synthesized membranes in a DCMD bench-scale system by measuring the permeate flux, salt rejection rate, and energy consumption, and compare the results to industry standards to assess their commercial viability.
3. Optimize the permeate flux of synthesized membranes in a pilot-scale DCMD system by varying the feedwater quality and duration of tests and characterizing the effect of

these parameters on the permeate flux and energy consumption of the system while maintaining a stable system performance.

4. Enhance the process efficiency by controlling wettability and fouling of membranes.
5. Developing a computational model using Python software that can accurately predict and optimize the permeate flux considering the experimental DCMD operating conditions.
6. Investigate the effect of porosity on mass and heat transfer properties of polystyrene membranes using mathematical modelling.
7. Optimize the surface membrane temperatures of the hot and cold stream in DCMD to achieve optimum flux and desirable energy efficiencies.
8. Perform a detailed energy analysis of the pilot-scale DCMD system and identify the key factors that affect its performance and viability.

1.3 Methodological approach

The accomplished milestones of this study have been divided into 6 different work packages as per the following:

WP1. Background and Literature Review.

T1: Collecting research articles.

T2: Reading and examining research articles.

T3: Writing a literature survey.

WP2. Synthesis of electropsun polystyrene membranes for DCMD applications.

T1: Preparation of polymer solution for membrane synthesis process.

T2: Optimization of electropsun parameters.

T3: Characterization of membranes before DCMD testing.

WP3. Test the desalination performance of membranes in DCMD bench-scale system.

T1: Preparation of synthetic brine.

T2: Optimize flux and wettability of membranes by changing DCMD process conditions.

T3: Characterization of membranes after DCMD testing.

WP4. Pilot-scale optimization of permeate flux in DCMD.

T1: Investigate effect of varying brine concentrations on fouling behavior of membrane at long processing hours.

T2: Conduct fouling tests for flux enhancement.

T3: Examine the membrane properties including the wettability and surface characterizations after DCMD tests.

WP5. Study the effect of porosity on mass and heat transfer properties using mathematical modelling.

T1: Study the effect of porosity change of electropsun membranes on the permeate flux.

T2: Optimize surface membrane temperatures from both hot and cold sides of the membrane to maximize the obtained theoretical flux.

T3: comparative analysis between experimental flux with respect to theoretical and prediction-based fluxes.

WP6. Conduct comprehensive analysis of energy performance at pilot-scale.

T1: Estimate specific energy consumption (SEC) utilizing the calculated values of specific thermal energy consumption (STEC) and specific electrical energy consumption (SEEC) for the whole duration of the DCMD test.

T2: Statistically correlate flux with salt rejection, contact angle, and SEC consumption.

1.4 Research gap and contribution

Membrane-based separation systems have become of greater demand in water purification processes due to their simplicity of use and reasonable design costs. Membrane distillation (MD) is a well-known non-isothermal membrane separation process that utilizes the difference in vapor pressure, as the driving force, in generating purified permeate of improved quality. The performance of Direct Contact Membrane Distillation (DCMD) systems greatly assists in incorporating the low-cost desalination of wastewater in industrial desalination plants using abundant waste heat from other industrial processes [17][18].

There have been recent investigations on the operating process parameters in MD for seawater desalination and wastewater treatment distillation for the treatment of highly saline brine (i.e. feedwater) using electrospun membranes [19–24]. Yet, the use of brine from Qatari desalination plants in DCMD was rarely reported in literature. In fact, based on literature, only 2% of the research groups (12 articles) utilizing real or synthetically prepared produced water (i.e. brine) comparable to Qatari desalination plants in DCMD were reported. In the GCC region, four studies worked on synthesizing polystyrene membranes [25–28] from which only one has employed these fabricated PS membranes for the treatment of synthetic brine [25].

Out of the total number of similar research studies found in the literature, only a few papers have been made on synthesized PS membranes. The research contribution of this study to existing research gap in wastewater treatment using electrospun PS membranes in DCMD is clearly mentioned in Table 1.

Table 1. Research gap identified in related publications.

Ref.	Year	Contribution relevant to this study	Research gap
[29]	2023	The work included heat and mass transfer model to evaluate the effect of thermal conductivity on porous nanocomposite membranes in DCMD.	MD performance with respect to thermal efficiency was not explored at pilot scale.
[30]	2023	The study explored the performance of synthesized PPO/PS membranes at concentrations up to 35000 ppm NaCl. Humic acid (HA) in feed solution resulted in 20% drop in flux due to fouling.	Feedwater did not mimic that of real wastewater water. The operation time of DCMD performance did not exceed 4 hours. Long test durations were not performed.
[31]	2021	The work explored the potential of high-impact polystyrene membranes for treating dye wastewater.	Energy consumption of the DCMD process was not included in the study.
[27]	2021	The work applied mathematical modeling to validate experimental flux for PS/GNP membranes at lab scale with 80% porosity.	A scale-up MD system along with the effect of membrane porosity on the flux was not addressed.
[26]	2020	The study incorporated activated carbon in PS membranes and performed DCMD tests using 7 g/L feed achieving an optimum flux of 6.3 $kg.m^{-2}.h^{-1}$.	The effect of membrane porosity on the flux was not mentioned. And the feed salinity was not comparable to either that of wastewater or produced water.
[32]	2020	The work evaluated the desalination performance of SAN4-HIPS membrane. Fouling occurred after 48 hours of DCMD using real industrial textile wastewater treatment.	Long-term DCMD performance was not presented.
[33]	2019	The research group synthesized PS membranes using electroblowing. The membrane porosity was 74.7% after hot-press.	Thermal efficiency and energy performance were not included.
[28]	2016	The research tested electrospun PS membranes in DCMD for 10 hours. Porosity of membranes was 82-86%.	A pilot-scale study was not studied.
[34]	2014	The study tested electropsun PS membranes using NaCl as the feed for 10 hours.	Higher concentrations for the feed mimicking that of industrial brine was not considered.

Hence, in this work, synthetically produced water was used as the feed component in the system (i.e. thermal brine) in two different types of DCMD modules (bench-scale and pilot-scale units). Both commercial and synthesized polystyrene membranes were employed throughout the work. The effect of synthetic brine on fabricated polystyrene membranes was investigated and obtained results were compared with that in literature, the effect of varying porosity on mass and heat transfer with respect to energy performance was investigated, and computational predictions were performed to find the membrane's optimum surface temperatures with respect to maximum thermal and evaporation efficiency.

This work includes the operation of a high-tech pilot-scale DCMD unit with emphasis on the effect of varying brine concentrations on its energetic performance with a deep insight on the effect of membrane fouling over long periods of time. This cannot be achieved through conventional bench-scale DCMD setups. Hence, the output of this study greatly contributes to existing DCMD technologies in the petrochemical industries worldwide towards the production of fresher water. The successful implementation of this study significantly contributes to existing DCMD technologies in the petrochemical industries, specifically in the gulf desalination plants, towards the production of fresh water. The findings of this research could open up opportunities for the utilization of the fabricated membranes as filtration materials for commercial purposes.

CHAPTER 2: LITERATURE REVIEW

This chapter provides a comprehensive overview of the literature and research related to wastewater treatment using membrane technologies, with an emphasis on direct contact membrane distillation. In this chapter, the research gaps were addressed and critically analyzed based on existing literature that is relevant to the topic of this thesis to ensure a clear understanding of the research problem and the significance of the study.

2.1 Produced water treatment technologies

Desalination and water treatment is the fundamental origin of consumable water in the nations of the Gulf, for example Saudi Arabia, Qatar, Kuwait, Oman, and the United Arab Emirates [35]. In these nations, desalination represents 40 percent of the water utilized for civil and industrial aspects. Desalination of produced water in the Gulf's petrochemical industry is a continuing challenge to major research groups in the field. With a focus on produced water from desalination plants, it has become crucial to define and follow specific protocol in wastewater purification technologies. Only 0.03% of the total 70% of earth's water is consumable by humans. The demand of wastewater treatment and desalination is expected to expand as per the World Health Organization to protect up to 4 billion of the world's population from running out of clean water access [36,37]. Desalinated water provides most of the water used in commercial processes. Qatar's wastewater from oil-field extractions is expected to be around 490 million m^3, which is about half the yearly desalination plants' demand for fresh water in the whole GCC region. Interestingly, the oil and gas producing countries have a substitution advantage in that they can reuse drained water from oil and gas fields, thus preserving and expanding the size of green land for a longer time. In terms of economic advantage, the amount of water provided

by the oil and gas industry is five times that of commercially produced oil from the same resource in the region [38][39].

This fact presents an excellent opportunity to rethink traditional wastewater management methods and implement novel desalination techniques. Treated produced water may be used for non-human purposes such as agricultural drainage, landscaping, building, road construction, and salinity flashing [1][40]. Several studies attempted to examine advanced biological treatments which are considered promising techniques for eliminating residuals from actual produced water. The effect of biodegradation of certain organic compounds existing in fluids during hydraulic fracturing was evaluated by Akyon et al. [41]. Another group analyzed an algal process with a highest result of 100% of the total dissolved solids eliminated from the water flux [42]. Additional approaches have also been evaluated. For instance, acid active shrimp shell as well as montmorillonite have successfully been used for the removal of heavy metal species (at efficiency of 65–93 percent) and crude oil (87 percent) from oilfield PW [43].

Nevertheless, several research groups focused on membrane distillation (MD) of hydrophobic membranes for seawater desalination and wastewater treatment [19–24]. Membrane distillation is a well-known thermally driven process that utilizes the difference in vapor pressure, as the driving force, in generating purified permeate of improved quality. At the liquid-vapor interface of the hydrophobic membrane, a temperature gradient exists leading to a selective transport of contaminants from one side of the porous membrane to the other. For this reason, in MD, it is always preferred to have a non-wetted membrane with pore sizes ranging between 10 nm and 1 μm [44]. Table 3 lists the existing contaminants that can be eliminated using specific membrane technologies.

From this point rises the importance of employing membrane-based separation systems in water desalination processes. Other than their simplicity of use and reasonable design costs, using membrane technologies has many benefits for produced water treatment, such as [45]: minimal environmental impact, reduced energy costs, highly automated installations, no requirement for chemical additives, and during such processes, the membrane can be used to reuse the waste streams. In membrane technologies, the crossflow operation mode is preferred in purifying high concentrations of saline solutions. This is because the flow of the feed is perpendicular to the flow of the permeate. This helps in reducing the amount of accumulated species on the surface of the membrane during the desalination process [46]. Similar work was done on produced water from shale oil and gas, with an emphasis on permeate flux and membrane fouling [47–50]. A list of five wastewater treatment technologies is mentioned in Table 2 with emphasis on the main benefits and limitations for each technology.

Nowadays, many technological advancements in the field of water desalination are majorly focusing on treating seawater or brackish groundwater, while brine with higher salinity (>35,000 mg/L) gained a little amount of consideration and was rarely reported in the literature. Reverse osmosis (RO) is one of the economically widely used wastewater treatment technologies for the purpose of desalinating ultra-high salinity brine (<45,000 mg/L) [15]. Membrane distillation is a temperature-dependent process that functions based on vapor-liquid equilibrium (VLE) and needs a heat source to be supplied to attain the requisite latent heat of vaporization of the feed solution [18]. It is considered as a single hybrid process unit consisting of thermal evaporation and membrane separation[51]. A

number of factors immediately contributing to figuring out the exact wastewater treatment technology which needed to be applied are listed in Figure 2.

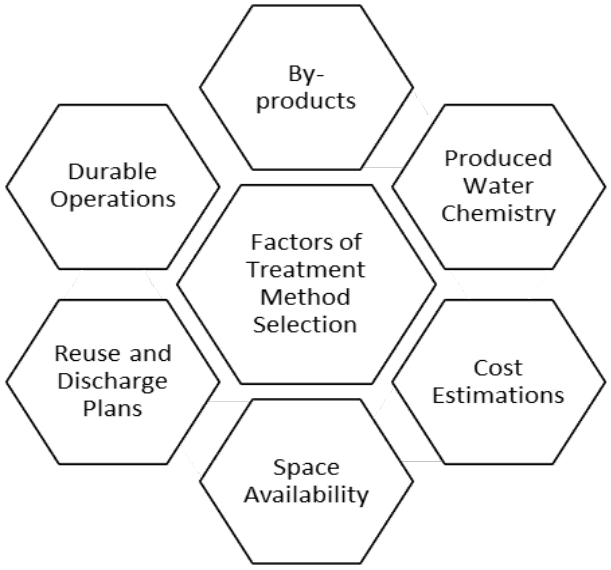

Figure 2. Aspects influencing the selection of produced water treatment techniques.

Table 2: Advantages and drawbacks of PW treatment technologies.

	Produced Water Treatment Methods				
	Microfiltration	Ultrafiltration	Reverse Osmosis	Adsorption	Ion-Exchange
Advantages	☑ High recovery of fresh water	☑ High recovery of fresh water	☑ Compact module ☑ Removes dissolved contaminants	☑ Cheap ☑ Efficient ☑ Compact	☑ Low energy required ☑ Continuous treatment possible
Drawbacks	☑ High energy required ☑ Low efficiency	☑ High energy required ☑ High membrane fouling	☑ Requires high pressure ☑ Small traces of grease may cause membrane fouling	☑ Low efficiency at high feed concentrations ☑ High retention time	☑ Requires pre-treatment ☑ Requires post-treatment

Table 3: Contaminants in wastewaters and their corresponding membrane technologies

Type	Main Contaminants	Treatment Aim	Technologies	Limitations
Produced water	☑ Drilling fluid additives ☑ Oil and grease ☑ Divalent cations	☑ Reduce salinity ☑ Oily compounds elimination	☑ MD ☑ FO ☑ NF ☑ RO	☑ Large water consumption ☑ High total dissolved solids ☑ Disposal regulations ☑ High membrane fouling
Municipal wastewater	☑ Microbial pathogens ☑ Micropollutants ☑ Phosphates ☑ Ammonia	☑ Degradable organic materials ☑ Microbial removal ☑ Eliminates nutrients	☑ MF ☑ UF ☑ NF ☑ RO	☑ Need for potable reuse ☑ Large footprint ☑ Treatment plant odor ☑ High membrane fouling

2.2 Innovative MD membranes

For water desalination purposes, six MD configurations exist: direct contact membrane distillation (DCMD), air-gap membrane distillation (AGMD), permeate gap membrane distillation (PGMD), sweeping gas membrane distillation (SGMD), vacuum membrane distillation (VMD) and vacuum multi-effect membrane distillation (V-MEMD)[52],[53]. DCMD has the simplest operation mode. This configuration has become of high research interest due to its special features: (i) Low operating temperatures, (ii) Low operating pressure, (iii) High rejection rates, and (iv) Low requirements for a membrane's mechanical strength. In fact, the Direct Contact Membrane Distillation (DCMD) does not involve any expensive apparatus for it to function [54]. Thus, based on literature, more than 60% of MD research work deal with the DCMD configuration. Among all MD configurations, characterized by the mode of vapor recovery on the permeate side, the simplest and easiest to operate is Direct Contact Membrane Distillation (DCMD). It is the most studied MD configuration and can be carried out in any desired membrane configuration, such as flat sheet, spiral wound, capillaries, or even hollow fiber [55].

2.2 Electropsun membranes in DCMD

To date, commercial membranes are the common contributors to the MD process as, until now, there is no commercial membrane that is specially designed for MD [56]. Nonetheless, recent review articles reported valuable summaries on water purification technologies and porous membrane materials with referral to membrane properties in MD [57–62]. The majority have stated that the best technique used to produce thin distillation

membranes is electrospinning. This effective method generates very thin membranes with fiber sizes ranging from nanometer up to submicron. The most common types of polymers used for membrane distillation processes are: polytetrafluoroethylene (PTFE), polyvinylidene fluoride (PVDF), polypropylene (PP) and Polystyrene (PS) [21,22,69,70,24,46,63–68]. Polystyrene, as an abundant thermoplastic polymer, is largely abundant and can reach up to several million tons of annual production [56]. Also, it has been distinguished for its competitive cost compared with PVDF and PTFE [71].

Jalloul et al. [72] synthesized an electropsun poly(vinylidene fluoride)-co-hexafluoropropylene (PVDF-HFP) membrane with fiber diameters below 300 nm. When heat pressed, the flux became greater than 37.5 kg/m^2.h with a salt rejection rate of 99.99%. the overall performance of the modified electrospun membrane was similar to that of commercial PTFE membranes. Essalhi and Khayet studied the effect of membrane thickness of electrospun poly- vinylidene fluoride (PVDF) membranes ranging from 144.4 mm to 1529.3 mm [73]. The concentration of the feed solution was twice of that of actual seawater (60 g/L). The decline in permeate flux was more likely to occur for membranes with thinner thicknesses (< 400 mm).

Niknejad et al. developed a new triple-layer membrane consisting of high- impact polystyrene (HIPS) as the top layer and PP as the support layer binded with styrene−butadiene rubber (SBR) in between [56]. This study was first to use SBR as the mid-layer in electrospinning where the peeling test was performed to measure the membrane's toughness. The cold-pressed electrospun HIPS/SBR/PP membrane resulted in enhanced mechanical strength and showed rejections rates above 99.9%. Hou et al. fabricated poly(vinylidene fluoride-co-hexafluropropylene) (PVDF-HFP)/Silica

nanoparticles (SiNPs) flat-sheet hybrid membranes by electrospinning [74]. As a result of overlapped nanofibers and existence of beads, the surface of the membrane showed a rough and hierarchical structure. The addition of Silica nanoparticles reduced the porosity and increased the thickness of the membrane at the same time. When tested in DCMD using a 35 g/L NaCl feed for 240 hours, the highest flux was achieved at 48.6 kg/m^2 h.

Ren et al. [75] synthesized a nanofibrous membrane of TiO_2 coating fluorosilanized with low surface energy material of 1H,1H,2H,2H-perfluorododecyl trichlorosilane (FTCS) which was employed to modify the virgin polyvinylidene fluoride electrospun nanofiber membrane (PVDF ENM). Results have exceeded that of commercial PVDF membrane with 40.5 LMH and 73.4 LMH using 3.5 wt% NaCl and real RO brine, respectively. Deka et al. [76] reported the fabrication of electrospun polyvinylidene fluoride-co-hexafluoropropylene (PVDF−HFP) membranes. The novel membrane showed excellent anti-wetting MD performance for seven continuous days using 3.5 wt% of NaCl.

2.2.2 Membrane wettability and porosity

Wetting mechanisms in membrane distillation are still not fully understood and various mechanisms have been proposed. Capillary effects, diffusion, fouling and scaling, adsorption, hydrophobic–hydrophobic interaction, electrostatic attraction, microbial growth, and secretion of hydrophilic extracellular polymeric compounds are examples of the associated mechanisms in membrane wetting [77–79]. Adsorption and the hydrophobic–hydrophobic interaction have both been widely hypothesized and researched. In the MD process, the balance between the absolute pressure on the feed side, the capillary pressure brought on by surface tension, and the vapor pressure, determines the driving force. The hydrophobic membrane is compromised into becoming more hydrophilic with

deposition of mineral salts on membrane surface or in membrane pores, resulting in membrane wetting [80]. The hydrophobic tail segment of surfactants, organics, or oils typically enables them to adsorb on the surface and pore walls of MD membranes through hydrophobic–hydrophobic interactions, diffusion, or electrostatic attraction, decreasing the hydrophobicity of the membrane surface and pores[81–83]. The degree or level of membrane wetting can be categorized as (a) nonwetting, (b) surface wetting, (c) partial wetting, and (d) entire wetting when taking into account the performance of the MD process [84,85]. Surface wetness typically happens as a result of surface phenomena and is linked to prolonged use. When a membrane is only partially wet, some areas are left open to water flow while the distance between the feed and the permeate is narrowed in other areas. If the wetted membrane area is not big enough to affect permeate quality, the MD process can still go on. A fully wet membrane produces a low-quality permeate since the feed just passes through the membrane, which results in poor MD performance [86].

The evolution of membrane wetting entails the displacement of a solid-liquid interface with a solid-air (vapor) contact during the MD process. The conductivity measurements are a straightforward in-situ technique to describe partially wetted membrane on a broad scale [87,88]. Moreover, the wetting rate is defined as the slope of the observed rise in permeate conductivity over time, in which the wetting time can be determined when it begins to rise. The soaking time has specifically been defined as the period of time between the time the permeate conductivity rises over 50 or 20 S/cm or the time the salt rejection decreases below an acceptable level (such as 99%) [89].

Taylor et al. found that PTFE membranes displayed the best antiwetting behavior among all membranes investigated in that study. They identified pore wetting based on a

threshold value of 5% for the normalized specific salt flux (i.e., the ratio of salt flux to water flux divided by salt concentration in feedwater) [90]. In contrast to conductivity monitoring, Lin's group employed a single-frequency impedance to monitor wetness, enabling earlier identification of impending wetting-based membrane breakdown [91]. Ahmed et al. created an electrochemical apparatus and electrically conductive membrane to enable real-time wetness detection based on electric current monitoring. Following an MD test that revealed partial pore wetting, concentration profiles of magnesium and calcium were determined as a function of membrane thickness in the permeate direction [92].

A recent study by Francis and Hilal [93] proposed an effective procedure in efforts to minimize the pore wetting of commercial PTFE membranes by electrospraying carbon nanotubes (CNT) for testing in DMCD. Results showed that the cake layer formation on the surface of the functionally modified PTFE-CNT membrane was minimized exhibiting a much more narrowed pore size distribution in comparison with the PTFE membrane. In addition, a high rejection rate of 99.99% was noted after a continuous MD operation of 24 hours with an 8.3% increase in flux as a result of the successful uniform deposition of CNT. Hence, not only would the modified membranes have improved wettability, but will also lead to the improvement in the shelf life of the membrane and reduce the amount of chemicals needed to clean the membrane to prevent fouling.

2.3.3 Performance evaluation of membrane technology

The treatment of real produced water was conducted by Al-salmi et al. [94] using polypropylene (PP). When increasing the temperature of the feed stream from 40 to 80 ^{o}C, the permeate flux increased up to 7.74 kg/m^2.h. a high percentage of 99% of salt rejection

was achieved for all tests. Pre-treatment of the produced water lead to an increase in permeate compared to the untreated feed. The research group conducted several optimization tests to recover permeate flux affected by salts scaling and oil depositions to enhance the quality of the distillate. In further attempts to remove contaminants using new synthesized membranes, Shirazi et al. developed membranes using commercial granules of high-impact polystyrene for the treatment of industrial textile wastewater [32]. Membranes were prepared using a gas-assisted electrospinning technique and cold pressing was done before all DCMD tests. Results depicted a high rejection range of 99.28-97.93%. The permeate flux was almost 16% higher than that achieved from commercial PTFE membranes. The flux started to decline after 48 hours of operation time in DCMD. It was concluded that this decline was attributed to surface fouling rather than partial pore wetting.

Pawar et al. [95] researched the treatment of real produced water for both laboratory and pilot-scale systems. Salt rejections higher than 99.7% and flux of 1.86 were achieved with no impact on the distillate quality over five days of MD operation. The study showed a negligible effect of treated and untreated produced water on the permeate flux at different feed temperatures of 40 and 60 ^{o}C. However, at a higher feed inlet temperature of 80 ^{o}C, the permeate flux further declined as the membrane was more potentially to be fouled at that point.

During long-term DCMD operations at high temperature, both the flux and salt rejection decline. This behaviour is due to 2 interrelated phenomena. Firstly, the vapor pressure of the feed elevates at a faster evaporation rate that increases the concentration polarization, hence leads to the deposition of more crystalline salts at the feed/membrane interface. This leads to the deterioration of the second key phenomenon, liquid entry

pressure (LEP), due to the raise in the membrane's surface energy. The overall weakening effect of salt accumulation on the feed's side of membrane surface causes pore wetting where liquids pass through the membrane pores, lowering the rejection efficiency. Also, previous studies have observed that pores expand to some extent at increasing feed temperatures which also cause a further decay in both the permeate flux and rejection rates [96][97].

2.4 Pilot-scale MD Modules

Numerous membrane designs that tackle critical challenges like wetting and fouling in MD applications have been investigated in the laboratory scale, but only a few have been successfully scaled-up and brought to market for commercialization and field validation. A durable membrane innovative designed in MD applications should be capable of being scaled-up in a membrane production facility and be easily assembled into large industrial-scale modules for field deployment. Li et al. fabricated a new tri-bore PVDF hollow fiber membrane on industrial-scale hollow fiber spinning equipment [98]. A number of optimisation tests were done to improve the flux to be greater than 5 $L/m^2.h$ in DCMD using a feed concentration of 3.5% NaCl. The rejection percentage was maintained higher than 99.9%. To assess the reproducibility of the membrane, random fiber samples were taken from each one of the 10 batches and synthesized accordingly using defined spinning conditions.

In another recent study by Ebrahimi et al. [99], a flat sheet superhydrophobic PVDF membrane were designed and modified using TiO_2 to assess its ability to recover nitrate from saline feedwater. The outcome for the test flat sheets in DCMD were evaluated and

reported using a pilot scale. The resulted flux of 2.3 kg/m^2.h was used in MATLAB to investigate the removal of nitrate from the inlet saline feed with a surface area requirement of 0.5 m^2 of the membrane. Throughout the process, the electrical conductivity of the permeate remained steady. These findings suggest that the nitrate ions were unable to pass through the membrane, causing their concentration in the feed to increase as pure water permeated the membrane. In general, the flux obtained from this system was not up to the expected standard, which is a drawback that requires improvement.

Ali et al. [100] highlighted the importance of utilizing better correlations for heat-transfer coefficients to develop a more reliable and accurate predictive model that can be applied across a wider range of operating conditions. The research group developed a dynamic model for producing desalinated water using DCMD. Two different types of dynamic model structures, lumped parameter and spatial, were assessed. To validate the models, experimental data was collected by conducting step tests on the inlet hot stream temperature of a DCMD pilot plant. However, both model structures were unable to accurately replicate the dynamic response. The overall discrepancy between the model and plant data was approximately 3%, which is reasonable given the random uncertainties associated with plant operation.

Furthermore, Huang and Arning [101] evaluated the performance of PTFE and PVDF hollow fiber membranes in DCMD. The lab-scale systems measured water flux and salt rejection as a function of module packing density and length. At 10% module packing density, the PVDF demonstrated higher water flux than the PTFE, with values of 17.3 LMH and 9.4, respectively. This was potentially due to their thinner membrane wall and higher porosity. However, the water production rate per module increased due to the larger

membrane surface area. In the case of the 50% module packing density, the long module produced 53% more water flux and presented a 42% higher module water production rate, due to the 2.7 times larger surface area of the membrane. A pilot-scale DCMD system was implemented to the second largest geothermally-heated greenhouse in the USA for a 22-day field testing. The results showed that the pilot scale DCMD system was robust and could withstand actual environmental fluctuations at the facility. The water flux and production rate of the long modules could be improved by raising the fluid flow rate on the shell side, though this would increase pumping energy costs. Salt rejection exceeded 99% in all experiments.

In an attempt to lower the MD operational costs, Park and Lee et al. [102] analysed the thermal energy efficiency of PP and PVDF hollow fiber membrane modules in DCMD in a pilot scale unit. The effective membrane areas of 2.6 m^2 and 7.6 m^2 were noted for PP and PVDF membranes, respectively. When subjected to similar conditions, both MD membranes exhibited varying flux and performance ratios. The variation in flux had an impact on the heat transfer across the membrane. Also, the performance ratio showed to be in linear relationship with the flux and highly dependent on it in pilot scale. Research findings show that comparing the thermal efficiencies of different MD modules solely based on flux was not feasible. These findings imply the properties of the module must be taken into account when choosing the operating conditions for MD.

Kim et al. [103] developed multi-physics computational fluid dynamics (CFD) simulations for hollow fiber membranes in DCMD. The group researched a scalable mesh production technique by implementing mathematical algorithms to enhance the scalability of the CFD simulation from lab scale to larger, pilot-scale modules. It was concluded that

the amount of time it takes to mesh any number of fibers is the same as that for a single fiber. As a result, the time required for meshing is not influenced by the number of fibers. Both theoretical and experimental outcomes were in very good agreement.

Dow et al. [104] conducted a pilot trial investigation utilizing waste heat from gas-fired power station at a temperature of approximately 40 °C to recover water from saline demineralization regeneration waste. The trial ran for three months without requiring membrane or module replacement and achieved 92.8% water recovery, with a flux of around 3 $L/m^2.h$. Results showed that membrane fouling had a minimal impact on flux and thermal energy demand, only becoming apparent at the end of the trial. Membrane analysis after the trial revealed that fouling was mainly due to inorganic scale. Fouling on the permeate side was also observed and was attributed to corrosion of the cooling heat exchanger. The treatment potential was estimated at up to 8000 Liter per day, making it practical for supplying water to various industrial, residential, or agricultural sites.

2.5 Fouling effect on MD performance

To date, commercial membranes are the common contributors to the MD process as, until now, there is no commercial membrane that is specially designed for MD [56]. Nonetheless, recent review articles reported valuable summaries on water purification technologies and porous membrane materials with referral to membrane properties in MD [57–62]. For instance, Yang et al. [105] provided an excellent overview of new polymeric membranes and compared different classes of polymeric membranes for water purification applications. The research group determined that the fouling resistance and permeability can be improved by the addition of microporous support.

Consequently, the major drawback in membrane-based processes is the buildup of undesirable biomass and calcium residues on the membrane surface from the feed side, which is known as fouling and scaling, respectively. These phenomena hinder the membrane's hydrophobicity, porosity, as well as pore size acceptable for MD processes [106]. The accumulated foulants may either be natural organic substances (organic compounds) or carbonate and chloride salts (inorganic compounds) [107]. Generally, organic and inorganic fouling are considered major challenges in large-scale membrane distillation processes that must be properly addressed to avoid minimal salt removal [108], increased energy consumption [109], and process shutdown [110]. When using industrial brine as the feed in the water treatment process, microfiltration (MF) and ultrafiltration (UF) techniques are mainly used as pre-treatment methods to reduce the fouling potential of non-dissolved contaminants.

Horseman et al. [111] indicated that gypsum scaling could be prevented by combining the use of superhydrophobic membranes and periodic gas purging in the MD system. Results have not shown any significant flux decline with high effectiveness in eliminating salt crystals from the membrane surface. With changing operating process parameters, membrane scaling can be delayed but cannot be completely avoided. Previous studies have shown that the purging efficiency during the MD scaling mitigation process is highly dependable upon the initial concentration of the brine.

Mansi et al. have recently reviewed the effect of varying process conditions on the fouling behaviour of the membrane using standalone membrane technologies for the reclamation of produced water [112]. The article showed that membrane distillation (MD) and forward osmosis (FO) exhibited notable process steadiness against high concentrations

of crude oil and salts of 1000 ppm and 150,000 ppm, respectively. Furthermore, hybridization of both technologies showed promising results at pilot scale. Another study on anti-scaling investigation was conducted by Rahimnia and Pakizeh where porous polyphenylene oxide and polystyrene membranes (PPO/PS) were prepared by polymer casting [30]. The fouling resistance of the prepared flat sheets was tested using feedwater consisting of NaCl, Na_2SO_4, and $CaCl_2$. Despite flux decline, all tests showed a rejection rate greater than 99.9%. The synthesized PPO/PS membrane showed satisfactory anti-fouling and anti-wetting performance with little to no deposition of foulants on the membrane surface after four hours of MD operation time. Similarly, flux reduction was noted by Ebrahimi et al. [99] for modified and unmodified PVDF-TiO_2 membranes. This reduction over time was attributed to two possible reasons. The first possibility is that the membrane pores become clogged or fouled, leading to a reduced surface area for water vapor to pass through. The second possibility is that the driving force for the process, which is the temperature difference between the feed and permeate, decreases. To address fouling of the pores, each membrane was immersed in a 0.2% NaOH solution with a pH of 12 at room temperature (25°C) for 15 minutes. Following this treatment, the modified membrane was able to recover up to 95% of its initial flux, while the unmodified membrane recovered only about 60% of its initial flux after being washed and reused.

2.6 Optimization and mathematical modelling in DCMD

In Direct-Contact Membrane Distillation (DCMD), the two liquid streams become in direct contact with the membrane from both sides, as illustrated in Figure 3. A complex heat transfer system occurs that is limited to the membrane thickness in DCMD. Therefore,

the system's permeate flux (i.e. mass transfer rate) impacts the heat flux and heat transfer coefficients in the two counter-current streams [25][113][114][16]. The feed temperature in the system and the type of membranes used in DCMD must be optimized in such a way that condensation is prevented within the pores of the membranes. Furthermore, the type of polymer membrane material employed in DCMD systems depends mainly on the specific requirements and constraints of the application, such as the type of feed solution being treated, the desired separation performance, the operating conditions, and the cost. Polystyrene (PS) membranes are commonly used in DCMD processes. They are known for their good thermal stability, chemical resistance, and mechanical strength, which makes them suitable for a wide range of MD applications [25][115].

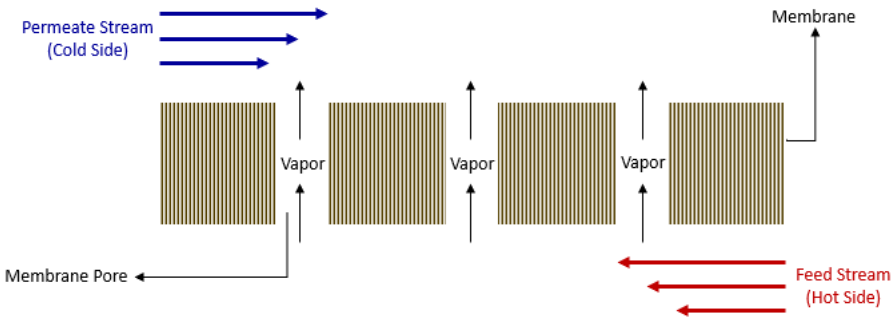

Figure 3. Illustration of Direct-Contact Membrane Distillation

In DCMD, heat inside feed and permeate solutions transfers in a form of a sensible and latent heat, and convective heat. Therefore, mechanisms of heat conduction and heat convection are essential to be considered within the study of heat evolution inside a DCMD module. The pores in the membrane allow the water vapor to pass through while blocking the impurities. The size and distribution of the pores can have a significant effect on the

mass transfer properties of the membrane. If the pores in the membrane are too small, the mass transfer rate will be limited because the water vapor will have difficulty passing through the pores. On the other hand, if the pores are too large, the membrane may be less effective at separating impurities from the water vapor. Figure 3 shows a schematic diagram of the counter current DCMD module.

In addition to pore size, the thickness also play a key role in impacting the heat transfer mechanisms at the membrane boundary where the feed and the permeate solutions are affected by each other [116]. Porosity can also affect mass transfer properties by influencing the surface area of the membrane available for mass transfer and it can also affect the permeability of the membrane. Therefore, the selection of a membrane with the appropriate pore size, thickness, and porosity is key to optimize the mass and heat transfer properties of the system.

2.7 Energy efficiency in MD processes

Membrane distillation systems take advantage of high temperature wastewater channels in order to bring down the need of feedwater heating. A fundamental drawback of the MD process lies in its lower energy efficiency when compared to other treatment technologies such as Reverse Osmosis [117]. However, when it comes to energy constraints, MD processes require an energy range of 120.6-1701.8 Wh/m^3 for heating of the feedwater compared to only 2.5–7.0 kWh/m^3 for the RO process. This huge amount of energy requirement hinders the commercialization potential of advanced MD systems. From an industrial viewpoint, The desalination and treatment of high-salinity brines are inherently energy-intensive [118]. Particularly in MD processes, due to latent heat needed for the evaporation of the feed, the energy requirement significantly rises. The criteria

behind evaluating the energy performance of an MD system are divided into two main parts: (i) standard measures directly related to the fundamentals of the system, and (ii) developed measures based on the specificity of the employed system [51]. The evaluation of the Specific Energy Consumption (SEC) is a common parameter used to evaluate the energy efficiency of MD systems [119,120]. Although the different types of MD systems are very promising in terms of energy efficiency effectiveness, most of them have not exceeded 10 years of continuous application. Hence, more experimental and theoretical are needed to fully assess the overall MD operations [121].

Membrane technologies that are thermally-driven based can treat large capacities of seawater, up to 55,000 m^3/day, while the membrane technology plants can treat 500–5000 m^3/day of seawater depending on the size of the treatment plant. Current patterns show that membrane distillation costs are declining as a direct result of economies of scale (enormous plants). The specialists suggested that every case should be assessed carefully before choosing the technology for treatment with membrane processes as being the most versatile and promising technology for future applications [122]. The expenses of desalination rely principally upon the sort of desalination process utilized, the nature of the influent and effluent, the yield limit of the plant, and the accessible choices for waste removal. The overall cost includes the cost of removal, labor, investment in land and equipment, operational and maintenance, energy consumption, and environmental costs [123].

Table 4 shows a comparison between the thermal and membrane technology methods in terms of cost. The highest costs are attributed to the capital and electricity costs. Thermally-driven membrane processes are more expensive than pressure-driven ones. Thus,

membrane technology is considered a feasible method for saline water treatment [124]. However, the total costs can be further reduced depending on the size of the treatment plant. A smaller plant will require less labor and less energy compared to a large plant [125].

It was discovered by a previous study that raising the feed pressure up to 6.586 MPa significantly lowered the specific energy consumption (SEC) to 0.323 kW h/m^3 in the system with two energy recovery devices. Freshwater supplied from RO system makes it beneficial in arid areas [126]. Given that 40% of the world's population are 100 km away from a seawater source, much research has been made on the different desalination technologies to reduce the capital and operational costs. Currently, the operating costs and energy requirements for desalination using reverse osmosis and thermal distillation are 0.5–1.2 (USD/day. m^3) and 0.8–1.5 (USD/m^3), respectively. In contrast, the energy cost of former techniques is about 4–5 (kWhelec/m^3) and 10–16 (kWhelec/m^3) respectively [127]. This means that the desalination technologies are very energy intensive.

Table 4: Different desalination techniques and the associated costs.

Cost Parameter	Membrane Technology	
	Thermally-Driven	Pressure-Driven
Capital cost (US \$/m^3)	0.449	0.301
Energy (US \$/m^3)	0.555	0.25–0.27
Labour (US \$/m^3)	0.128	0.128
Chemicals (US \$/m^3)	0.024–0.045	0.018–0.054
Membrane replacement (US \$/m^3)	0	0.001–0.072
Maintenance (US \$/m^3)	0.018–0.032	0.018–0.032
Total costs (US \$/m^3)	1.10–1.15	0.45–0.877

It is interesting to note that the main environmental concern that is associated with all desalination processes is the energy intensity. Energy as either electricity or steam produced using non-renewable sources of energy leads to gas emissions. For example, 1 m^3 of desalinated water by generally requires 1 L of fuel. The other environmental issue is the brine and its disposal which affects the marine life [128]. Interestingly, unlike other pressure-driven membrane technologies, the DCMD process does not usually require a pre-treatment step for actual wastewater. This is owing to the low sensitivity of MD to membrane fouling at low operating pressure [32]. The elimination of any pretreatment procedure minimizes both the cost of operation as well as carbon footprint of the whole process.

Membrane Distillation (MD) technologies, either used alone or in combination with other innovative separation processes, are better alternative options that are designed for complete salt removal. This is because: (i) membrane distillation desalinates thermal brine and generates a permeate that is suitable for immediate reuse [129], and (ii) RO technologies may mostly be used in cases where the salinity of brine is minimized to levels close to that of seawater [130].

Owing to MD's low-temperature requirements, many research studies have utilized waste heat and integrated direct contact membrane distillation with other low-grade heat sources. For instance, Li et al. provided insights into the potential benefits of combining DCMD with a phosphoric acid fuel cell (PAFC) in terms of energy efficiency, power output, and exergy efficiency [131]. Stored heat in the tank was used to deliver sustained energy for the DCMD subsystem and hence the overall energy efficiency was increased up to 82.2%. Shafieian and Khiadani [132] developed a novel solar membrane-based

desalination system in an attempt to enhance the production rate of freshwater. The proposed DCMD solar system showed a maximum thermal efficiency of 78%. In another study, Soomro and Kim [133] integrated DCMD with a parabolic-trough (PT) plant. Mathematical modelling was conducted to evaluate the desalination performance of the integrated system. Simulated results showed an increase in permeate flux and evaporation efficiency of 20.01 $kg/m^2.h$ and 54.98%, respectively at bulk feed temperature of 45°C. Zhao et al. [134] integrated DCMD with a dye-sensitized solar cell (DSSC) for the cogeneration of electricity and high quality water by transmitting sunlight. Numerical expressions were performed to calculate the hybrid system's maximum energy efficiency of 45.35%. The efficiency showed to improve by increasing the inlet temperature of the feed.

CHAPTER 3: MATERIALS AND METHODS

3.1 Experimental

This chapter aims to provide a comprehensive and detailed discussion of the materials, equipment, analysis, and procedures employed in the research project. The focus will be on presenting a thorough description of the bench-scale experimental set-up and the pilot-scale setup utilized in the study and provide a clear understanding of the research methodology and characterization techniques used to evaluate the research findings.

3.1.1 Materials

3.1.1.1 Membranes

The 200x250 mm sized PTFE membrane filters were commercially obtained from Sterlitech Corporation (WA, USA). Large-sized polyethylene membranes with an effective area of 0.01 m^2 (dimensions of effective area: 175 × 125 mm) were used without further modification from Aquastill, NL. The pore size range of the PE membranes was 300–700 nm with a mean thickness of 15.5 ± 1.53 μm. Furthermore, polystyrene pellets (PS, Mw = 192,000) were purchased from Sigma Aldrich Chemie GmbH TAUFKIRCHEN, Germany and used as it is. N,N-dimethyl formamide (DMF) for analysis was purchased from ACS.

3.1.1.2 Synthetic brine

Synthetic brine has been used throughout this work as the feed solution. Real produced water has numerous of elements that cannot be controlled under experimental conditions. In addition, due to confidentiality with oil and gas industry in Qatar, obtaining produced water was very difficult. In line with literature proposed procedures, synthetic brine solutions were prepared. Chemicals used for the preparation of the feed solutions consisted of a mixture of calcium chloride dehydrate (147.01 g/mol, purity 99.9%, CAS:

7791-18-6, Manufacturer: Sigma-Aldrich, St. Louis, MI, USA), potassium chloride LR (74.55 g/mol, Code:0001276, Breckland Scientific Supplies, Stafford, UK), magnesium chloride (95.21 g/mol, purity > 98%, CAS: 7786-30-3, Sigma-Aldrich, St. Louis, MI, USA), sodium chloride (58.44 g/mol, purity 99%, CAS: 7647-14-5, Sigma-Aldrich), magnesium sulfate 7-hydrate (120.37 g/mol, purity 99%, CAS: 10034-99-8, Surechem products Ltd.), potassium bromide analytical reagent grade (119.0 g/mol, CAS: 7758-02-3), strontium chloride (158.53 g/mol, CAS: 10476-85-4, Sigma-Aldrich), and boric acid (61.83 g/mol, purity > 99.5%, CAS: 10043-35-3, Sigma-Aldrich). All chemicals were used as received without additional purification [25]. The concentration of each chemical component is listed in Table 5.

Table 5: Detailed chemical constituents in prepared synthetic brine [25].

Components of feed	**Feed Concentration (ppm)**	
	C1	**C2**
Na	23,876	11,938
Mg	2,520	1260
Ca	765	382
K	793	396
Sr	11	5
B	9	4
Cl	42,682	21,341
SO_4	4,229	2,114
HCO_3	726	363
Br	67	33

An amount of 20 L feed was prepared with compositions similar to that in industrial thermal desalination plants in Qatar [135]. Quantities of 1200 g of sodium chloride was mixed with 5 L of boiled distilled water and kept stirring for 1 hour. After that, we added

58, 28, 112 and 108 grams of calcium chloride dehydrate, potassium chloride, magnesium chloride and magnesium sulfate, respectively. They were kept stirring for 2 hours to assure complete melting of all chemicals. At the end, small amounts of boric acid, potassium bromide and strontium chloride (1, 2 and 0.4 grams, respectively) were added and left for another 1 hour. Following this procedure, two different concentrations with conductivities of 100 mS/cm and 50 mS/cm were separately prepared to study the effect varying feed concentration on the permeate flux.

3.1.2 Electrospinning

A custom-made electrospinning system was used for membrane fabrication in this work (Figure 4). An amount of 20 grams of polystyrene (molecular weight: 192,000) was dissolved in 60 mL DMF and 40.0 mL Acetone. PS and DMF were first set to stir in a beaker. This was followed by a continuous stirring for Acetone/PTFE at room temperature up to 24 hours to assure the dissolving of the polymers. Spinning parameters used were as followed: Volume of polymer solution: 10 mL, Voltage: 14 kV, distance between the needle and collector: 15 cm, needle diameter: 20 gauge needle, Flow rate: 6 mL/hr, and Drum RPM: 560 RPM. Fabricated membranes were then left in oven overnight to get rid of any residuals. The solution was not pushed fully into the needle before the HV was applied to avoid formation of large drips. Afterwards, they were cold pressed at 1 Ton for 1 min. Sample masses of 0.1629 g, 0.1420 g, 0.1342 g and 0.0510 g were taken for PS-MA, PS-MB, PS-MC, and PS-MD, respectively. The specific properties of electropsun membranes are listed in Table 6.

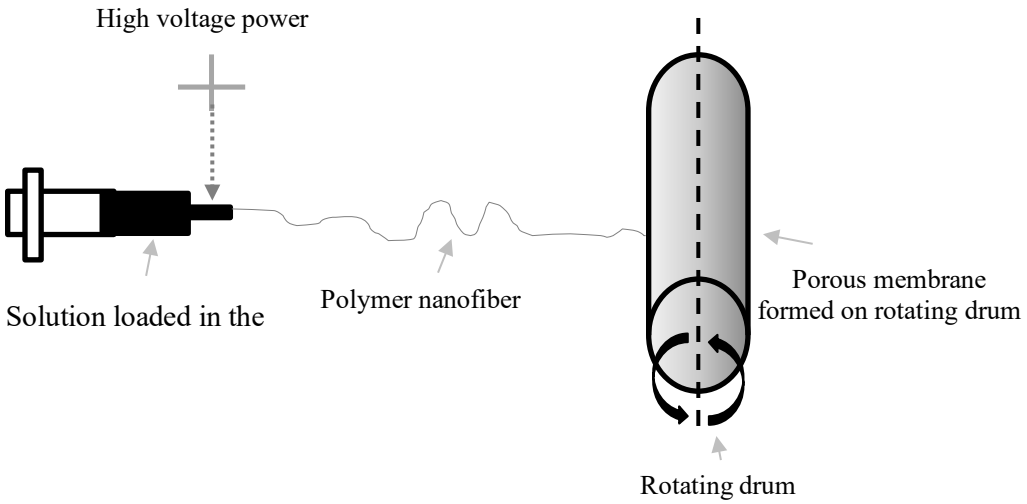

Figure 4. Schematic of Electrospinning technique [136]

Table 6: Detailed specification of commercial and synthesized membranes in DCMD

Membrane material	**Source**	**Mean Thickness (µm)**
PTFE-MA	Commercial	72.94 ± 3.35
PTFE-MB	Commercial	102.62 ± 17.56
PS-MA	Electrospun	190.82 ± 3.18
PS-MB	Electrospun	156.57 ± 15.15
PS-MC	Electrospun	136.97 ± 12.88
PS-MD	Electrospun	143.51 ± 14.20

**Note: MA, MB, MC, and MD refer to the electrospun PS membranes A, B, C and D, respectively.*

3.2 Characterization of membranes

3.2.1 Membrane thickness measurements

A micrometer was used to estimate the membrane's thicknesses. The mean thickness was then calculated on the basis of 5 different measured sides and corners of the

membrane.

3.2.2 Contact angle meter (CAM)

An optical contact angle (OCA 35) from DataPhysics Instruments GmbH (2013 model) was used as the main indicator of hydrophobicity. This device provided an automated control of the sample position in the x-y-z direction. Contact angle diagrams were generated from the surface free energies of the membrane sample. Distilled water was injected in the dosing needle. The dosing volume and dosing rate of the liquid syringe system were 1 μl and 4 $\mu l/s$, respectively. The flat membrane was placed on a glass plate, and the sharp tip of the syringe was positioned on the top of that membrane's surface. Measurements were recorded at three different locations.

3.2.3 Scanning electron microscopy (SEM)

An FEI Quanta 200 environmental scanning electron microscope at 2.0 keV to obtain a clear idea on the membranes' microstructures. The Scanning electron micrographs were taken for membranes before and after the DCMD test. Prior to analyzing our membranes and investigating their surface measurements by SEM, they were first dried under vacuum at room temperature for 3 hours to eliminate moisture and obtain unblemished scanning images. After that, we sprayed the samples with a thin layer of gold. This electrically conducting metal helped create a critical layer on our non-conductive material, which therefore inhibited electron charging and reduced thermal damage at higher resolutions. We designed our own gold sputtering target for this purpose. ImageJ software (National Institutes of Health, USA) was used to estimate the average pore size from different locations on the membrane's surface.

3.2.4 Atomic Force Spectroscopy (AFM)

An atomic force spectroscopy (AFM) was used to study the structural change on the membrane surface, providing deeper insights into the formation of crystals and accumulation of foulant on the membrane during all DCMD experimental work.

3.3 MD Performance

It is a fact that membrane performance is considered an essential key indicator of the filtration effectiveness for different types of membrane-based technologies. This success factor replies mainly on the ability of the membrane to maintain stable and high permeate flux throughout the entire duration of MD operation [56]. In addition, the membrane's potential for achieving complete salt rejection is another criterion of improved desalination performance. This means that all salt particles are effectively separated from the highly saline feed solution, which leads to achieving very high salt rejection rates and resulting in high quality water.

3.3.1 Salt Rejection and Flux Calculations

The salt rejection rate (R) was estimated using the equation [137]:

$$R\ \% = \frac{C_f - C_p}{C_f} \times 100 \quad (1)$$

Where: $\mathbf{C_f}$: the conductivity for the feed

$\mathbf{C_p}$: the conductivity for the permeate

The permeate flux of a porous membrane (J) is mostly known as the applied transmembrane pressure driving force divided by the resistance to mass transfer [138,139]. An electronic balance was used to collect the permeate in a large 5L tank and the change

in permeate weight was continuously recorded over time. Similar to Miller et al. [140], the resistance to permeation as a function of the permeate volume per unit membrane area was calculated. Therefore, the permeate flux was calculated as per equation 3:

$$J = \frac{\Delta M}{\rho_w A \Delta t} \quad (2)$$

Where: **J**: the permeate flux [LMH]

ΔM: the difference in permeate mass [Kg]

ρ_w: the density of distilled water [1 Kg/L]

A: the membrane effective area [Bench scale unit: 0.00206 m^2]

Δt: the difference in time [H]

3.4 Membrane Fouling

In this work, a Humic Acid sodium salt with technical grade (CAS: 68131-04-4) was purchased from Sigma-Aldrich. A stock solution was prepared, as the foulant, by dissolving an amount of HA in deionized water. A standard concentration of (50 ppm) of Humic Acid was prepared by dissolving HA in DI. The working solutions of required concentration were prepared by sequential dilution of the standard solution. The control foulant concentrations were measured using a UV-visible spectrophotometer at λ_{max} = 600 nm at initial concentrations of 15–45 mg/L. Consequently, the fouling performance of the polyethylene membranes was tested in the pilot-scale DCMD system. The HA rejection was calculated based on the HA concentration obtained by the UV spectrophotometer. The initial HA concentration was measured by taking a sample from the feed before starting the DCMD experiment (the control), and the final HA concentration that is collected from the permeate is the measured value. The rejection values were calculated for different HA

concentrations using the difference between the control and measured concentrations divided by the control adsorption.

The dynamic fouling tests for the polyethylene membranes were investigated using 15, 25, 35, and 45 ppm of the Humic Acid (HA) foulant. Three fouling cycles were conducted per experiment. Basically, the first cycle included the evaluation of pure water flux before fouling (J_1) for pure distilled water for 1 h, followed by the second cycle that includes the foulant in the feed resulting in the foulant flux (J_p). Finally, the third cycle was performed by backwashing the membrane using deionized water without applying any forms of external heat. The pure water flux after fouling (J_2) was recorded. The following fouling ratios were calculated to assess the antifouling properties of the polyethylene membrane in the pilot DCMD system:

$$\text{Flux recovery ratio, FRR [\%]} = \left(\frac{J_2}{J_1}\right) \times 100 \quad (3)$$

$$\text{Reversible fouling ratio, } R_r \text{ [\%]} = \left(\frac{J_2 - J_p}{J_1}\right) \times 100 \quad (4)$$

$$\text{Irreversible fouling ratio, } R_{ir} \text{ [\%]} = \left(1 - \frac{J_2}{J_1}\right) \times 100 \quad (5)$$

$$\text{Total fouling ratio, } R_t \text{ [\%]} = \left(1 - \frac{J_p}{J_1}\right) \times 100 \quad (6)$$

3.5 Energy Consumption Analysis

An important aspect of MD is the thermal energy consumption linked to the heat of the feed stream [9]. In this respect, the specific thermal energy consumption (STEC) is

often used, calculated as the energy to supply to the feed recirculating inside the module, divided by the permeate production per time (kW h/m^3) [129]:

$$STEC = \frac{Q_f \times c_p \times \left(T_{fin} - T_{fout}\right)}{Q_p} \quad (7)$$

where Q_f is the feed flow rate (kg/h), c_p is the specific heat of the feed (kJ/kg. K), T_{fin} is the feed temperature at the module inlet (K), T_{fout} is the feed temperature at the module outlet (K), and Q_p the permeate flow rate (L/h). Due to the fact that in DCMD processes, both the hot feed and the cold permeate water are brought into contact with the membrane under atmospheric pressure, the total pressure is assumed constant at 1 atm, resulting in a negligible viscous flow [141–143].

Another important performance indicator in an MD system is the specific electrical energy consumption (SEEC). It is defined as the amount of electrical energy consumed to produce a unit mass of pure water [51]. In the current MD pilot unit, the specific electrical energy consumption (SEEC) was calculated based on three main sources in the system: the permeate pump, the feed pump, and the unit's control panel. When calculating the specific thermal and electrical energy consumptions, the specific energy consumption (SEC) (kWh/m^3) is defined as the amount of total energy supplied (heat and electrical energy) to produce a unit mass of the product [144,145]. SEC was used in this work to evaluate the energy performance for a large pilot unit capacity of 207.31 m^3/h.

$$SEC = STEC + SEEC \quad (8)$$

3.6 Optimization mathematical modelling

3.6.1 Heat transfer

3.6.1.1 Heat transfer from the feed side to the surface of the electropsun membrane:

Convection is used to transfer heat through the feed boundary layer, and Newton's law of cooling governs this process by the following equation:

$$Q_f = h_f\left(T_{b,f} - T_{m,f}\right) \quad (9)$$

Where Q_f is the convective heat flux, h_f is the boundary layer heat transfer coefficient at the membrane's feed side, and $T_{b,f}$ and $T_{m,f}$ are the average feed temperature for the bulk and surface of the membrane from the feed side, respectively. The transfer of heat across the membrane can be categorized into two segments: the first being the transfer of heat through the membrane by conduction, which includes the polymer matrix and pores filled with gas; the second being the transfer of heat through the membrane by the latent heat of water vapor movement.

3.6.1.2 Second Stage: Heat transfer through the membrane layer

The conducted heat transfer across the membrane (Q_C) is added to the evaporative mass flow (Qv) through the membrane pores to obtain the total heat flux across the membrane (Qm).

$$Q_c = \frac{k_m}{\delta}\left(T_{m,f} - T_{m,p}\right) \quad (10)$$

$$Q_v = J_w \Delta H_v \quad (11)$$

The enthalpy of the water (ΔH_v) can be calculated using the following equation:

$$\Delta H_v = \left(\left(1.7535 * T_{m,f}\right) + 2024.3\right) \quad (12)$$

The effective thermal conductivity of the membrane (k_m) is equal to the product of the thermal conductivity of the membrane solid (k_{mem}), and the thermal conductivity of the

membrane gas, k_{gas} (air and water vapor).

$$k_m = \left(\left(\frac{\epsilon}{k_{gas}}\right) + \left(\frac{1-\epsilon}{k_{mem}}\right)\right)^{-1} \quad (13)$$

The total heat flux across the membrane (Q_m) can be described as the following:

$$Q_m = Q_c + Q_v = h_m\left(T_{m,f} - T_{m,p}\right) + J_w \Delta H_v \quad (14)$$

3.6.1.3 Third Stage: Heat Transfer from the Membrane Surface to the Permeate Stream

Convection is used to transmit heat across the boundary layer from the permeate side membrane surface to the permeate bulk. The permeate heat flux, Q_p, depends on the permeate heat transfer coefficient (h_p) and temperature difference between bulk permeate temperature ($T_{b,p}$) and the interfacial membrane temperature ($T_{m,p}$) at the permeate side. In this work, the DCMD process is assumed to be a steady-state process in order to calculate both the surface temeprature at the feed and permeate sides of the membrane. The overall heat transfer flux of the feed, membrane, and permeate sides of the module, are assumed to be at steady state conditions ($Q_f = Q_m = Q_p$).

$$Q_p = h_p\left(T_{m,p} - T_{b,p}\right) \quad (15)$$

In the DCMD process, the vapor pressure difference arising from the temperature difference between the two surfaces of the membrane is the driving force for water vapor transfer across the membrane. The temperature difference between $T_{m,f}$ (the membrane/feed interface) and $T_{m.p}$ (the membrane/permeate interface) are the driving force for water vapor transfer through the pores of the membrane. However, one of the limitations in DCMD systems is the change in the membrane/interface temperature with

respect to bulk temperature in the process. This occurs due to heat lost from the feed stream membrane surface side and heat gained from the permeate stream side of the membrane surface. $T_{m,f}$ and $T_{m.p}$ were calculated using the following equations:

$$T_{m,f} = \frac{k_m\left(T_{b,p} + \frac{h_f}{h_p}T_{b,f}\right) + \delta(h_f T_{b,f} - J_w \Delta H_v)}{k_m + h_f\left(\delta + \frac{k_m}{h_p}\right)} \quad (16)$$

$$T_{m,p} = \frac{k_m\left(T_{b,f} + \frac{h_p}{h_f}T_{b,p}\right) + \delta(h_p T_{b,f} + J_w \Delta H_v)}{k_m + h_p\left(\delta + \frac{k_m}{h_f}\right)} \quad (17)$$

In this work, the DCMD process is assumed to be a steady-state process in order to calculate both the surface temeprature at the feed and permeate sides of the membrane. A number of assumptions were made to assess the significance of the different heat transfer mechanisms using the pilot DCMD system, such as: Operating conditions are at steady state, negligible heat loss, the membrane pores have uniform sizes, constant physical properties of water, the water flow is laminar in the x-direction, and constant total pressure of 1 atm. As such, the heat balance guaruntees that the three consecutive heat transfer methods satisy the following equation:

$$Q_f = Q_m = Q_p \quad (18)$$

After a certain period of time, the concentration polarization in the desalination process influences the transfer as a result of salt molecules building up on the membrane surface. The ratio of the solute concentration on the feed membrane surface ($C_{m,f}$) to the concentration of the feed bulk ($C_{b,f}$) is known as the concentration polarization coefficient (ϕ):

$$\phi = \frac{C_{m,f}}{C_{b,f}} \tag{19}$$

$$C_{m,f} = C_{b,f} * \exp\left(\frac{J_w}{k_s * \rho_{b,f}}\right) \tag{20}$$

Where $\rho_{b,f}$ is the density of the feed flow, and k_s represents the solute mass tranfer coefficient as follows:

$$k_s = Sh * \frac{D_e}{D_h} \tag{21}$$

Where D_h is the hydraulic diameter of the hot channel and Sh is the Sherwood number, which is determined using the Graetz-Leveque equation for laminar flow:

$$Sh = 1.86\left(Re * Sc * \frac{D_h}{L}\right)^{\frac{1}{3}} \tag{22}$$

In the following equations, Sc represents the Schmidt numbers, Re represents the Reynolds number, and Pr represents the Prandtl number:

$$Sc = \frac{\mu_{mf}}{\rho_{b,f} * D_e} \tag{23}$$

$$h = \frac{Nu * k}{D_h} \tag{24}$$

$$\Pr = \frac{v}{\alpha} = \frac{\mu * c_p}{k} \tag{25}$$

Where k is the average thermal conductivity of the fluid at the membrane feed side, and Nu is Nusselt number that is determined by the equation shown below:. For a flat plate module and laminar flow (Re < 2100), the Nusselt number can be used for both the feed and permeate side of the membrane using the following equation:

$$Nu = 1.86 \left(\frac{RePr D_h}{L}\right)^{\frac{1}{3}} \quad (26)$$

3.6.2 Mass transfer

In the following equation, J_w is the permeate mass flux, and De is the equivalent diffusion coefficient:

$$J_w = D_e * \Delta p_m = D_e * (P_{wf}^0 - P_{wp}^0) \quad (27)$$

P_{wf}^0 and P_{wp}^0 are the partial pressures of water at the feed and permeate sides of the membrane, respectively:

$$P_{wf}^0 = \exp\left(23.1964 - \frac{3816.44}{T_{mf} - 46.13}\right) \quad (28)$$

$$P_{wp}^0 = \exp\left(23.1964 - \frac{3816.44}{T_{mp} - 46.13}\right) \quad (29)$$

Considering the effect of salinity in the feed solution, the permeate flux can be represented as the following equation:

$$J_w = D_e(P_{wf}^0 * \gamma_{wf} * x_{wf} - P_{wp}^0) \quad (30)$$

For an aqueous solution of NaCl, the γ_{wf} can be expressed as the following:

$$\gamma_{wf} = 1 - (0.5 * x_{NaCl}) - (10 * x_{Nacl}^2) \quad (31)$$

There are three different sorts of mechanisms that account for the movement of gases and vapor through porous media, which are the Poiseuille flow model, the molecular diffusion model, and the Knudsen model. The Knudsen flow and molecular diffusion models can be used with DCMD. Trans-membrane hydrostatic pressure is not applied since the feed and permeate solutions are retained inside the membrane module at a constant pressure (about 1.0 atm). The Poiseuille flow in this situation is insignificant. The ratio of

the Knudsen diffusion to the molecular diffusion was used to calculate the combined influence of the molecular and Knudsen diffusions. The governing mechanism in the mass transmission is determined by this ratio. Considering the effect of salinity The effective, Knudsen, and molecular diffusion coefficients are D_e, D_k and D_m, respectively. The following are the mathmatical expressions for D_e, D_k and D_m:

$$D_e = \left(\frac{\alpha}{D_k} + \frac{1-\alpha}{D_m}\right)^{-1} \tag{32}$$

$$D_k = \left(\frac{3 * \delta * \tau}{2 * \epsilon * d_{pore}} * \left(\frac{\pi * R * T_m}{8 * Mol_w}\right)^{0.5}\right)^{-1} \tag{33}$$

$$D_m = \left(\frac{R * T_m * \delta * \tau * P_{air,pore}}{Mol_w * \epsilon * PD_{w,a}}\right)^{-1} \tag{34}$$

The following expression, $PD_{w,a}$ can be employed in the temperature range of 273-373 K, is used to compute the value for water-air, and Tm is the mean temperature across the membrane surfaces

$$PD_{w,a} = 1.895 * 10^{-5} * T_m^{2.072} \tag{35}$$

$$P_{pore} = \frac{P_f + P_p}{2} \tag{36}$$

$$T_m = \frac{T_{mf} + T_{mp}}{2} \tag{37}$$

The fictitious route across the membrane is frequently related to the membrane porosity ϵ, as in the Mackie-Meares equation, and τ is the membrane thickness which is frequently constant.

$$\tau = \frac{1}{\epsilon} \tag{38}$$

The steps followed to calculate the theoretical model in this work is depicted in Figure 5.

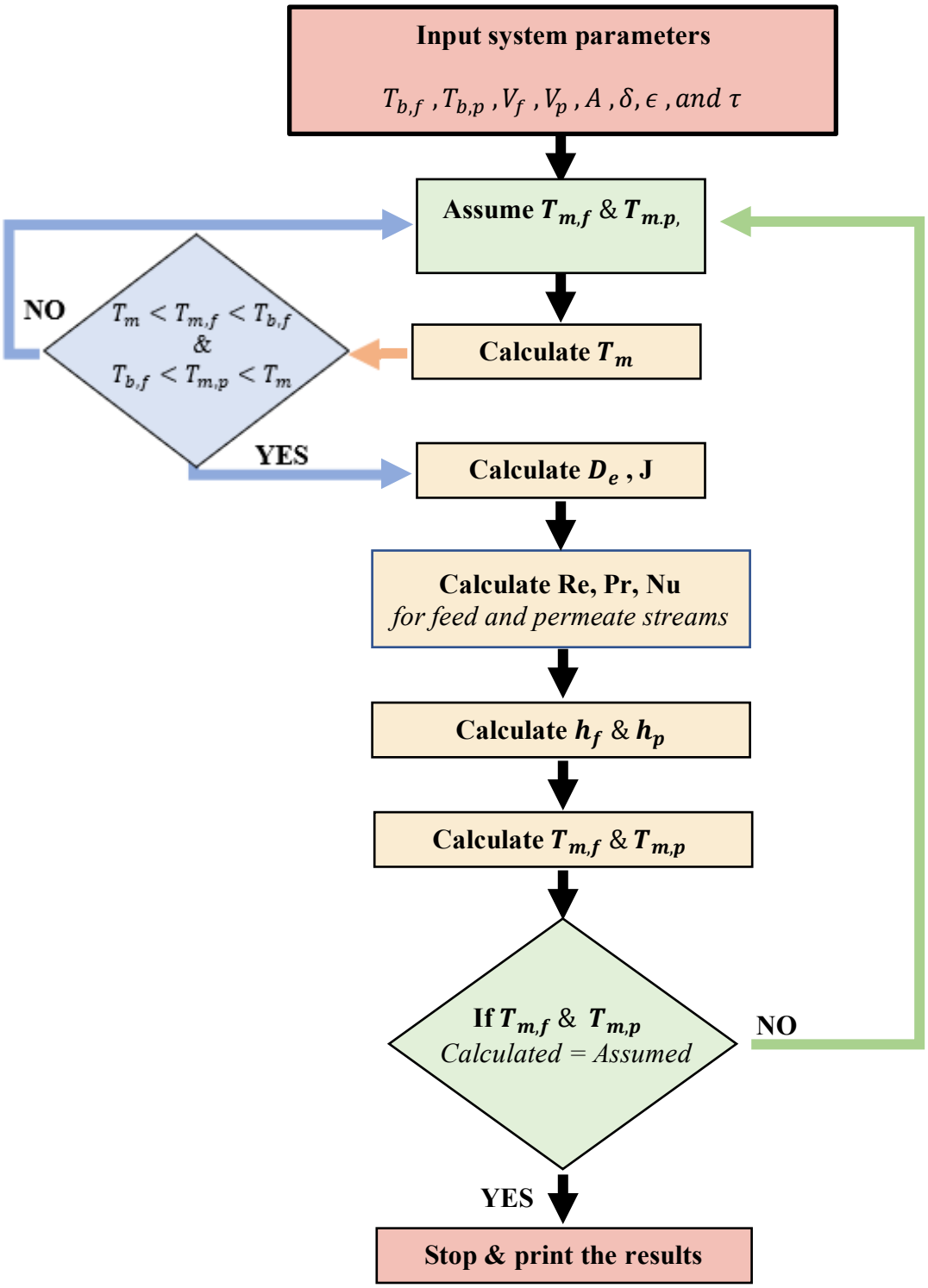

Figure 5. Flowchart for numerical optimization model in direct contact membrane distillation.

3.7 DCMD Modules

3.7.1 Bench-scale system

The direct contact membrane distillation configuration consist of two different liquid channels: (i) Hot side containing thermal brine as the feed and (ii) a cold side containing distilled water. The flow here is counter-current since both channels have opposite flow directions. As illustrated in Figure 6 below, the separator between both channels is the membrane. During the distillation processing, the thermal brine is heated, and its purified vapor passes through the pores of the membrane up to the cooled side of distilled water where it condensates.

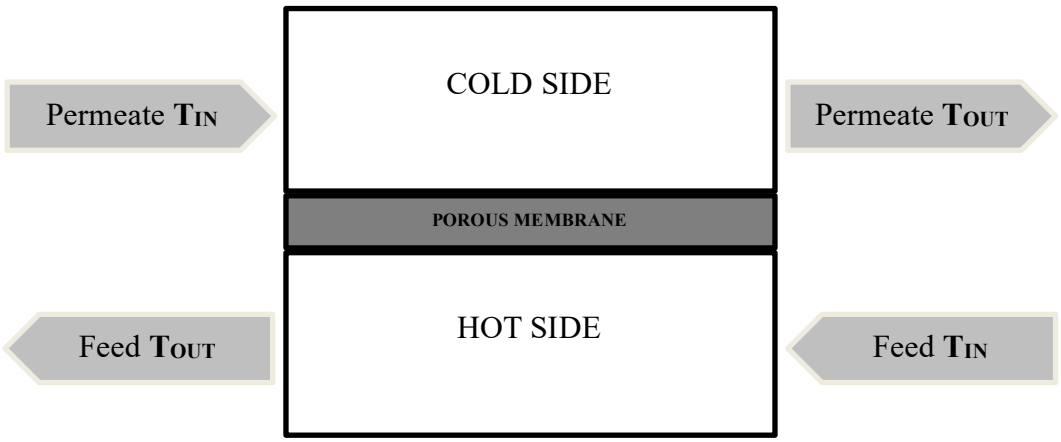

Figure 6: Direct Contact Membrane Distillation (DCMD).

Different flow rates were used to test the desalination performance of electropsun membranes, however, due to the low mechanical strength of the pure polystyrene membranes, pore wetting occurred at high flow rates. Hence, the optimum flowrate at which pore wetting did not occur and stable flux was maintained was set to be 5 rpm. This

unit is equivalent to a value of 0.03 L/min. The optimal process parameters are listed in Table 7.

The synthetic brine was used as prepared without further treatment. The membrane was sandwiched between two low-foulant spacers and acted as a good support to allow equal distribution of the liquid onto the membrane surface without harshly affecting the membrane's tender structure. The addition of a spacer significantly increases the heat transfer coefficient of the hot side by almost 82% [146]. Prior to starting off with the direct contact membrane distillation process, an amount of 4 L of prepared brine were poured into an empty 5 L tank (the hot side). Similarly, an equal amount of distillate was poured into an empty 5 L tank (the cold side).

Table 7: Optimal parameters for DCMD experiments

	Feed (Thermal brine)	Permeate (Distillate)
Inlet Temperature [^{o}C]	60	20
Inlet Pressure [PSI]	0.13-0.52	0.13-0.52
Flowrate [RPM]	5	5

A laboratory-scale PTFE membrane cell, with an active membrane area of 20.6 cm^2, was purchased from Sterlitech Corporation and successfully used for all experiments in this work. The size of each membrane used in the DCMD tests were cut to fit the DCMD cell's active area dimensions of 4.52 x 4.52 cm^2. Temperature, pressure, feed weight, distillate weight, and time were recorded using a data acquisition system (National

Instrument).

The feed and permeate were circulated using two pumps (model: FH100X, Thermo Scientific, USA). RTDs (RTD-NPT-72-E, Omega Engineering, UK) were used to measure the temperatures of the both the inlet feed and outlet permeate streams. The MD data was collected using a data acquisition software (Model NI ENET 232, National Instruments, USA). There are four temperature and pressure probes positioned at the inlet and outlet for each of the feed and permeate streams, respectively. A schematic diagram showing the bench-scale DCMD system is clear in Figure 7.

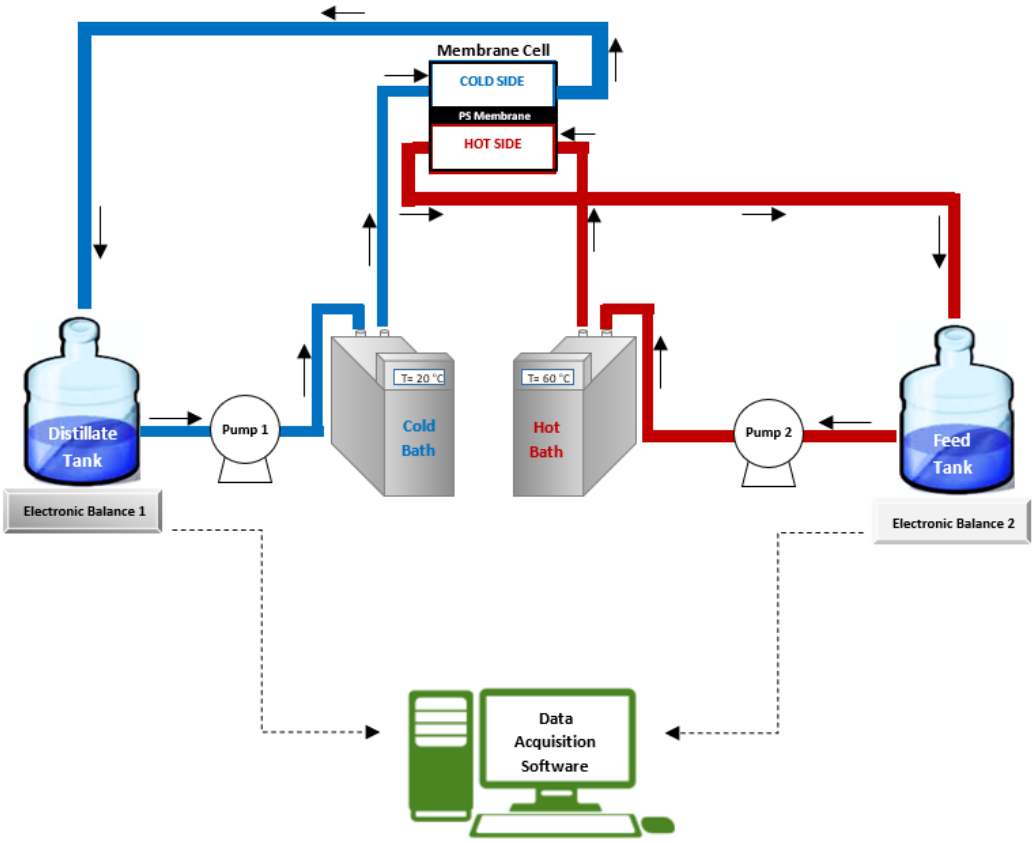

Figure 7: Schematic diagram for the bench-scale DCMD system used in Qatar University labs.

3.7.2 Pilot-scale system

A DCMD pilot unit was used for measuring the performance of the polyethylene membranes using synthetic thermal brine. The tanks are made from polypropylene, whereas the pumps are made by Pan World NH-100-PX. Due to the chemical resistance of the build-up materials, this pilot unit is suitable for testing our high-salinity brine with TDS values reaching up to 100 mS/cm. Furthermore, this large unit consists of four temperature sensors, two pressure sensors, and two flow meters. The process parameters are manually entered by tapping on the required setpoint using the electronic control panel located on the front side of the unit, as shown in Figure 8.

As for the recording of information, a built-in flash drive inside the pilot unit automatically saves the data each time the pump returns the distillate back to the brine. Electrical heating of 3KW is available inside the feed tank. The heating is automatically controlled and switches off if it exceeds the maximum allowable temperature. An external chiller is directly connected to the distillate tank.

In the DCMD pilot unit, three chambers were utilized: the brine, distillate, and distillate return tank. The brine tank was filled with 16 L of feed, and the distillate tank was filled with 16 L of distilled water to ensure a temperature gradient across the membrane channels. The distillate produced was collected in the distillate return tank until it reached the maximum level, where the distillate return pump started pouring back the excess amounts of produced distillate back into the brine tank (Figure 9).

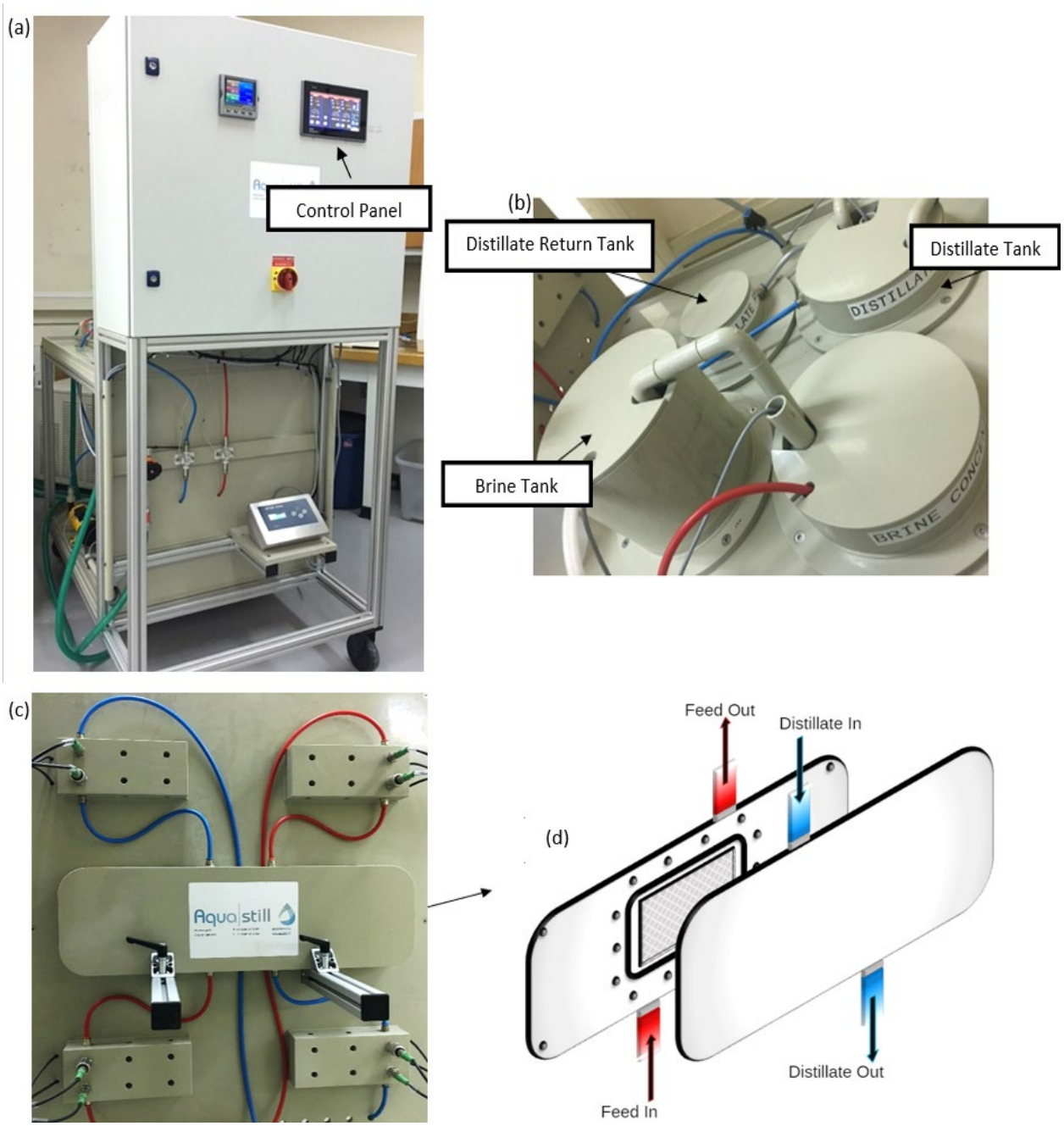

Figure 8. (**a**) Front side of the DCMD pilot unit at Qatar University labs, (**b**) the tanks on the backside of the pilot unit (**c**) Membrane channels from the back side of the pilot unit, and (**d**) 3D illustration of DCMD membrane holder showing counter current flows in the DCMD pilot unit.

This DCMD process was assumed to be (i) steady-state, (ii) no heat exchanged with the surrounding (isolated system), and (iii) counter-current flow direction. All experiments were performed using the normal operation mode for long periods of time (reaching up to 100 h). This DCMD pilot unit was used for operational DCMD testing hours of 20, 40, 60, 80, and 100.

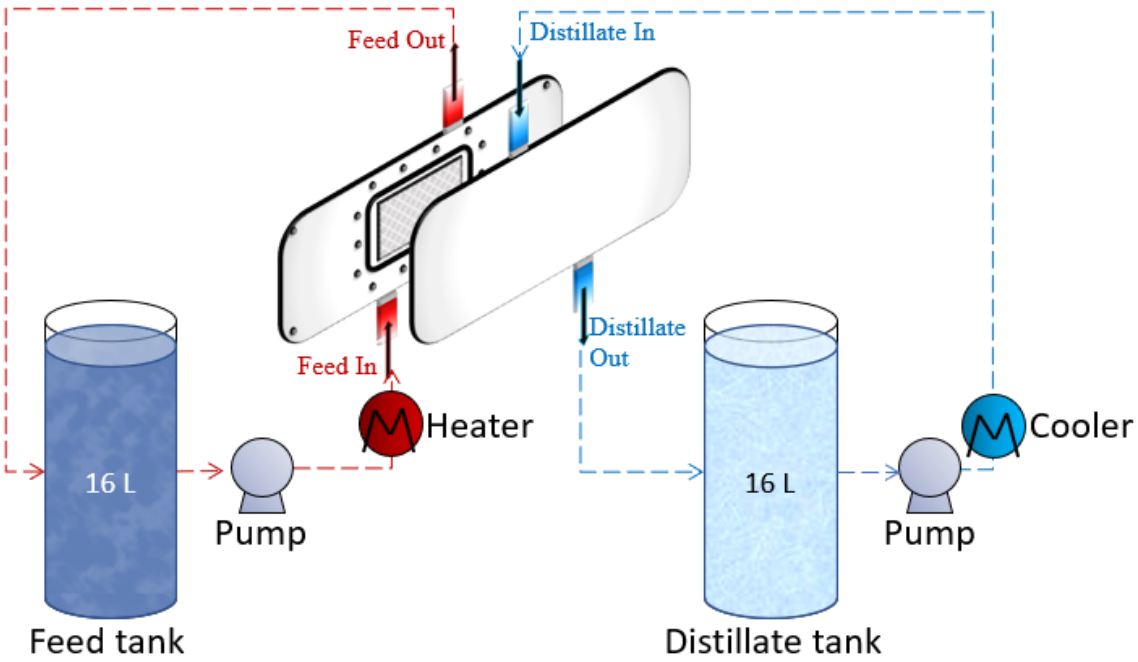

Figure 9. Schematic diagram for DCMD pilot unit.

CHAPTER 4: RESULTS AND DISCUSSION

This chapter aims to provide a comprehensive and in-depth analysis of the research gaps, as well as the research findings from applied experiments and numerical approaches, followed by thorough interpretation and discussion of the results. Moreover, this chapter provides a critical assessment of the research findings and its significance compared with existing data in literature, highlighting the contribution of the current research findings and its relevance and novelty in the investigation of the desalination performance in direct contact membrane distillation (DCMD).

4.1 Desalination performance of optimized electrospun polystyrene membranes using a bench-scale DCMD system

This section aims to establish a direct link between electrospun polystyrene (PS) membranes and industrial desalination plants in Qatar by mimicking real produced water. Therefore, synthetic brine was used as the feed component in the bench-scale DCMD unit and investigated the effect of the produced water on the synthesized PS membranes. The results were compared with similar work in literature. Overall, the research shows experimental data that contributes to a better understanding of the use of electrospun PS membranes in DCMD that may be suitable for long-term desalination applications at larger scale.

4.1.1 Wettability

The water contact angle is a direct measure of the membrane's hydrophobic behavior which is key in any MD process to help repel the liquid feed solution. It was found that at higher feed concentrations of 75,500 ppm, the water contact angle was significantly

lower than that in reduced concentrations of 25,200 ppm. This is because the higher amounts of salts, at constant process parameters of temperature, pressure and flowrate, result in an increase in the membrane's surface roughness. This property is key in dropping the water contact angle of fabricated polystyrene membranes. All contact angle measurements before and after DCMD are recorded in Table 8 for the two feed concentrations.

Table 8: Contact angle measurements before and after DCMD

	Before DCMD	After DCMD – C1	After DCMD – C2
PTFE-MA	139.80 ^{o} ± 4.77	134.78 ^{o} ± 3.57	132.96 ^{o} ± 1.13
PTFE-MB	145.90 ^{o} ± 4.17	130.1^{o} ± 1.03	129.6 ^{o} ± 1.21
PS-MA	134.3.60 ^{o} ± 4.44	119.4 ^{o} ± 1.20	128.8 ^{o} ± 2.05
PS-MB	129.84 ^{o} ± 10.44	116.3 ^{o} ± 1.21	132.34 ^{o} ± 1.17
PS-MC	139.90 ^{o} ± 7.02	127.00 ^{o} ± 1.57	131.43 ^{o} ± 1.79
PS-MD	146.10 ^{o} ± 5.08	137.69 ^{o} ± 1.21	138.64 ^{o} ± 3.38

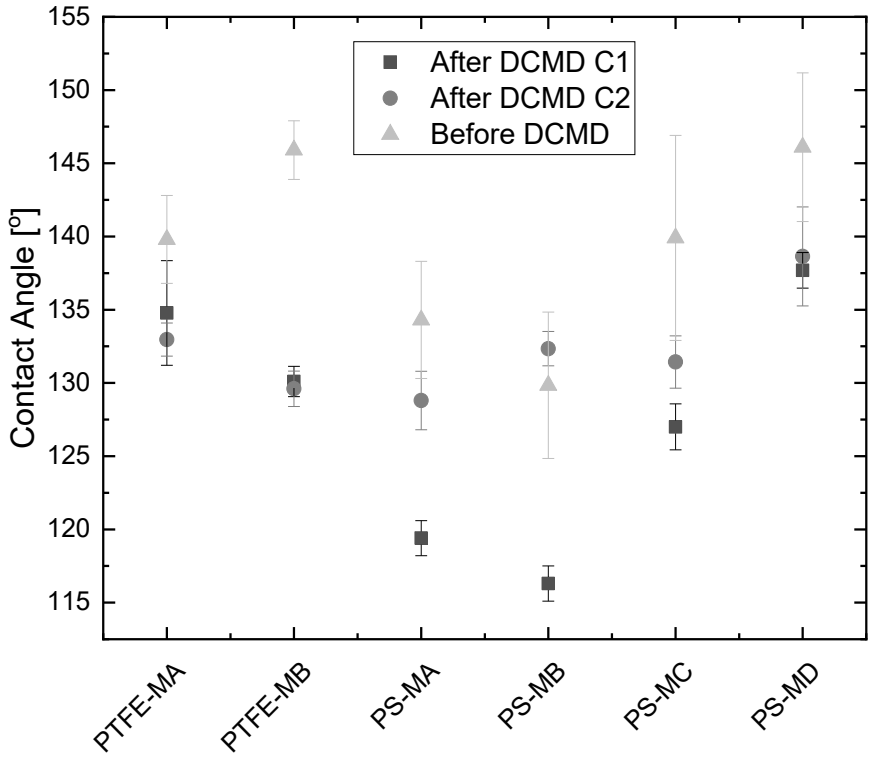

Figure 10. Contact Angles before and after DCMD

Unlike after membrane distillation, the high standard deviation in the contact angle measurements for the membranes before DCMD are due to the uneven surface structure of the electrospun membranes. However, after testing the membranes at both concentrations the surface became smoother due to direct exposure of hot and cold streams from both sides. The higher the feed concentration, the closer the contact angle measurements tend to be from the averaged point.

As shown in Figure 10, the lowest concentration, C2, has presented minimum percentage of decrease in contact angle as low as 1.9 for PS-MB. To be more precise, the

average reduction percentages for C1 and C2 are 8.49% and 5.54%, respectively. This shows the feed concentration effect in relation to water contact angle of electrospun polystyrene membranes.

4.1.2 Surface characterization

The changes in membrane morphology from before and after DCMD tests were made using SEM. Supplementary information was obtained from SEM micrographs at higher magnifications after a thin layer of gold was sprayed on the top of the membrane's surface prior to analysis. The accumulation of salt components on the membrane's surface called cake layers. This can be clearly seen in Figure 11. Both Polystyrene membranes A and B showed higher particle deposits coming from the synthetic thermal feed in compared to membranes C and D where there were less amounts. The depositions of such dense cake layers is greatly contributed to the ionic strength of the material. Particles accumulate mainly due to less repulsive forces. This was confirmed by the study of Vigneswaran and Kwon[147] where it was observed that the porosity of cake decreased with the increase in ionic strength. This is also related to both contact angle measurements and flux calculations. Thus, polystyrene membranes C and D exhibited higher contact angle and flux mainly due to the greater repulsive forces.

4.1.3 Permeate flux

Theoretically speaking, increasing the flowrate of the feed and permeate solutions would lead to a rise in the permeate flux. Due to the low mechanical integrity of the PS electrospun membranes, higher flowrates will raise the circulation velocity on both sides of the membrane and will therefore lead to pore wetting. Hence, the DCMD tests were performed at flowrates as low as 5 rpm. Permeate fluxes as low as 2.28 LMH occurred for

PS membranes of greater thickness of 190.82 μm. The lower the thickness the higher was the permeate flux. This confirms the inversely proportional relationship between the thickness of the membranes and the permeate flux. In fact, the larger the membrane thickness, the more prominent was the reduction in the permeate flux. A larger thickness is equivalent to a significant increase in the resisting mechanism of mass transfer resistance as well as a decline in heat loss.

Increasing the thickness of the membrane may be one way to help reduce heat loss in DCMD [148]. A previous study for Ali et al. [149] confirmed that membrane pore sizes exceeding 0.3 μm should not have a significant effect on the flux. Thus, larger pores do not greatly contribute to flux increase. Moreover, lower flux values were obtained using membranes of greater pore size (3.0 μm) in compared to membranes of other studies with smaller pores (0.22 μm). Permeate fluxes in DCMD for both fabricated and commercial membranes are listed in Figure 13. As the salt concentration in the thermal brine solution was reduced, from C1 to C2, the water vapor pressure became higher (greater driving force), and the thermal efficiency increased simultaneously [19]. Thereby, this lead to a definite increase in the permeate flux. Figure 12 clearly shows this occurrence along with the overall relation between the permeate flux and contact angle after the DCMD tests. Furthermore, Table 9 compares experimental flux data with that existing in literature.

4.1.4 Permeate conductivity

Due to the varying sizes, mass, and interaction between the different salt ions listed in Table 6, it would be challenging to measure the exact conductivity contribution of each individual ion in water. However, the overall conductivity of the permeate after DCMD can still be estimated using a conductivity meter. This meter helps estimate the amount of

charged particles for all different types of remaining salts in the distilled water after the experiment. Here, the lowest permeate conductivities were obtained for PS-MD: 1.2 µS/cm and 1.0 µS/cm for varying feed concentrations with conductivities of 100 mS/cm and 50 mS/cm, respectively. This confirms an enhanced water quality of 99% as listed in Figures 14 and 15 .

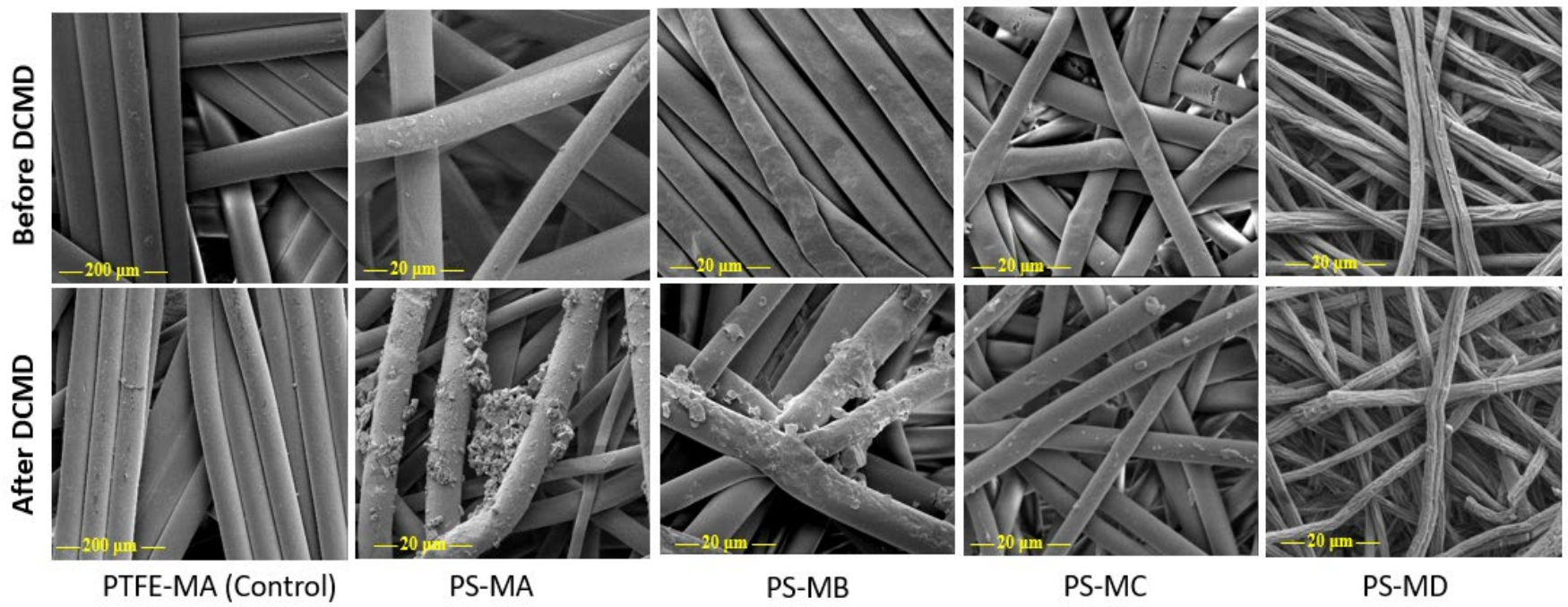

Figure 11. SEM Micrographs for PS membranes before and after DCMD.

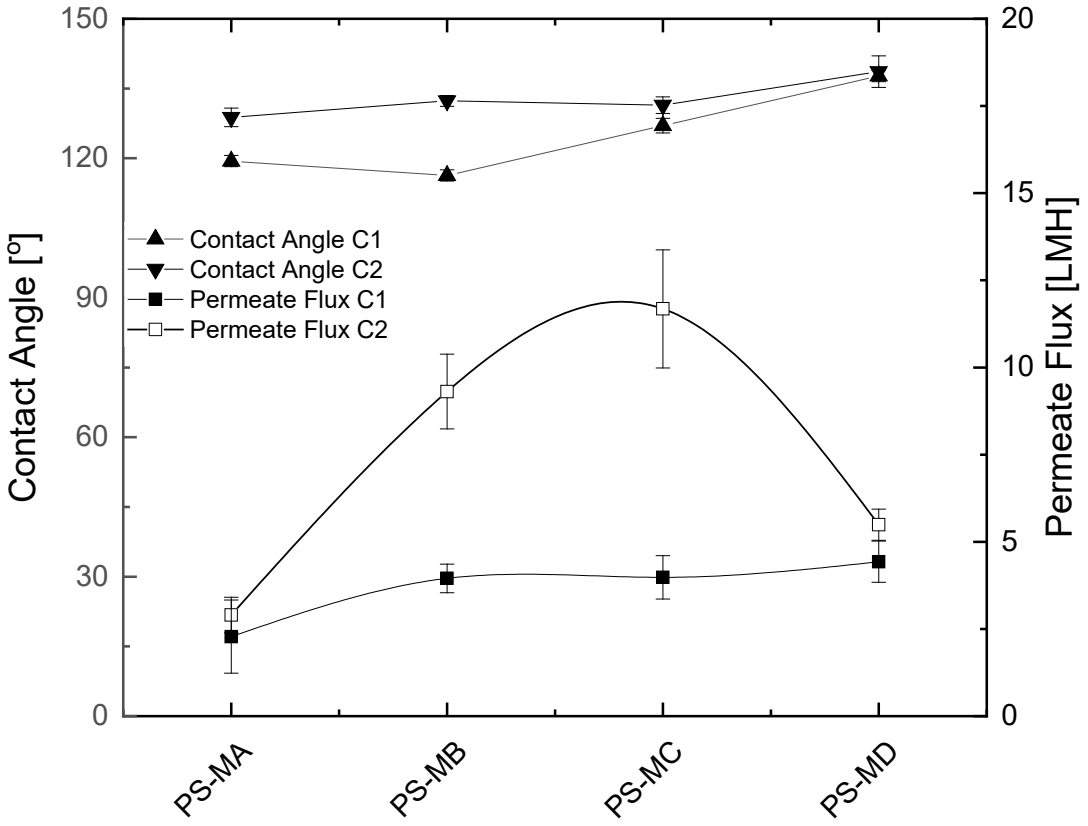

Figure 12. The relation between Permeate Flux and Contact Angle values after DCMD.

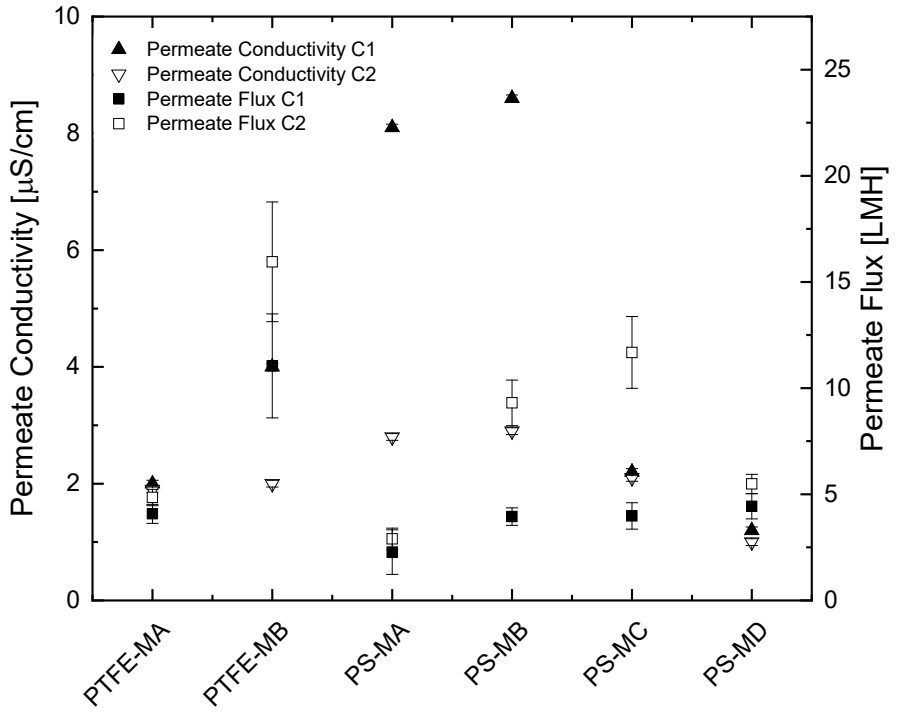

Figure 13. Permeate Conductivity and Permeate flux for each membrane after DCMD.

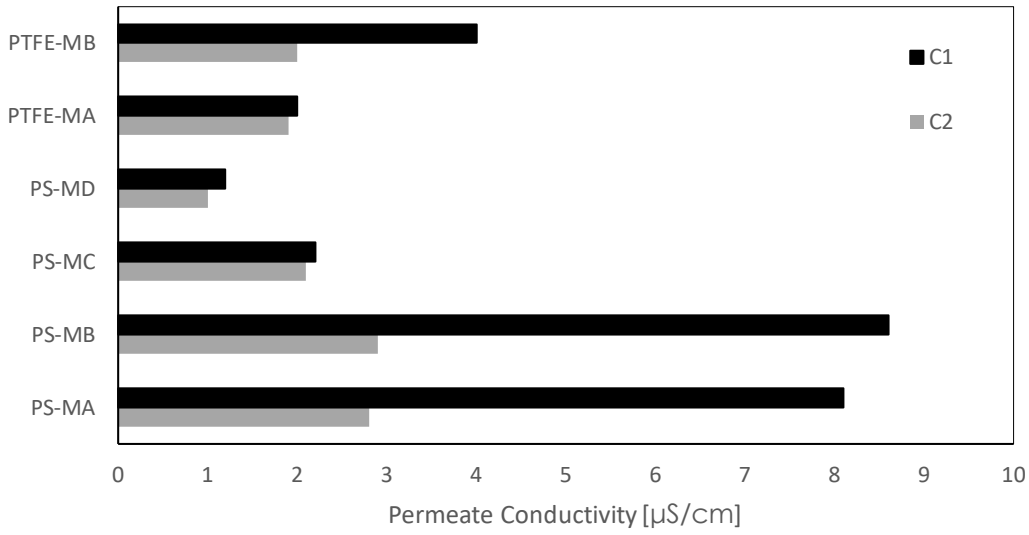

Figure 14. Permeate conductivity of membranes after DCMD.

Previous studies reported that at low inlet feed temperatures, the electrospun PS membranes displayed trivial change in the permeate conductivity. This is because the temperature difference in the middle of the hot and cold spots of the thermal and permeate regions in the MD process is not large enough to cause any vapor to move within the pores of the membrane to the colder side of the MD cell. Not only would higher inlet temperatures lead to significant increase in the permeates conductivity, but it also results in enhanced water quality [150].

4.1.5 Salt rejection

Another way of measuring the performance of the DCMD system as whole is through evaluating its salt rejection. Higher salt rejections indicate the removal of salt contaminants in greater quantities. Hence, this guarantees that the used membrane distillation system is functioning effectively. In this study, the calculated salt rejection values reached as high as 98% and 99% for high and low feed concentrations, respectively.

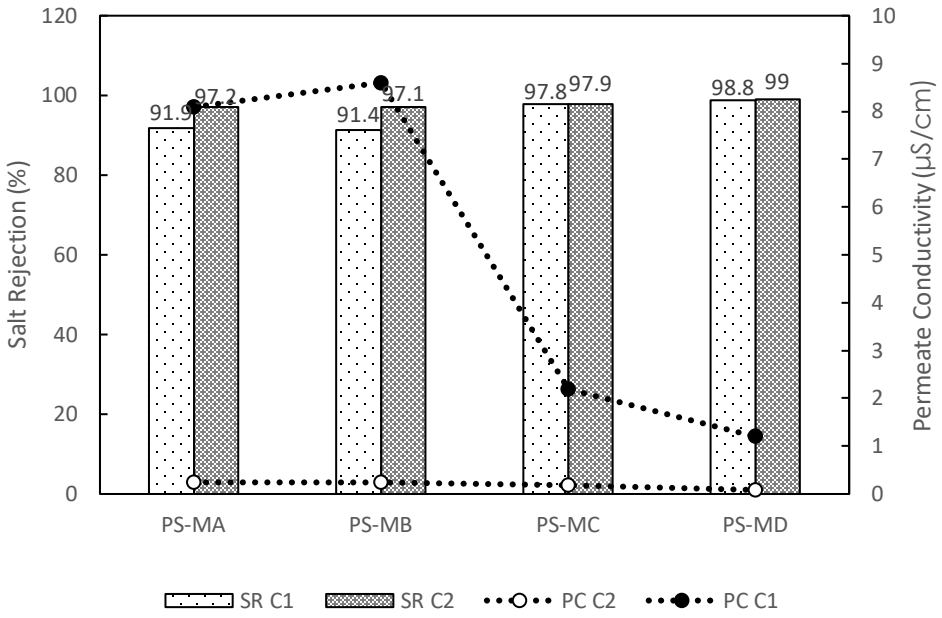

Figure 15. Trend showing relation between the conductivity and rejection rate after DCMD

Table 9: Optimum salt rejection and permeate fluxes from recent studies in DCMD configuration only

Membrane type	Membrane fabrication	Membrane thickness [µm]	Mean pore size [µm]	Feed type	Feed conc. [ppm]	Feed flowrate [L/min]	Feed inlet temperature [°C]	Distillate inlet temperature [°C]	Salt Rejection [%]	Permeate Flux [LMH]	Ref.
PTFE	Commercial	175	0.22	Synthetic brine	70,000	1.5	60	20	-	23.1	[146]
		175	0.22		58,000	1.5	70	30	99.9	-	[151]
		72.94	1.0		75,500	0.03	60	20	98.0	4.08	This work
		102.62	3.0			0.03	60	20	96.0	11.05	
		72.94	1.0		25,200	0.03	60	20	98.1	4.85	
		102.62	3.0			0.03	60	20	98.0	15.95	
		175	0.22	Sea water	41,600	1.5	70	30	99.9	-	[151]
PVDF	Commercial	110	0.22	3.5% NaCl	-	0.07	60	20	99.98	22	[136]
	Electrospinning	42	0.21	3.5% NaCl	-	0.07	50	20	-	20.6	[46]
		110	0.26	1% NaCl	-	0.32	50	24	98	20-22	[67]
		27-58	-	10% NaCl	-	0.31	65	20	-	10-30	[152]
PS	Electrospinning	147	0.44	Sea water	-	0.2	70	17	-	24.9	[24]
		-	-	20% NaCl	-	0.6	60	20	99.99	60.1	[153]
		136.97	5.2	Synthetic brine	25,200	0.03	60	20	98.8	11.68	This work

4.2 Pilot-scale investigation and membrane fouling effect on DCMD performance using synthetic brine

This section explores the operation of an innovative direct contact membrane distillation pilot unit, which can be scaled up for industrial applications. The investigation of long-term MD processes at large-scale is crucial to assess the energy performance of the whole system. This is because, in actual desalination plants, MD systems are operated continuously for extended periods, during which various factors can impact their energy efficiency. For instance, membrane fouling can occur over time, reducing the performance of the system and increasing energy consumption. Similarly, changes in the feedwater quality or operating conditions can also affect the system's energy performance. Conventional bench-scale DCMD modules are insufficient for this purpose. For this reason, the research findings from this work may pave the way for implementing this cost-effective membrane technology for the desalination of real wastewater in industrial desalination plants and improve their overall energy efficiency. Polyethylene membranes have been used for all the tests at optimum process conditions, with emphasis on the effect of varying brine concentrations on its energetic performance, and with a closer outlook on the effect of membrane fouling over long periods of time. This study will be used as a benchmark for the next section of this thesis.

4.2.1 Effect of long-term Pilot-scale test on membrane surface analysis

All membranes were dried immediately after removal from the DCMD pilot unit. Although pore wetting did not partially occur, the organic foulant has passed through the hydrophobic membrane leading to the proposal of an adsorption–desorption foulant migration mechanism. Despite the high hydrophobicity of polyethylene, there was a

significant rise in the deposition of salt particles on the membrane's feed side due to the immediate contact between the brine and membrane surface at harsh fouling operating parameters. SEM images for the membrane's feed side were taken every 20 h during the entire duration of the experiment (Figure 16).

It was confirmed that the amount of foulants penetrating through the membrane is largely dependent upon the adsorption strength of the membrane material. As a result, it hinders the membrane's functionality in terms of the formation of cake layers and clogging of pores [154][155]. This can be clearly seen in the zoomed-in SEM images in Figure 17, where larger cake layers were formed due to the use of highly concentrated feed (C1) in comparison to less concentrated feed (C2). The formation of cakey layers and foulant depositions (also known as membrane scaling) can be avoided by physically eliminating the crystals deposited on the surface of the membrane, which often leads to the blockage of pores [111]. Recent MD studies have demonstrated that Humic acid (HA) aggregates play a major role in the fouling process [156–160]. Hence, it was important to study the HA fouling effect on PE in our pilot DCMD system using synthesized thermal brine that mimics industrial wastewater in the GCC region.

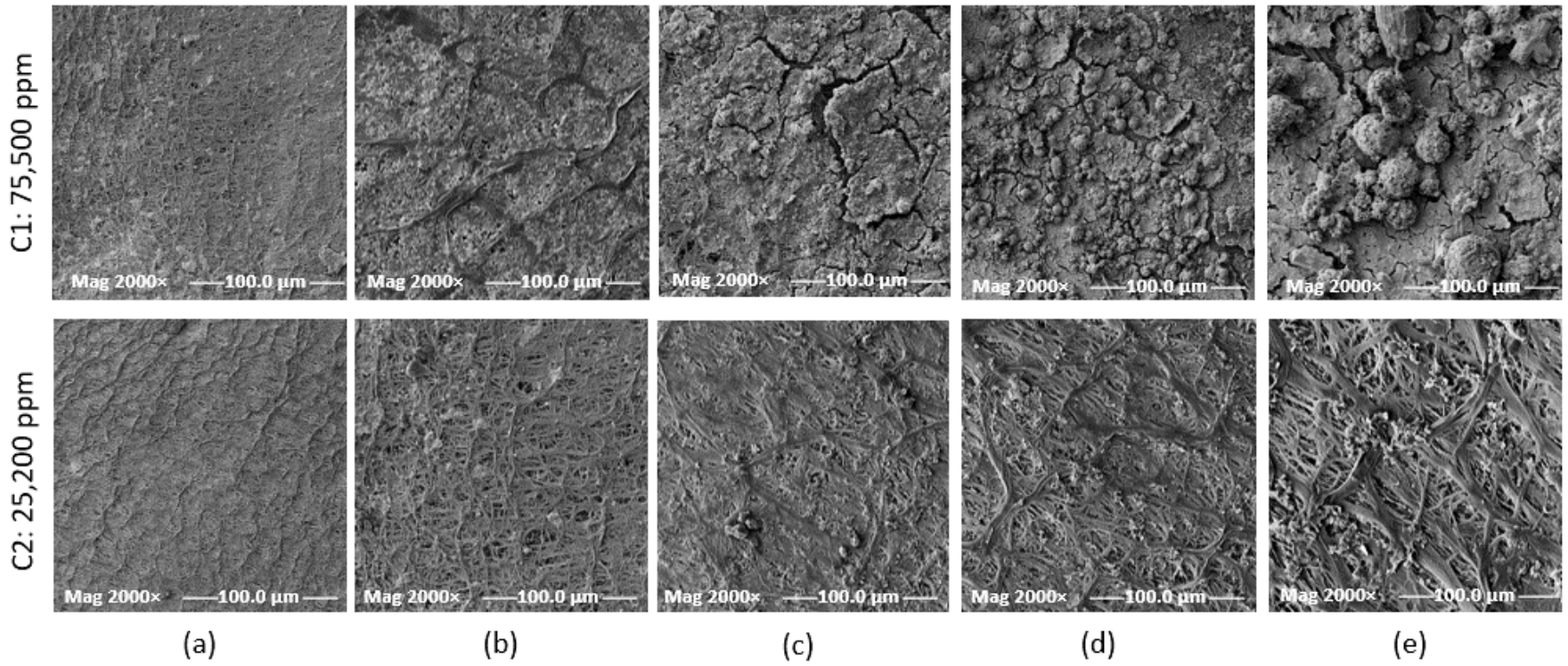

Figure 16. SEM images for PE membranes after (**a**) 20, (**b**) 40, (**c**) 60, (**d**) 80, and (**e**) 100 hours of pilot-scale DCMD tests using different feed concentrations.

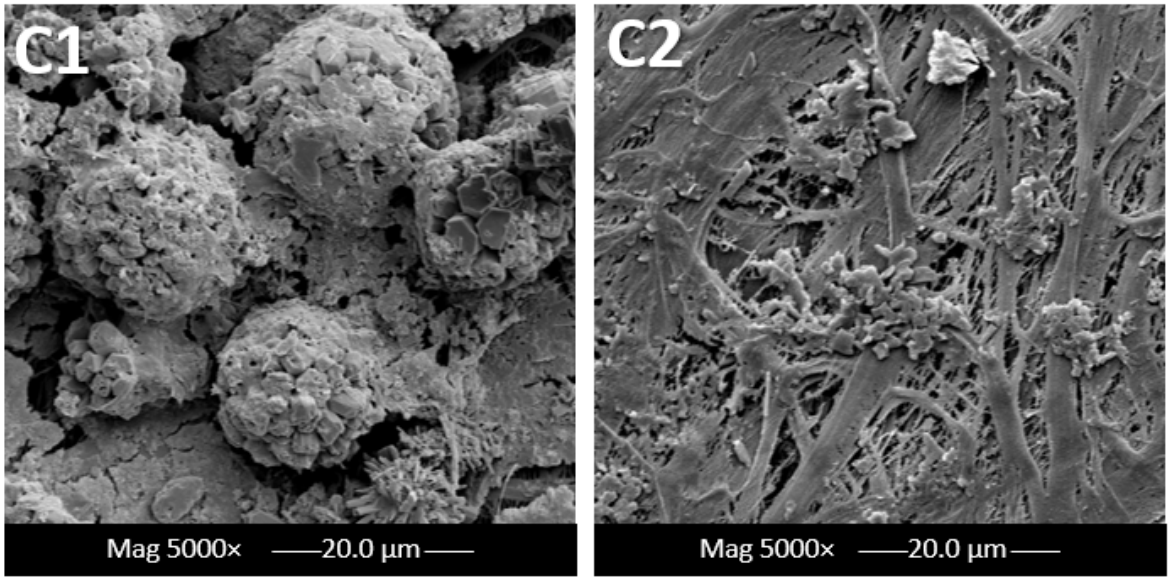

Figure 17. Magnified SEM images for PE membranes after 100 h at different concentrations immediately after pilot-scale MD tests.

According to Nthunya et al. [161], high porosity of superhydrophobic membranes were evident from the SEM micrographs where highly distributed voids were detected. High porosity in membranes is due to the slow demixing rate during phase separation. Membranes with high porosity tend to reduce their mechanical strength, which could potentially impact their overall performance. The presence of a hydrophilic coating layer on the membrane can help decrease the pore wetting and colloidal fouling.

To further confirm the surface morphology with respect to increasing the duration of the pilot process, AFM inspection was conducted for the feed side of the membranes that were continuously exposed to the concentrated brine. The surface topography of the commercial polyethylene membranes was denoted in Figure 18, Figure 19, Figure 20, at scan rates of 1.0 Hz and scan sizes of 20 µm and 5 µm, respectively. The root-mean-square

(RMS) roughness parameter was used as an indication of the material's surface roughness [162].

The measured RMS values for all membranes prior to DCMD was 81.39 nm (Figure 18). The surface roughness increased after 40 h of continuous testing, reaching a value of 213.1 nm (Figure 19). A further increase in the RMS value was noted after 100 h of testing with a maximum roughness value of 357.1 nm (Figure 20). The incremental increase is attributed to the accumulation of salt molecules and thereby the fouling of the membrane surface. Similar data trends were observed in previous studies [142,163].

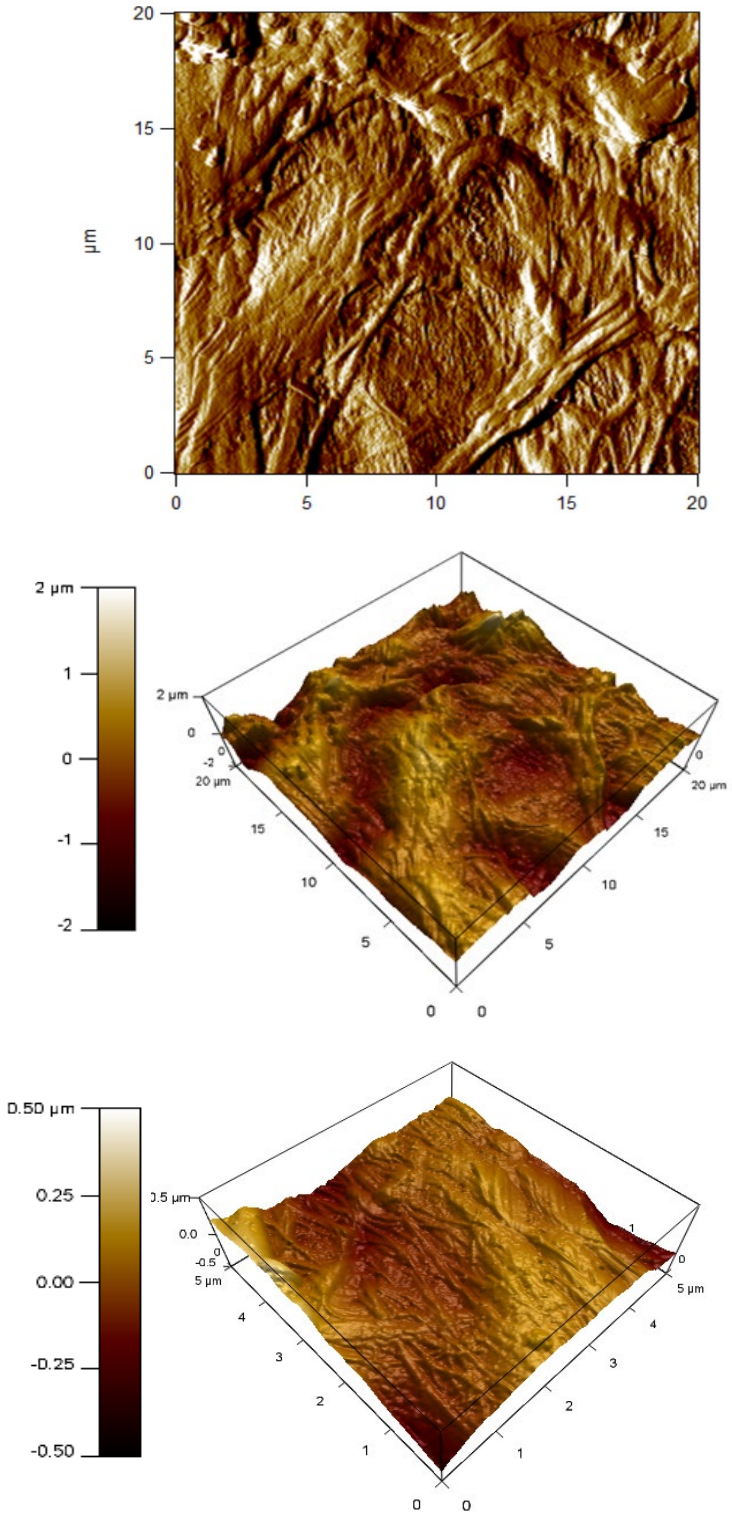

Figure 18. AFM images for PE membranes before pilot-scale DCMD tests.

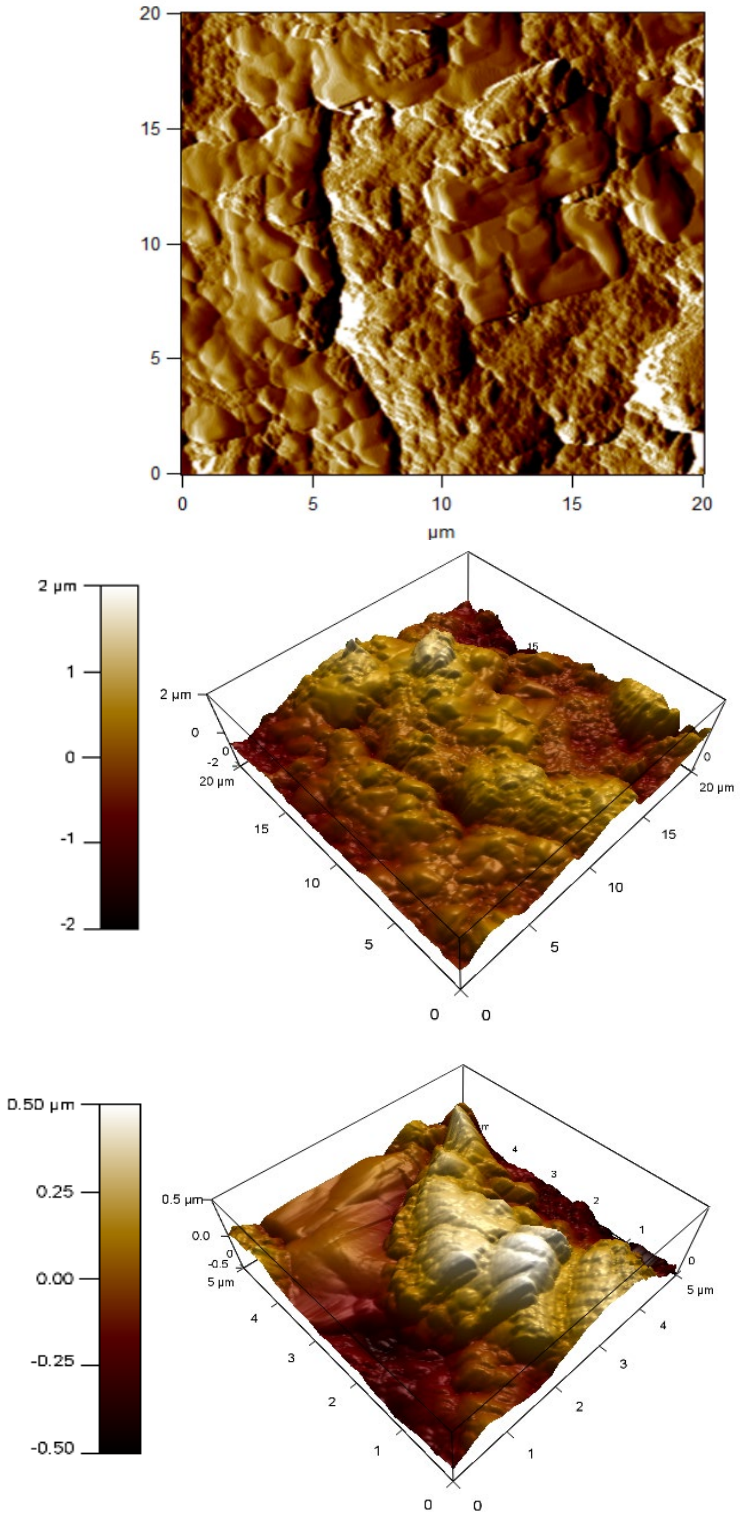

Figure 19. AFM images for PE membranes after 40 hours of pilot-scale DCMD tests.

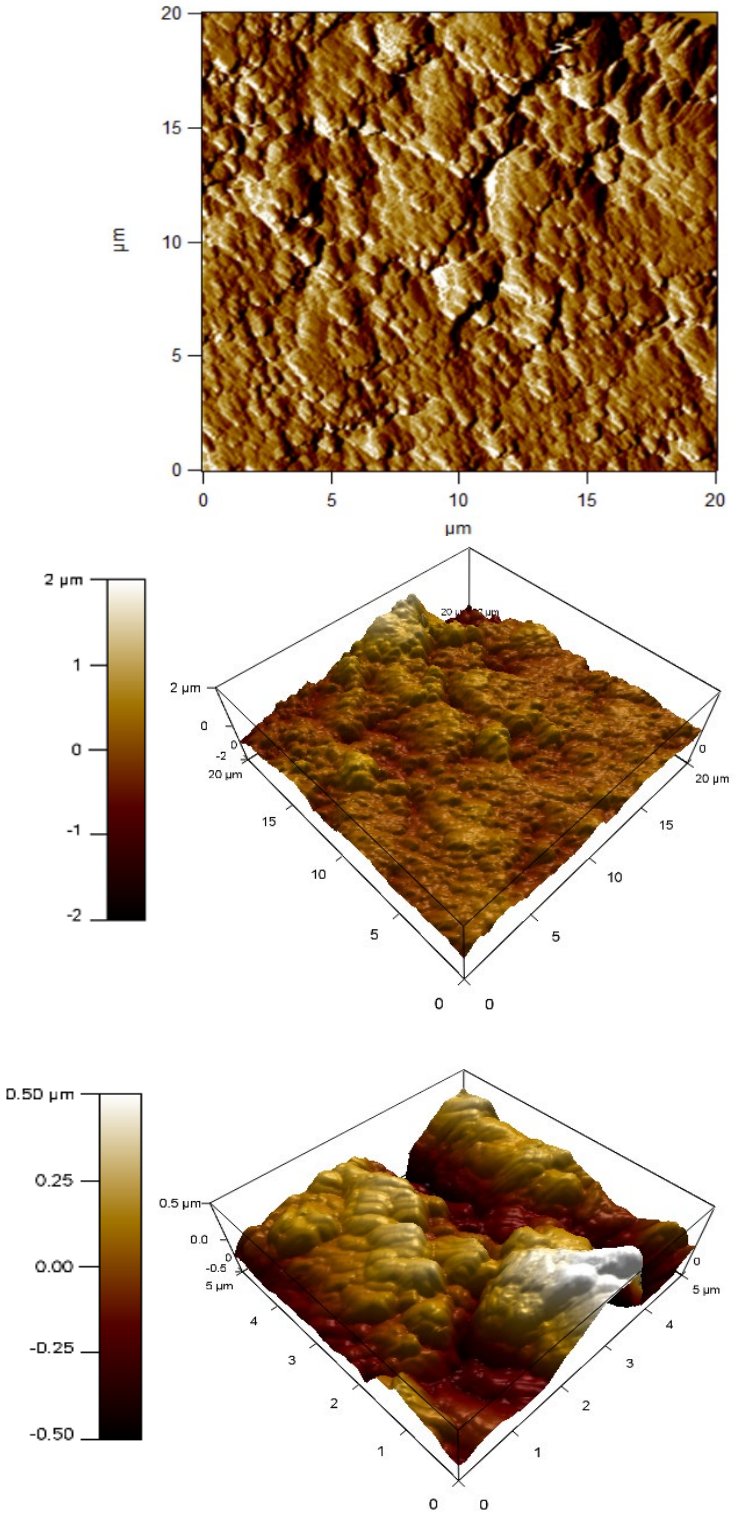

Figure 20. AFM images for PE membranes after 100 hours of pilot-scale DCMD tests.

4.2.2 Effect of long-term Pilot-scale test on membrane wettability

During an MD operation, pore wetting is one significant issue that causes failure of the whole operation. During the desalination of synthetic brine, the hydrophobic tails of the existing amphiphilic molecules become interconnected with the hydrophobic membrane pore surface. This leaves the hydrophilic head exposed and thereby renders the hydrophilicity of the membrane pores. Hence, this instantly impacts the membrane wetting properties revealed in Figure 21a.

At higher feed concentration, a much higher reduction was shown throughout the whole duration of MD pilot testing. A 4.3% loss in hydrophobicity was noted after the first 20 h, followed by a total of 94% reduction after the 100 h of testing was completed. In contrast, at a lower concentration, a lower drop of 2.6% was observed after the first 20 h, followed by a 37% decrease in the contact angle measurements. This huge reduction in the membrane's wetting behaviour for C1 compared with C2 emphasizes that, due to long periods of immediate exposure to highly concentrated feed, its pores have already become saturated with chemical compounds and salts, causing an increase in adhesive forces between the water molecules and the polyethylene molecules on the membrane surface.

These adhesive forces become greater than the cohesive forces within the water molecules. The existence of surfactants and organic compounds in the brine is a major contributor to pore wetting of the membranes was studied thoroughly in previous studies [164]. This significant absorption of brine into the membrane pores has thereby undermined the salt rejection rates denoted over a long period of time, as seen in Figure 21b.

Similar to wettability analysis, the drop percentage in salt rejection rates showed a linearly proportional relation with feed concentration. The evaluation of salt rejection rates in membrane distillation studies is actually complicated and requires a systematic approach due to many determining factors. This includes the feed solution, membrane properties, and operating process conditions [165]. In this work, the only changing variable was the feed solution, while other factors remained fixed. The interplay between various factors that affect salt rejection in membrane distillation is dependent on whether the feed solution involves inorganic salts and organics.

The presence of high amounts of salts and chemicals in the higher feed solution resulted in a higher potential for membrane scaling. Hence, a denser fouling layer at the membrane surface was produced, which therefore lowered the liquid surface tension and reduced the salt rejection compared to the moderate saline feed. The reduction in salt rejection rates for higher concentration feed was 21% in comparison with the lower ones of 2.3% during the entire MD operation process. This was visually reflected in Figure 22, showing the buildup of dense cake as confirmed by Vigneswaran and Kwon [147].

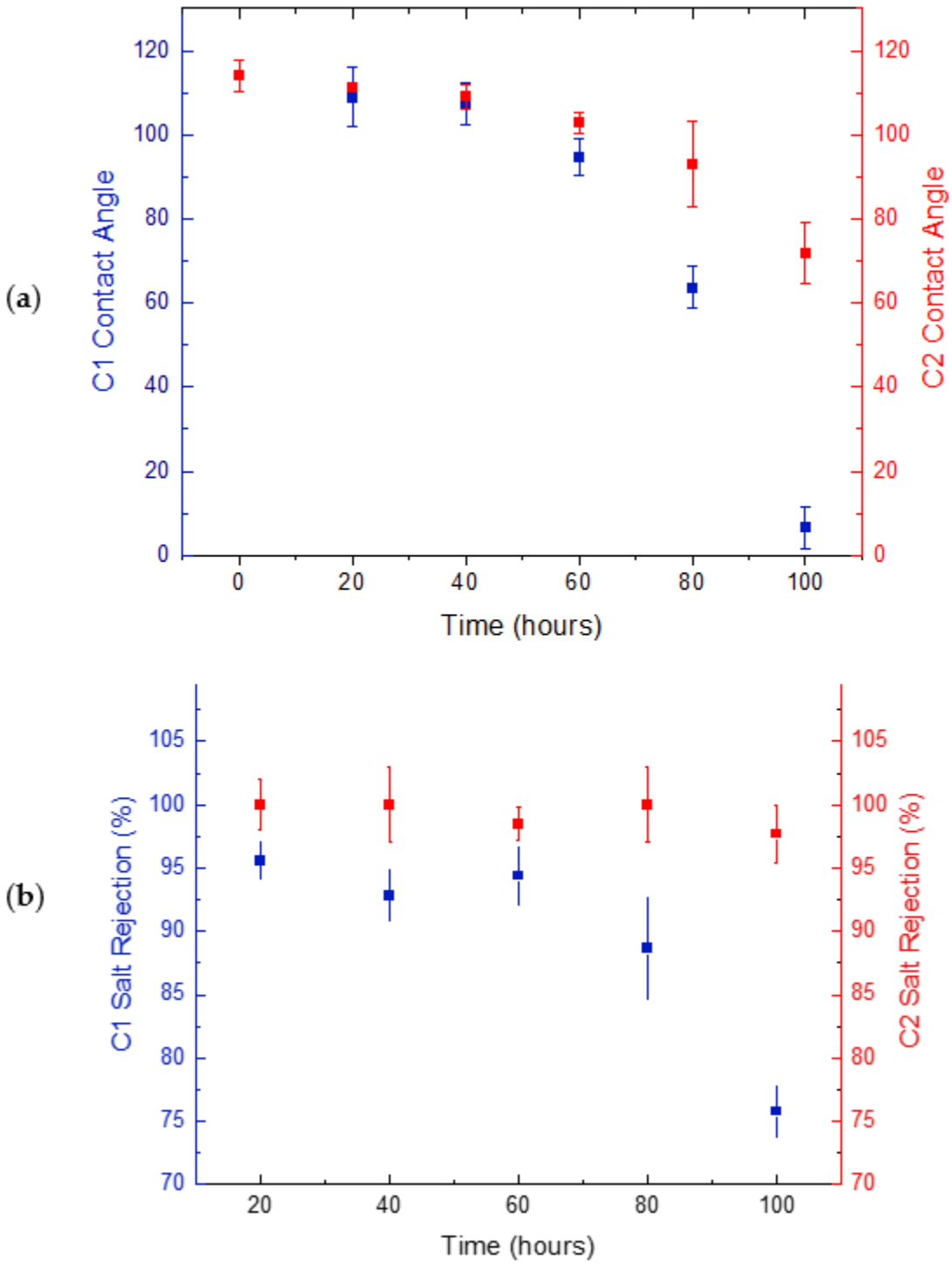

Figure 21. Contact angles (**a**) and salt rejections (**b**) of tested PE membranes during longtime DCMD operation at pilot scale.

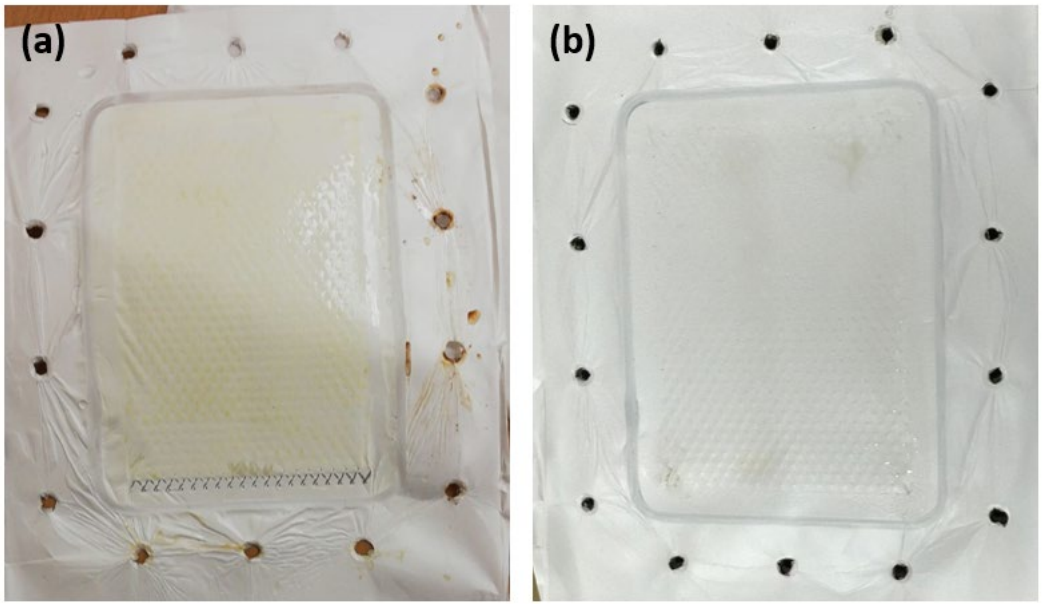

Figure 22. Images of PE membranes after 100 h of DCMD tests at concentrations of C1 and C2, (**a**) 75,500 and (**b**) 25,200 ppm, respectively.

4.2.3 Effect of long-term Pilot-scale test on permeate flux

In all MD operations, successful membranes are the ones that show enhanced performance over a long period of time with high stability. In this work, the commercial PE membranes were tested at equal permeate and feed flow rates of 70 LPH with effective areas of 0.01 m^2 and were noticeably affected by the 100-h experiment. The effect of varying concentrations on the water flux can be clearly seen in Figure 23, where both types of concentrated brines have eventually yielded a significant decline. The higher brine concentration of 75,500 ppm showed a rapid 20% flux reduction compared to the 25,200 ppm brine with only 3% reduction after the first 20 h. Similarly, after 100 h of intensive pilot-scale MD operation, the flux decline was nearly 90% and 80% for the highest and lowest feed concentrations, respectively. The decline in flux for C2 after 80 h of continuous

MD operation indicates that, at given operating parameters, the membrane was no longer able to maintain its hydrophobicity with time. This caused a collapse of membrane pores leading to pore blockage. This comes into agreement with previous studies where the flux reduction was majorly due to intensified velocity on both sides of the membrane that consequently led to pore wetting [25].

Moreover, a decline in permeate flux may also be attributed to membrane fouling over long durations of MD tests [18]. Furthermore, the reduction in water vapor pressure caused by continuous exposure to highly concentrated feed led to the decline in the permeate flux.

Zuo et al. [166] tested the durability of PE membranes at long-term operating conditions using a 3.5 wt% NaCl feed solution at constant operating process parameters. A high flux (123.0 $L/m^2 \cdot h$) was achieved at a high membrane thickness of 50 μm. McGaughey et al. [167] used commercial PTFE membranes using a bench-scale DCMD system designed for continuous long-term operation and showed that maintaining distillate-side hydrophobicity and/or internal hydrophobicity may be more important for long-term performance in an MD system. Another study by Mansour and Hasan [168] utilized real rejected brine using a pilot-scale DCMD unit. Each experiment lasted for 4 h. There was a 69% decline in the flux due to fouling formation with an optimum permeate flux and salt rejection of 16.7 LMH and 99.5%, respectively.

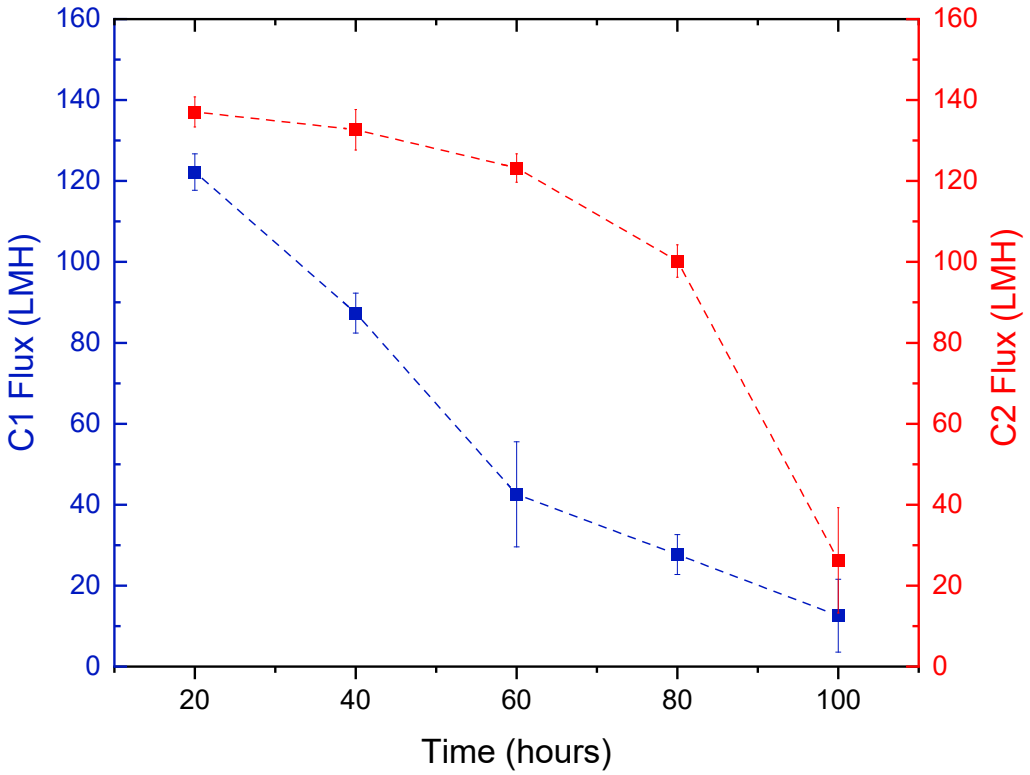

Figure 23. The effect of brine concentration on the permeate flux at longtime DCMD operations.

4.2.4 Effect of long-term Pilot-scale test on fouling behaviour

When a solution containing foulants is used as feed, a fouling layer is formed on the membrane surface by foulants deposition [169]. Crystals formed following MD applications lead to clogging of membrane pores and continue to grow within the pores, which allows penetration of foulants from the feed through the membrane leading to membrane wetting. Actually, the adsorption of foulants onto the surface or inside the pores of the membrane causes a rapid decline in the membrane flux, hindering the overall MD performance resulting in direct contamination of the permeate [14,40,47].

As depicted in Figure 24, at concentrations exceeding 25 ppm, the measured concentration reached 0.013 ppm with minimal change even at increasing foulant concentration up to 45 ppm. This indicates that a small change in the foulant's concentration will result in a significant change in fouling behaviour on the membrane's surface during the microfiltration process. In this work, the rejection rates of the HA foulant exceeded 98.5%. Similarly, Khayet et al. reported at least 96% of Humic Acid rejection using commercial PVDF membranes [170]. Previous studies have also reported similar findings [154]. As seen in Figure 25, the fouling flux became much less than that of pure water flux. Such fouling behavior is largely dependent upon the consecutive absorption and deposition of HA particles onto the membrane surface [171].

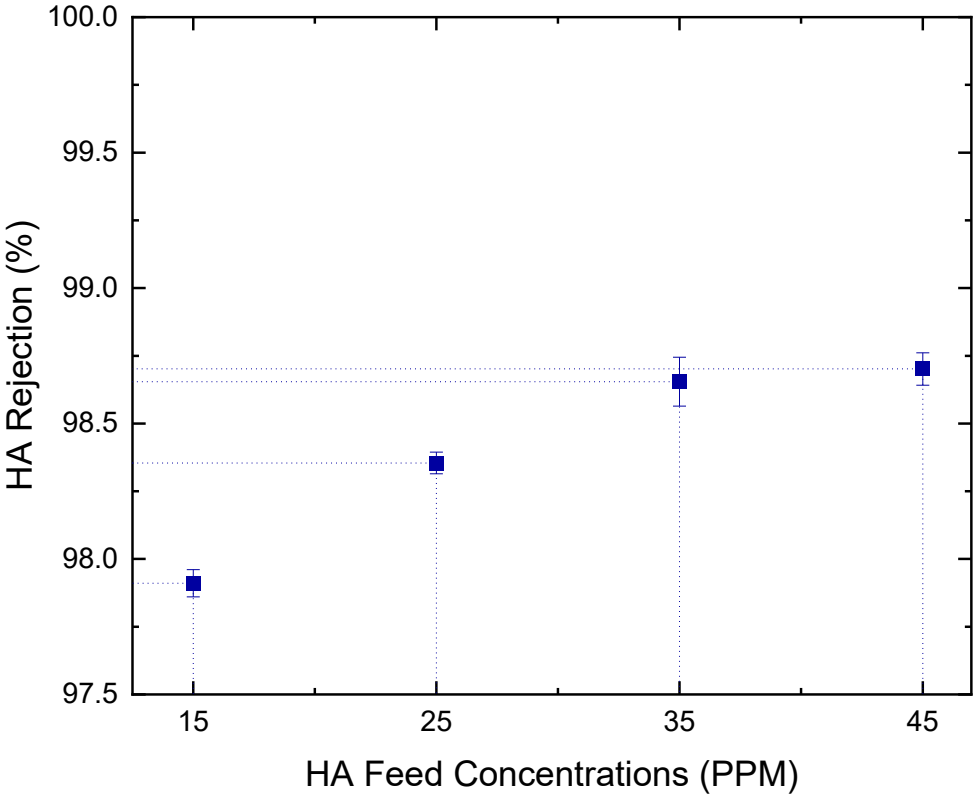

Figure 24. Humic Acid rejection rates at different foulant feed concentrations

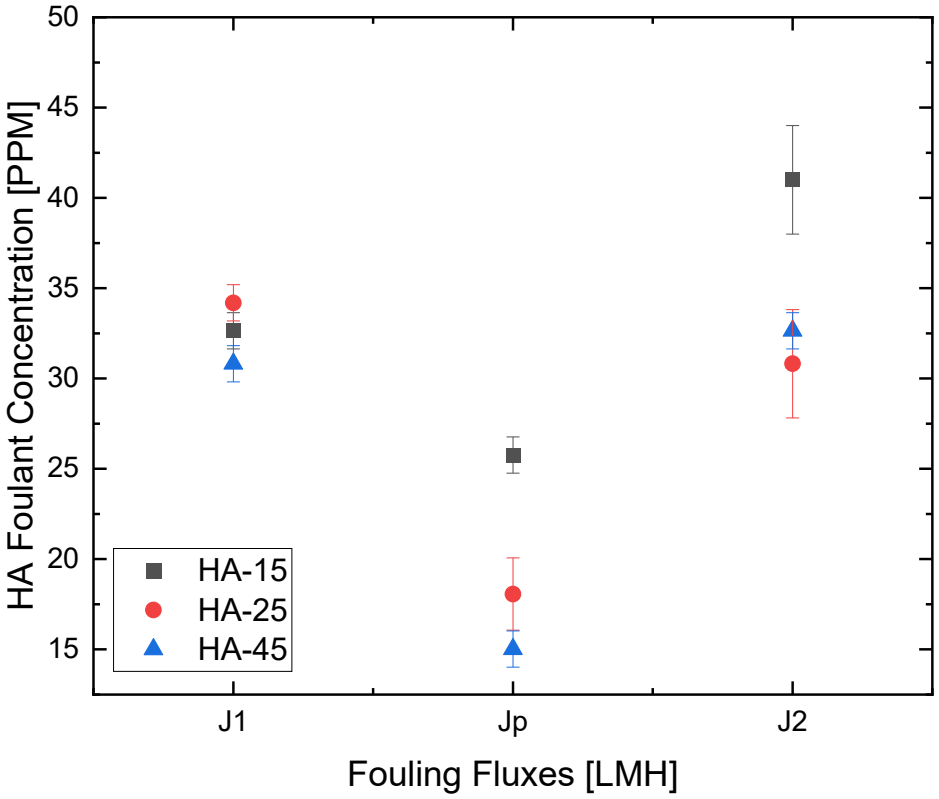

Figure 25. Calculated fouling fluxes at optimum HA foulant concentrations.

At increasing foulant concentrations, the foulant flux significantly declined by 21%, 47%, and 51%, respectively (Figure 25b). As confirmed by Cho et al., It was demonstrated that Humic Acid enhanced $CaCO_3$ deposition on the membrane surfaces, thereby expediting the scaling phenomenon [172]. Similarly, previous studies have shown that HA fouling of membranes causes a rapid and irreversible loss of flux through the membrane, which limits the successful application in water or wastewater treatment technologies [173][174]. However, interestingly in this study, the irreversible fouling ratio was only 4.5% for the 45 ppm compared to 14% for the 15 ppm of HA feed.

This implies that in our pilot MD system, hydraulic cleaning is not much needed for the elimination of HA adsorbed on the membrane. This also comes into agreement with the high flux recovery and reversible fouling ratios reaching up to 95% and 52%, respectively, at higher HA concentrations (Figure 26). This indicates that only water flushing would be sufficient for foulant removal in our MD pilot unit, as visually proven in Figure 27a–c. In fact, the increased R_r of membranes at increasing HA concentrations created a reversible adhesion between the polyethylene membrane surface and the HA molecules [173].

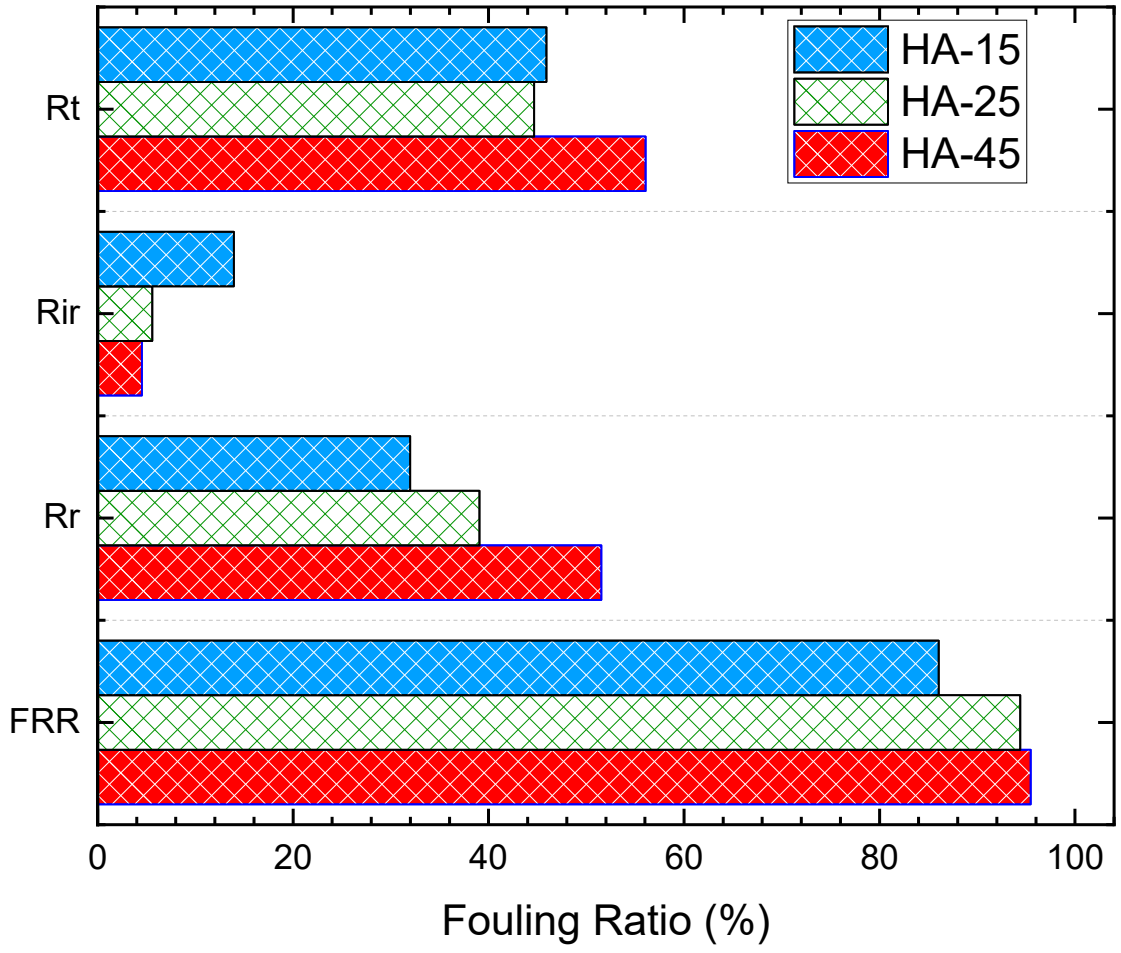

Figure 26. Calculated fouling ratios at increasing HA concentrations of 15, 25, and 45 ppm.

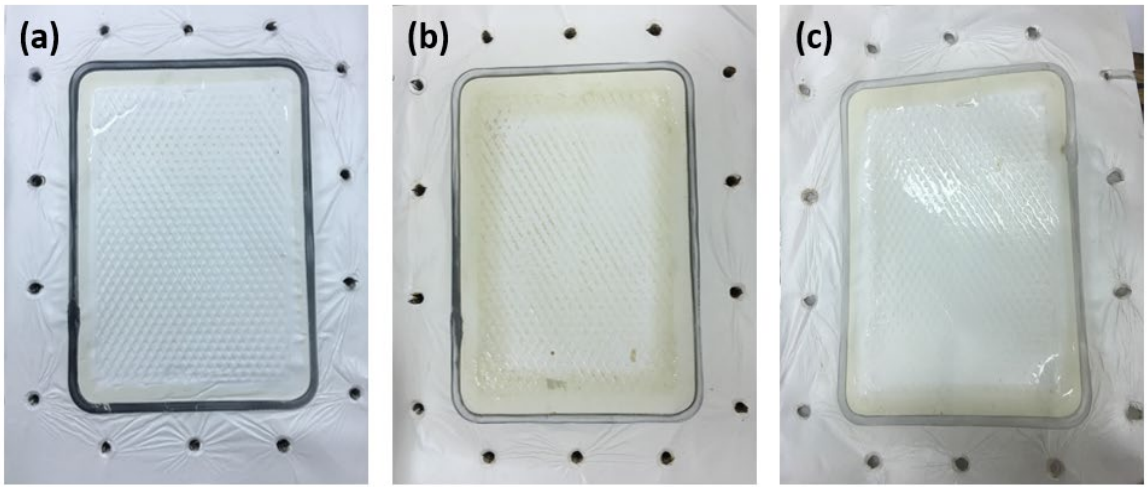

Figure 27. Visual effect of HA foulant on the membrane surface; (**a**) after the first wash with DI feed, (**b**) application of HA feed, (**c**) washing the foulant off the membrane using DI feed.

Srisurichan et al.[175] studied the fouling mechanism of hydrophobic PVDF membranes and used the cake filtration model to describe the HA aggregates on the membranes. The rise in total resistance was attributed to the existence of fouling layer resistance which significantly increased over time. Hence, a critical parameter to consider in terms of examining the anti-fouling performance against the membrane surface would be the adhesion forces at the interfaces [176][177]. As confirmed previously, with increasing feed concentrations, the electrostatic repulsive forces of HA with both HA and PE membranes promote the accumulation of the HA molecules resulting in a denser HA fouling layer on the membrane.

4.3 Optimization approach using mathematical modelling to investigate the effect of porosity on mass and heat transfer properties

This section aims to investigate the impact of porosity on combined heat and mass transfer properties in direct contact membrane distillation to improve the overall energy performance of the system using polystyrene membranes. To date, present literature has not yet explored the desalination potential of electropsun polystyrene membranes in DCMD at pilot scale. In addition, this work introduces machine learning (ML) and artificial intelligence (AI) to optimize the membrane surface temperature and provide insights into how the porous structure of polystyrene membranes affects the efficiency of the entire DCMD system. The study offers computational predictions to achieve maximum thermal and evaporation efficiency at the membrane surface temperature in the feed and temperature boundary regions. The accuracy of the theoretical model was enhanced through the utilization of optimization methods using Python. The data was simulated using python to find the membrane surface temperatures using the concept of iteration. Since most simulation models are performed on the basis of experimental work [12,13], in the DCMD pilot unit, experimental feed/permeate flow 40 LPH was used in the predictions to evaluate the optimum permeate flux at fixed inlet feed and permeate temperatures of 70 ºC and 20 ºC, respectively.

4.3.1 Theoretical vs predicted flux

From Table 10, an increase in Teflon percentage from 0.1% to 0.5% lead to slight reduction in experimental permeate flux by 1.8%. This decrease in permeate flux is attributed to the increase in membrane thickness from 190 µm to 199 µm. Furthermore, at a fixed porosity of 94%, the flux was enhanced by 2.7% and 0.44% with an addition of 1% for polystyrene membranes with 157 µm and 131 µm thicknesses, respectively. It can be

observed that the optimum flux has been achieved for the membrane at 14.05 LMH. This value is relatively higher than other membranes in DCMD as mentioned in literature and listed in Table 11. This is attributed to the presence of PTFE beads that acted as a template for the formation pores in the membrane, leading to an increase in its porosity. A membrane with a high porosity will have a larger surface area available for heat transfer, which thereby improves the efficiency of the process.

Table 10. Experimental, theoretical, and predicted permeate flux of polystyrene membranes at controlled paramters of T_{bf}=60 ºC and T_{bp}= 20 ºC.

Porosity	Thickness (µm)	J_{exp} (LMH)	$J_{theoretical}$ (LMH)	Error (%)	$J_{predicted}$ (LMH)	Error (%)
0.77	190	13.68	12.9032	6	15.24	11
0.89	199	13.43	11.5563	14	15.15	13
0.94	157	14.05	12.1535	13	15.26	9
0.94	131	13.74	13.1158	5	14.84	8

At the same time, a membrane with a high porosity may also be less durable and be highly wettable. Therefore, it is very important to optimize the porosity of the membrane in order to achieve improved desalination performance. Similar to previous studies, an optimized numerical model was used to evaluate the the experimental values of the membrane/liquid interface temperatures, the thermal effeieicncy of the system as well as the evaporation efficiency [178][116]. The predicted flux resulted in a similar trend as the experimental values. Nontheless, the theoretical flux showed a comparatively high error of 13% with that of experimental. This is because the applied theoretical model investigated a wider range of applicaibilities leading to a higher propbalibity of error in the obtained

flux, as presented in Figure 28. For this reason, optimization was perfomed using python in order to account for the variation of the surface membrane temperatures at both feed and permeate sides to accurately predict the flux.

From the depicted results in Figure 29, it can be noticed that there is a linear relationship between the permeate flux and the bulk feed temperature, and that can be seen by looking at the 89% porosity, as the bulk feed temperature increases from 60 ^{o}C to 70 ^{o}C and from 70 ^{o}C to 80 ^{o}C, the permeate flux increases from almost (11.9 to 14) LMH and from (14 to 16.2) LMH, respectively. Also, results show that there is no direct relationship between the increase of flux and the increase of membrane porosity, as for example the lowest porosity does not correspond with the lowest permeate flux, which means that the increase of flux is not proportional with the increase of the porosity. The same conclusion can be applied to the relation between the permeate flux and membrane thickness. It is worth mentioning that the lowest experimental flux was noticed at the largest thickness which is 199 μm at a porosity of 89%. However, the optimum flux was achieved at the highest porosity with slightly higher thickness which is 157 μm.

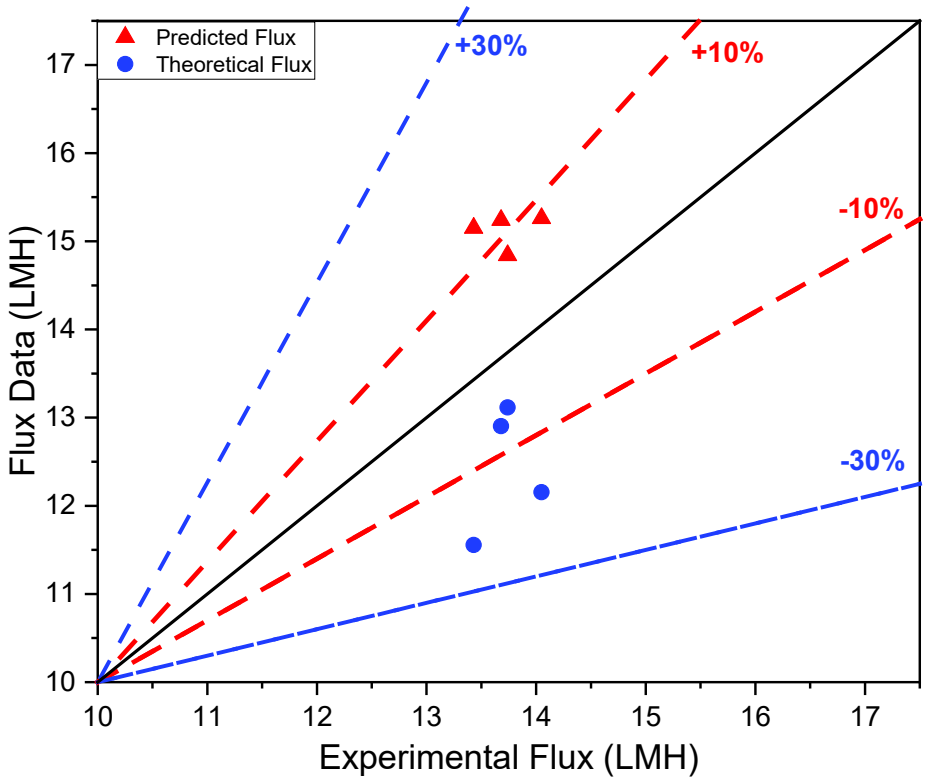

Figure 28. Experimental and numerical validation of the permeate flux for electropsun polystyrene membranes in DCMD.

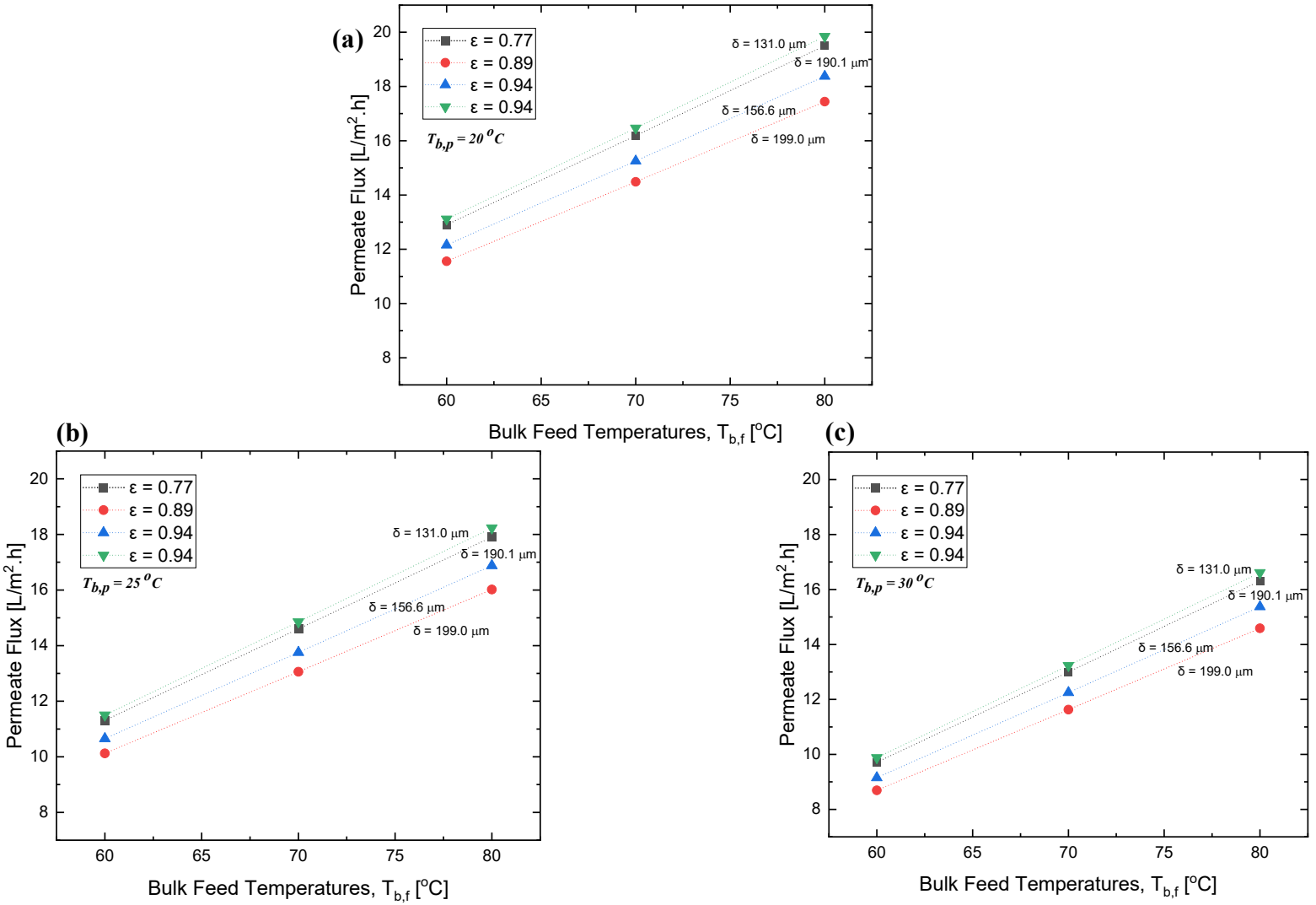

Figure 29. Relation of changing bulk feed temperature on membrane porosity and membrane thickness at $T_{b,p}$ of (a) 20 °C, (b) 25 °C, and (c) 30 °C.

Table 11. Comparison between the predicted flux in this work with various experimental performance for different membranes existing in the literature.

Membrane	**Feed Temperature** (℃)	**Feed Concentration** (g/L)	**Feed Flow Rate** (L/min)	**Experimental Flux** (**LMH**)	**Ref.**
PVDF	50	35	0.6	21	[141]
	80	0.45	6	51.5	[179]
PTFE	40-90	4.65	0.14-100	55-72	[180]
	60	Seawater	4.5	45.5	[181]
	38	Various	11-22	2-5	[182]
	60	Synthetic brine	0.03	4.85-15.95	[25]
PTFE-PP	60	30	0.04	12.2	[183]
PVDF-PTFE	60	20	0.5	19	[184]
PP	40-60	-	0.5-1.7	5-25	[185]
PE	80	3.5	1.5	123	[166]
	70	Synthetic brine	1.2	122.2	[186]
PS	60	Synthetic brine	0.03	2.9-11.68	[25]
PS-PS	65	7	0.05	8.1	[26]
PS-AC	65	7	0.05	6.3	[26]
PS-PTFE	60-80	Synthetic brine	1.5	13.68-14.05	Present work
PS-PTFE	60-80	15	1.5	Predicted flux 14.84-15.26	Present work

4.3.2 Effect of porosity on the thermal efficiency

At a low membrane porosity of 77%, the membrane showed a minimum thermal efficiency at all varying bulk feed temperatures. With a 15% increase in membrane porosity, a higher amount of water vapor was allowed to be transported across the membrane leading to more heat being exchanged between the two sides of the polystyrene membrane. This resulted in a 14.6% increase in thermal efficiency. Similarly, as depicted in Figure 30, a maximum thermal efficiency of 63% was reached when increasing the membrane porosity by 22%.

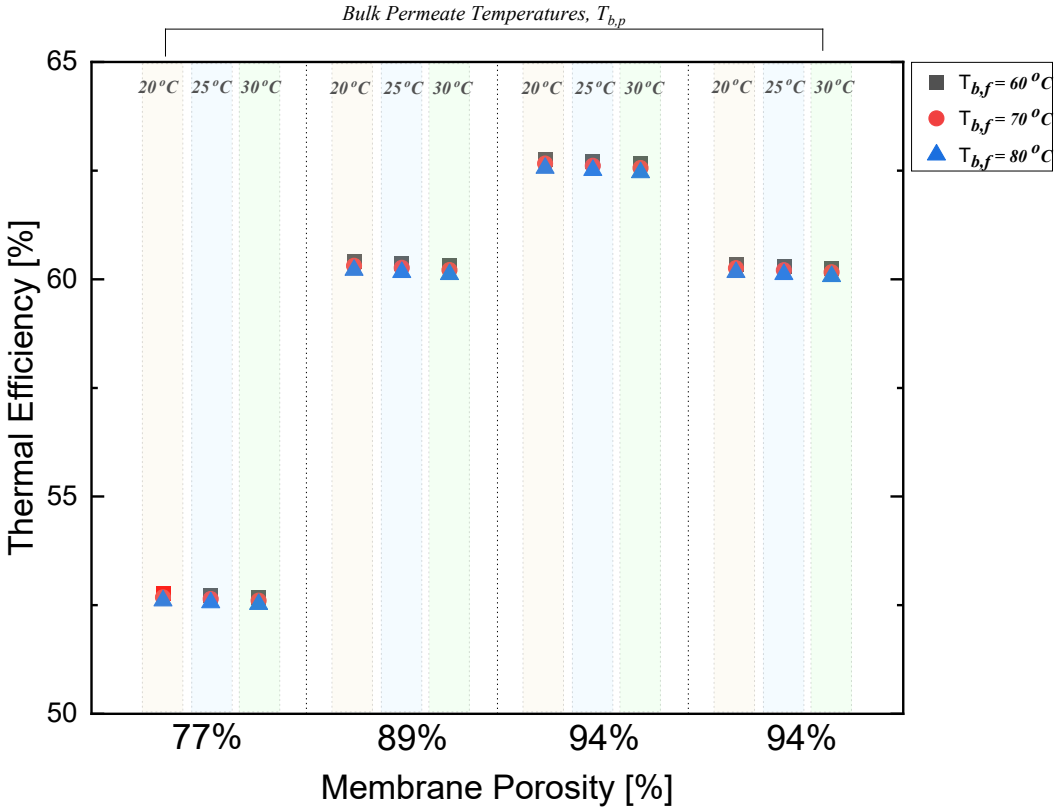

Figure 30. Effect of bulk temperatures on the thermal efficiency in DCMD.

Interestingly, at equal membrane porosity of 94%, increasing the membrane thickness by 14.5% resulted in a thermal efficiency drop by 4%. MD membranes with higher thickness have a higher thermal resistance, which hinders the heat transfer between both the hot and cold streams. This results in a lower temperature driving force across the membrane, which decreases the rate of mass transfer and reduces the thermal efficiency of the MD process [187]. Moreover, thermal efficiency of polystyrene membranes in DCMD is majorly affected by membrane fouling. As previously demonstrated, the accumulation of salt particles takes place on the membrane surface coming from the synthetic feed [25].

4.3.3 Effect of porosity on the evaporation efficiency

Membrane porosity shows to have a significant effect on evaporation efficiency with respect to changing bulk permeate and feed temperatures. A rise in the porosity from 77% to 89% resulted in a 5% increase in evaporation efficiency. Higher porosities allow for more efficient evaporation since there becomes a larger surface area available for water vapor to pass through. However, as the porosity continued to increase up to 94%, the ability of the membrane to properly reject the dissolved solutes, coming from the feed solution, decreased. This negatively impacts the evaporation efficiency and dropped it substantially by 5% (Figure 31).

As per the results of this work, as the porosity of the polystyrene membrane increases beyond 89%, the increased surface area for the evaporation becomes offset by the decrease in the solute rejection, resulting in a decrease in evaporation efficiency. In Figure 32 a-c, the relation between membrane porosity, thickness and bulk permeate temperature is illustrated. Taking the 60 C^{o} bulk feed temperature as an example, the

maximum permeate flux can be observed at a porosity of 94% with a thickness of 133 µm, the second highest permeate can be observed at a porosity of 77% with a thickness of 190 µm, and the third highest permeate flux can be observed at a porosity of 94% with a thickness of 156.6 µm, and the lowest permeate flux can be observed at a porosity of 89% with a thickness of 199 µm.

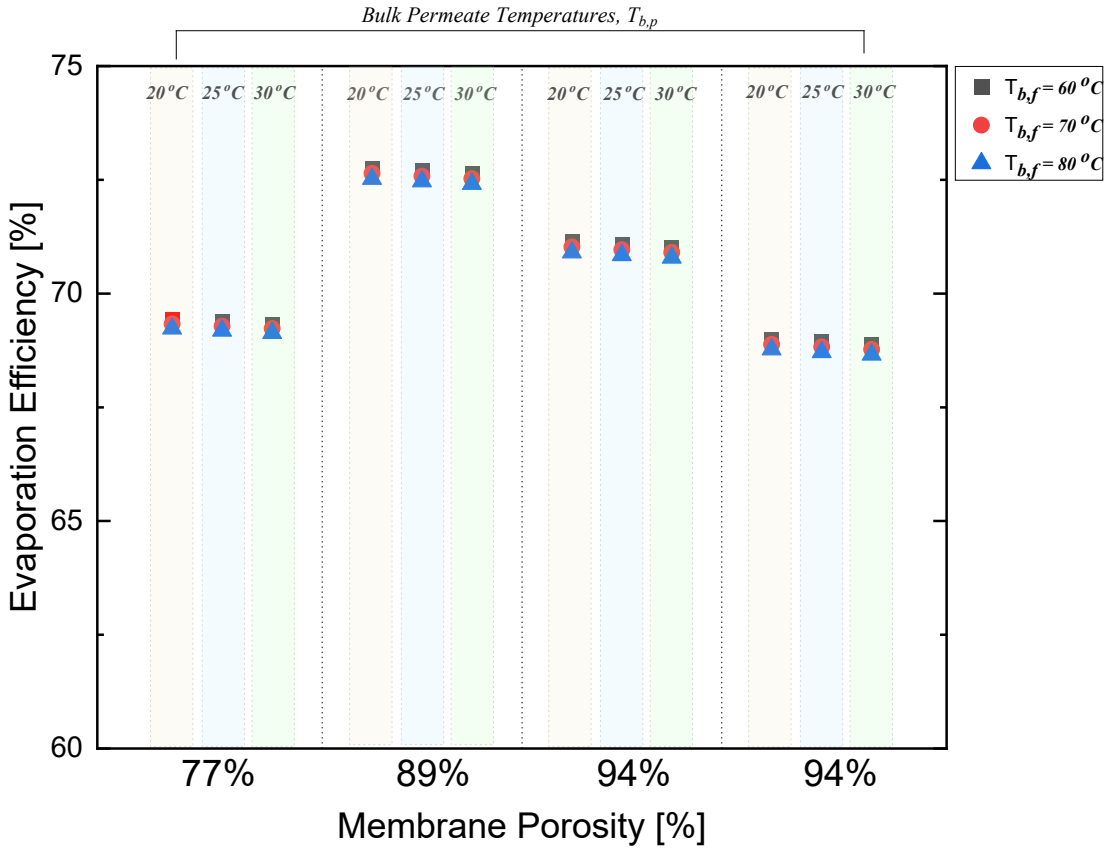

Figure 31. Effect of bulk temperatures on the evaporation efficiency in DCMD.

With an increase in bulk feed temperatures, the permeate flux increased by 51% due to the increase in vaporization of synthetic brine at higher temperatures [115]. This comes in accordance with Antoine's equation where the vapor pressure exponentially rises with an increase in feed temperature resulting in a rise in the permeate flux and enhances the overall MD process efficiency [188].

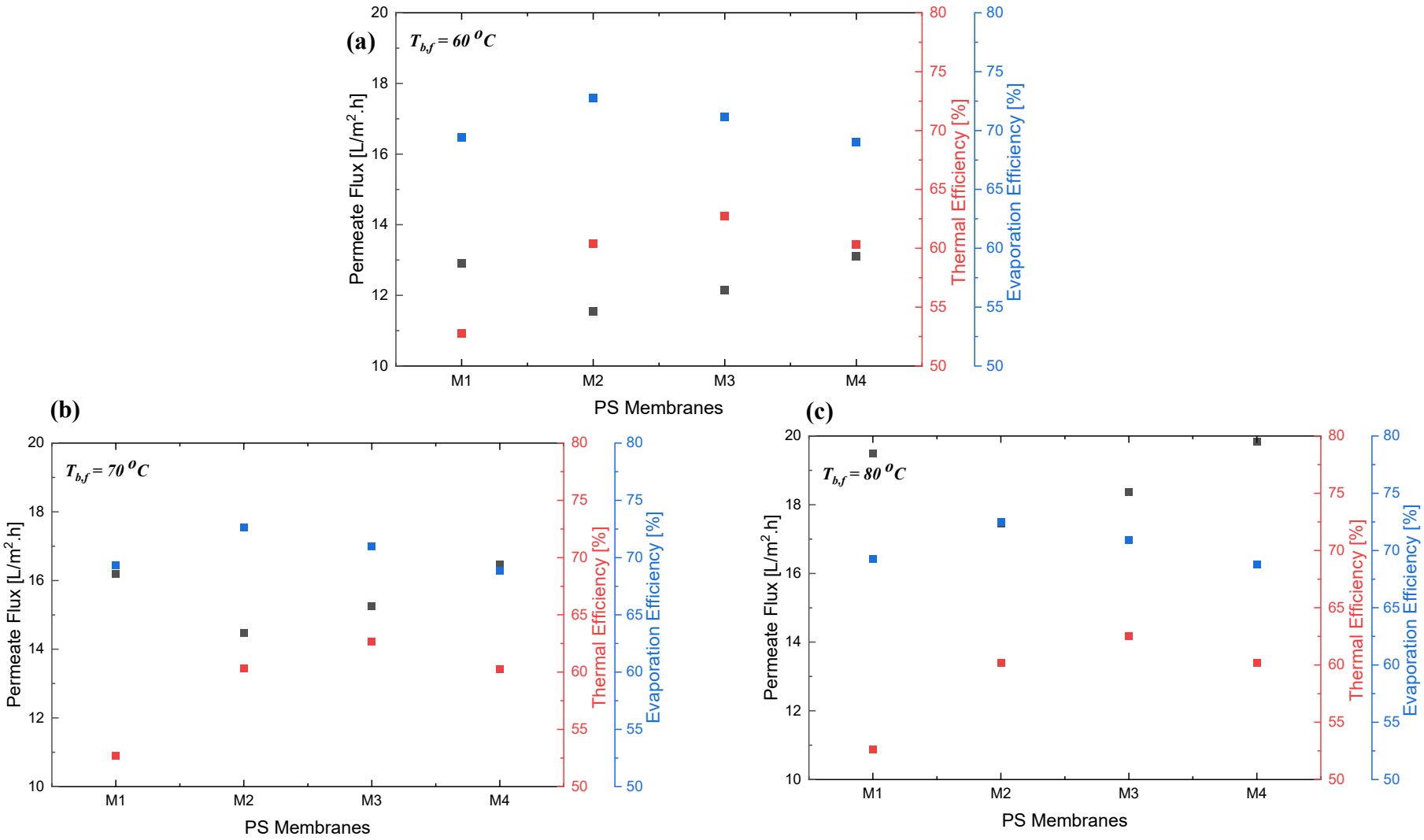

Figure 32. Permeate flux vs. thermal efficiency and evaporation efficiency of polystyrene membrane at $T_{b,p}$ =20 °C and $T_{b,f}$ = 60-80 °C, from (a)-(c), respectively.

Ni et al. investigated the effect of membrane characteristics of different membrane materials [189]. The study showed that with a decrease in membrane thickness, the permeate flux could be enhanced until a certain limit is reached. This limit is the threshold where permeate flux is no longer improved. Theoretically, based on literature, a reduction in thickness results in continuous increase in the permeate flux. However, this is not the case in experimental investigation. Once threshold is reached, the efficiency in membrane separation starts to decrease. Park and Lee investigated the energy efficiency in a pilot-scale DCMD system for hollow fiber modules [102]. The study showed that the thermal efficiencies for different MD modules cannot be directly compared in terms of flux.

Figure 33 demonstrates the relation between the permeate flux and membrane porosity by taking into consideration the change in the bulk permeate and bulk feed temperatures. At a constant porosity of 77% and a constant bulk permeate temperature of 20 ^{o}C, it can be observed that permeate flux is increasing as the feed bulk temperature is increasing from 60 ^{o}C to 80 ^{o}C. the same trend can be observed for the bulk permeate temperatures of 25 ^{o}C and 30 ^{o}C, and for the rest of porosities as well. At constant porosity and bulk feed temperature, a decreasing trend with respect to the permeate flux can be noticed. Looking at the 77% porosity membrane, the permeate flux decreased from 30 to 9 LMH when the bulk permeate temperature increased from 20 ^{o}C to 30 ^{o}C.

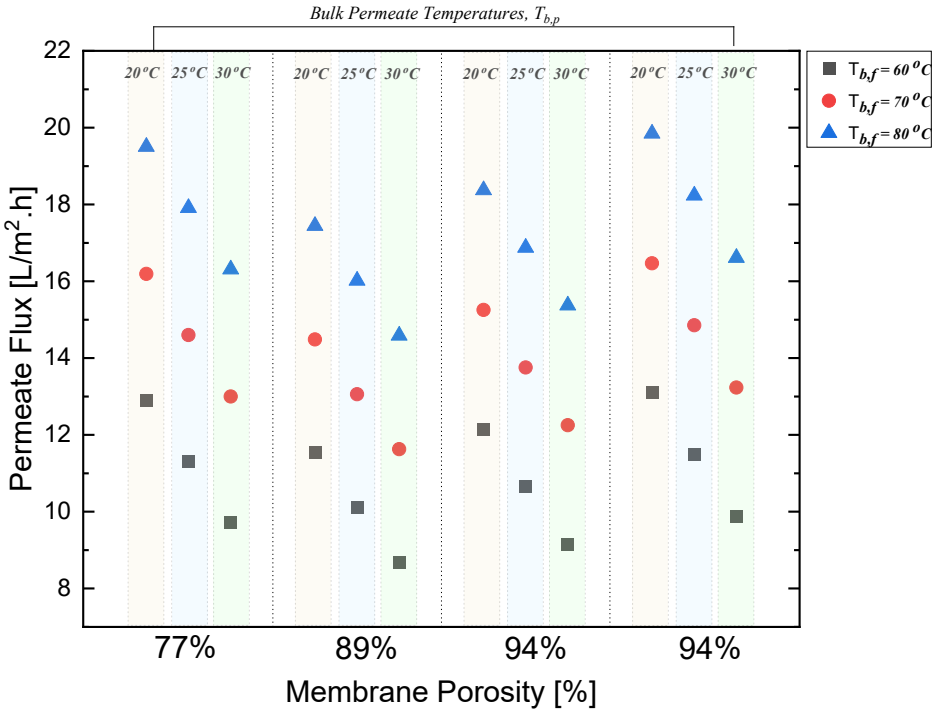

Figure 33. Effect of change in membrane porosity on permeate flux in DCMD.

At a constant bulk feed and bulk permeate temperature, and when increasing the membrane porosity from 77% to 94%, a non-linear relationship can be noticed. The permeate flux first decreased from 12.9 to 11.8 when the porosity increased from 77% to 89%, then the permeate flux increased from 11.9 to 12.1 then to 13.1 when the porosity increased from 89% to 94%, then stayed constant at 94%, respectively.

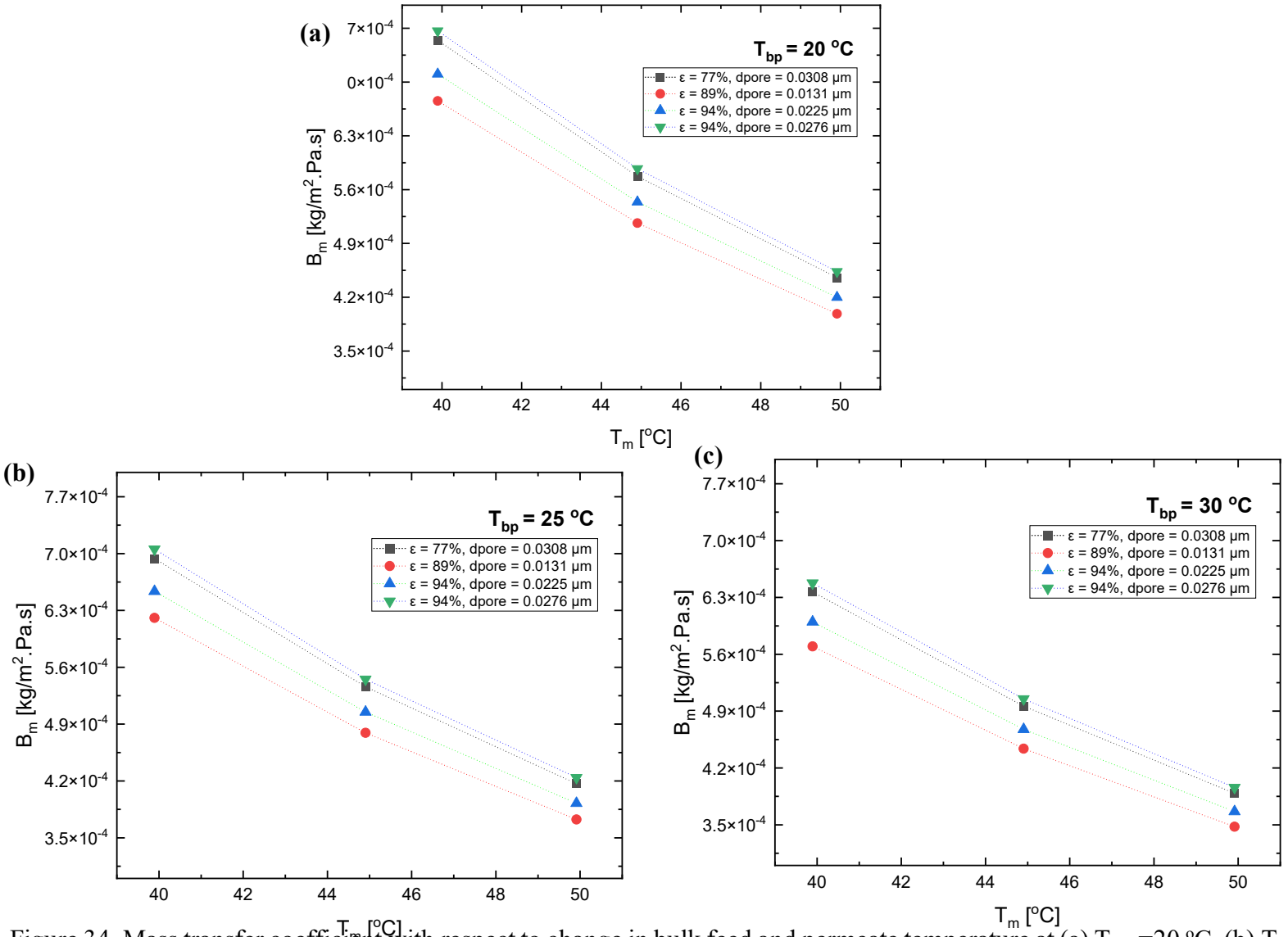

Figure 34. Mass transfer coefficient with respect to change in bulk feed and permeate temperature at (a) $T_{b,p}$ =20 °C, (b) $T_{b,p}$ =25 °C, and $T_{b,p}$ =30 °C.

4.3.4 Effect of porosity on the mass transfer coefficient

On the other hand, the design and manufacturing of various separation tools are usually quantified by the mass transfer coefficient. It is basically the function of of MD configuration, membrane temperature, and membrane characteristics [190]. From Figure 34(a) it can be seen that at a constant permeate flux and pore diameter the mass transfer coefficient values were decreased with the increase of the mean average temperature. The maximum mass transfer coefficient value occurred at the highest permeate flux of 94% with a pore diameter of 0.0276 μm, and the lowest mass transfer coefficient occurred at a permeate flux of 89% with a pore diameter of 0.0131 μm. Thus, it can be noticed that there is no direct relationship between the increase of the permeate flux, pore size diameter and the variation of the mass transfer coefficient. The same conclusion can be made for Figure 22 (b and c).

In Figure 34 (b and c), the bulk permeate temperature has been increased from 20℃, to 25℃ and 30 ℃. Looking at the membrane with a 94% permeate flux with a pore diameter 0.0276 m at 40 ℃ mean average temperature, as the temperature increase from 20℃ to 25℃ and from 25℃ to 30 ℃, the mass transfer coefficient decreases from 7.7×10^{-4} pa. s to 7.0×10^{-4} pa. s, and from 7.0×10^{-4} pa. s to 6.4×10^{-4} pa. s. And this is due to the fact that an increase in temperature can cause the fluid in the pores to become more viscous, which can lower the mass transfer coefficient. This occurs since the fluid becomes more resistant to flow, and also the diffusion through the pores becomes more difficult.

4.4 Comprehensive evaluation of desalination performance and energy efficiency of pilot-scale DCMD system

This section contributes directly to the development of cost-effective and sustainable MD technologies in the region. However, its energy efficiency and long-term performance in practical applications are still unclear. the long-term performance of a DCMD system can also be affected by the accumulation of fouling or scaling on the membrane surface. This can drastically reduce the system's performance over time, leading to increased energy consumption. Additionally, changes in the feedwater quality or operating conditions can also impact the system's long-term performance, further complicating its evaluation. Hence, an overview on the energy performance is highlighted providing valuable insights into the potential of DCMD as a viable desalination technology.

4.4.1 Specific Electrical Energy Consumption (SEEC) of DCMD Pilot Unit

As a result of membrane fouling, there is a rapid increase in the optimum energy required for desalination either by decreasing productivity (flux) or increasing the required driving force [191]. Over the period of 100 h of continuous MD process, a positive linear relationship between both SEEC and the number of operating hours can be noted in Figure 35. This was an expected behavior as more electrical energy is required to provide more power for the entire duration of MD. Currently, the industry is focusing on using equipment with minimal usage of power at the pilot level [192]; however, the challenge still arises in the uncertainties of the energy usage within the specific boundaries of the entire MD pilot unit. Assuming continuing operation over a minimum of 20 h per day, the total electrical

energy consumption for one pump, including pilot unit capacity, would be 131.01 kWh. Moreover, since the operation of MD at a large scale is performed based on two pumps for both the heating feed and cooling permeate tanks, then the total specific electrical energy consumed for the whole pilot unit would be 138.61 kWh/m^3.

4.4.2 Specific Thermal Energy Consumption (STEC) of DCMD Pilot Unit

Generally, in DCMD, the pumps, electrical heating inside the feed tank, and external water coolant running through the coolant spiral inside the distillate tank, all lead to the consumption of electrical energy. In Figure 36, the overall heat input raised, resulting in an increase in the pilot system's STEC from starting points of 35.51 and 43.667 kWh/m^3, for C2 and C1, respectively. This agrees with some findings in the literature [193].

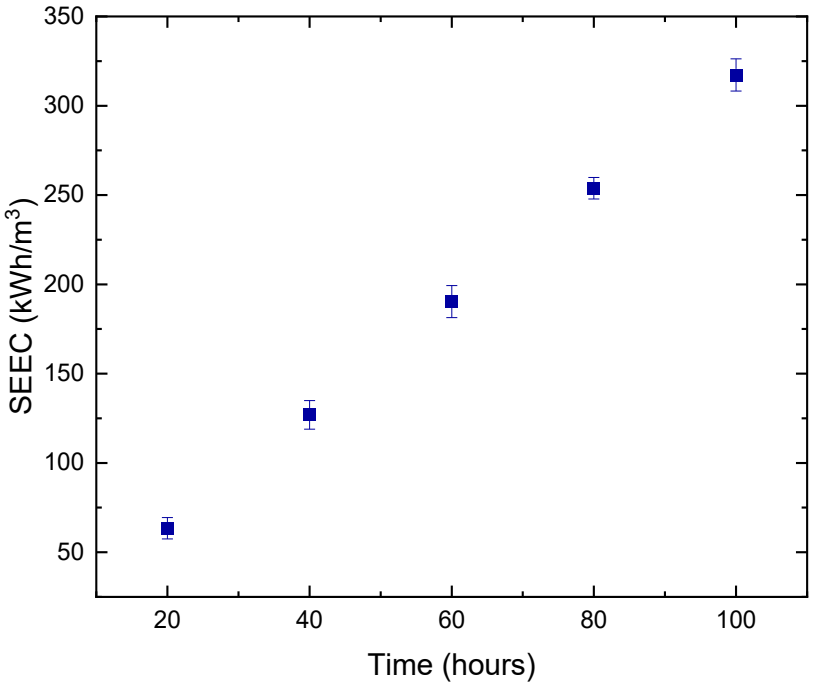

Figure 35. Specific electrical energy consumption calculated over time for MD pilot unit.

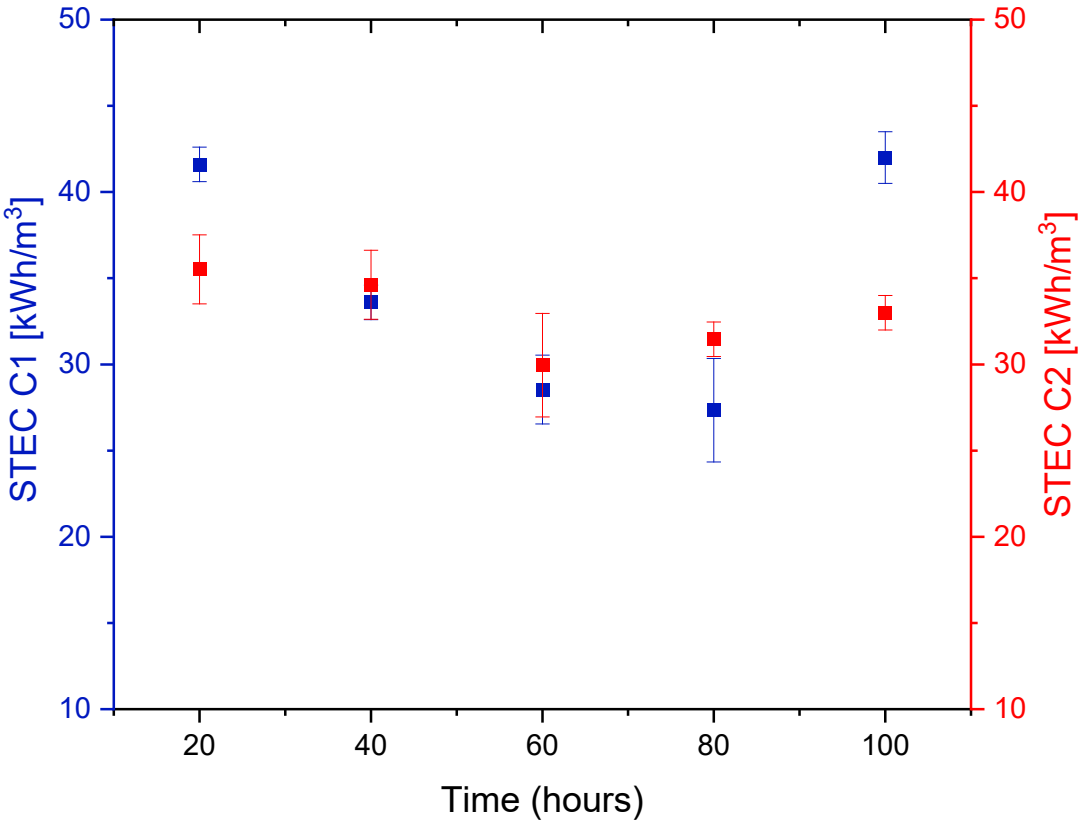

Figure 36. Influence of different feed concentrations on specific thermal energy consumption in pilot scale.

Feed salinity plays a significant role in determining the thermal energy consumption of an MD system. With the reduction in feed concentration, as presented in Figure 37a, there was a 19% drop in STEC after the first 20 h. The total reduction in STEC at higher feed concentrations was greater than that of lower concentrations, with 37% and 21%, respectively. This was due to the direct effect of feed salinity on the viscosity and mobility of the stream passing through the membrane, which in turn affects the vapor pressure of the solution [19]. In this work, the feed and permeate inlet temperatures were fixed at T_{Fin} = 70 °C, T_{Pin} = 20 °C, respectively. The flowrates of $Q_F = Q_P$ = 70 LPH were equal for both the feed and permeate streams, respectively. The specific heat capacity was assumed constant in the whole pilot system. The minimal values of the STEC between 40 and 90 h of continuous DCMD pilot operation were reached as a result of the fouling effect on the system's thermal performance. The formation of the fouling layers on the membrane surface raised the overall membrane thermal resistance and lowered its overall heat transfer coefficient.

As depicted earlier, as a function of operating time, an increase in the attachment of foulants onto the membrane surface took place. In the presence of inorganic compounds and chemical substances, both high ionic strength and large particles concentrations increased the membrane fouling to an extent where water flux rapidly declined. At fixed inlet conditions, the increased buildup of the fouling layers acted as extra resistance to heat transfer and hindered the effectuality of the pilot system. This, in turn, intensified the amount of consumed energy in the pilot system; hence the STEC value increased. Interestingly, the total SEC reduction after 100 h of pilot operation at lower feed concentration was only 3% compared to that of 15% at higher concentration (Figure 37).

The depicted outcomes provided a better insight into the relationship between membrane fouling and specific energy consumption. Previous studies have worked on the reduction in energy consumption and thus improving the thermal efficiency of the MD operation by linking the DCMD with a whole heat exchanger for latent heat recovery [194] and by brine recycling for water recovery purposes [195], where optimization between feed and distillate flow rates is necessary for lower energy consumption.

Table 12 lists the findings of this work and compares them with previous attempts on DCMD systems using different types of membranes at different operating parameters. Despite the large unit capacity of our system, we were still able to achieve an optimum specific energy consumption of 107.1 kWh/m^3 and 90.8 kWh/m^3 after 20 h and 100 h of membrane exposure to different feed concentrations, respectively. This signifies an optimum energetic performance for the DCMD pilot unit used in this study. However, the lack of clarity on whether only the energy used by the main equipment should be included or excluded in the analyses is one form of arising uncertainties, especially at the process level [196]. Thus, comparing the results of this work effectively with other studies is challenging [51].

4.4.3 Specific Energy Consumption (SEC) of DCMD Pilot Unit

SEC is generally used for benchmarking energy use in industrial processes to compare and evaluate the overall MD energy performance. The age of equipment and the capacity of the pilot unit are a few factors that influence the SEC. For instance, while newer equipment is more likely to be more energy-efficient compared to older equipment, it may require several years for optimization of newly installed equipment.

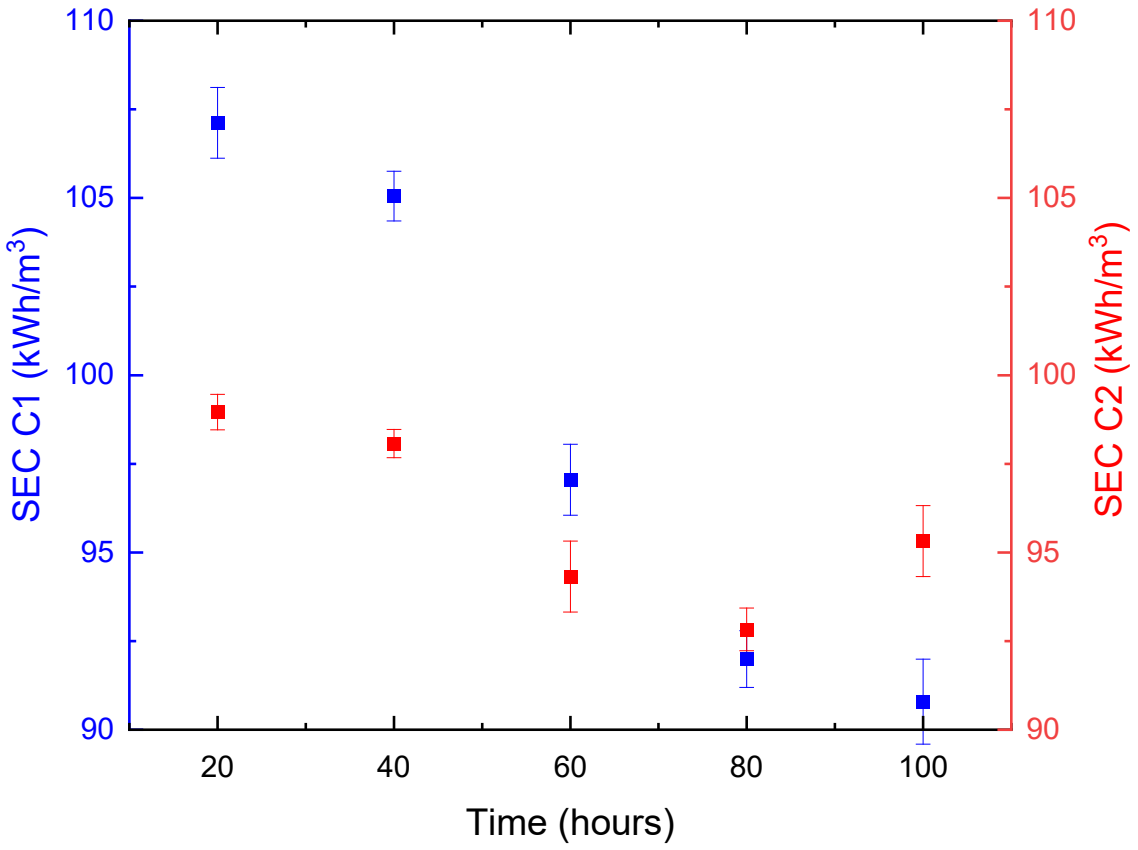

Figure 37. Influence of different feed concentrations on specific energy consumption in pilot scale.

Table 12: PWP and SEC values recorded in previous studies for DCMD systems only

Membrane	Feed Type	Temperature Inlets [°C]		Duration of MD [hours]	PWP [LMH]	SEC [kWh/m^3]	Plant Capacity [m^3/h]	Ref
		Feed	Permeate					
PP	Distilled Water	59.2	14.3	3	56.2	3550–4580	-	[197]
PVDF	Simulated RO Brine	80	30	-	10.80–12.6	130–1700	-	[198]
PTFE	Wastewater	60	18-21	840–1800	2–5	1500	3.85	[104]
PE	Synthetic Brine	70	20	20	122.2	107.1	207.31	This work
				100	12.6	90.8		

This work showed optimum SEC achieved with higher permeabilities at much lower MD duration in comparison with other systems operating at higher times and at lower unit capacities. This variation can be attributed to many factors, such as the location, size, and rate of permeate production used for an MD pilot system [199–201]. The considerably high amounts of energy consumption (ranging from 95.3 kWh/m^3 to 107.1 kWh/m^3) that are required to produce permeate with drinking water standards signify the importance of utilizing low-grade thermal energy by creating a hybrid MD-integrated system that outperforms other desalination systems. Results obtained from this work can create a solid basis to identify ways of enhancement in the energy efficiency for full-scale industrial processes.

4.4.4 Statistical correlation

One of the main statistical measuring elements was used in this study to better investigate the strength of the linear relationships of all data sets. The Pearson Correlation was used as per the following equation [202]:

$$Correl(A,B) = \frac{Covariance\,(A,B)}{Std.Dev\ A\ \times Std.Dev\ B} \tag{39}$$

In this study, the outcome of all correlations is plotted in Figure 33. The correlation results suggest that the permeate flux is greatly affected by the percentage of salt rejection (Figure 38a) as well as the water contact angle of the membrane (Figure 38b), with coefficients of 0.963 and 0.919, respectively. Furthermore, a moderate positive correlation was found for the plot relating CA with SEC (Figure 38d). However, a weak correlation factor of 0.359 was depicted for the flux with respect to STEC (Figure 38c). This may prove that there is a nonlinear relationship between both parameters but does not necessarily imply that there is no relationship between both sets of data. In fact, despite the low correlation, a directly proportional relation can still be seen at 40 h and beyond the whole duration of the DCMD process. Generally, the outcomes of this work have not shown any negative correlation coefficients, which proves that all sets of data obtained from this study are moving in the same linear direction. The coefficient of determination (R^2) was also calculated, showing a data-relation magnitude ranging from 0.768 to 0.993. This showed a high variance proportion in the dependent variables predicted from the independent variables [203].

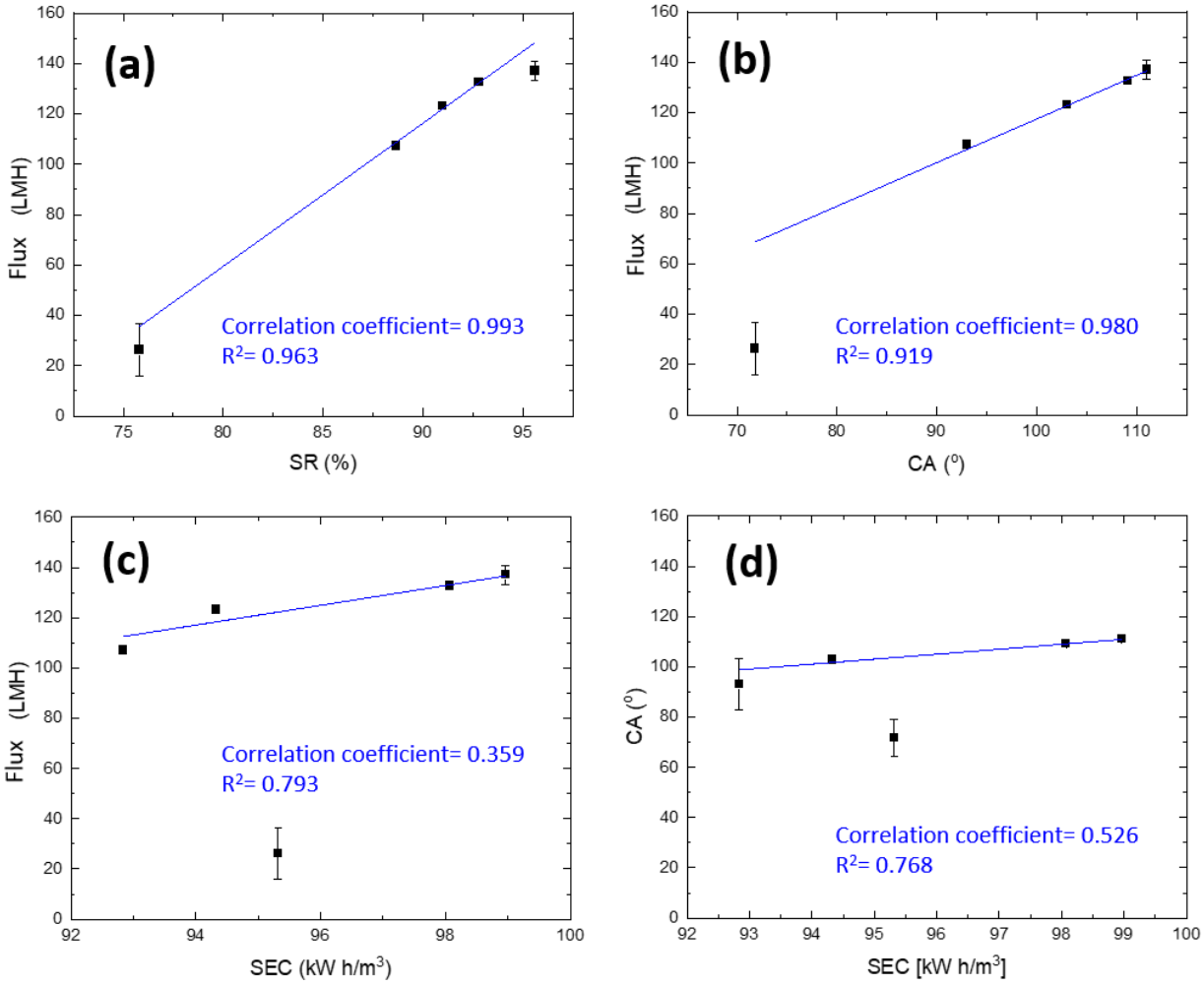

Figure 38. The correlations of the calculated water flux with (**a**) salt rejection, (**b**) contact angle, (**c**) specific energy consumption, and (**d**) the correlation of the contact angle with the specific energy consumption.

CHAPTER 5: CONCLUSIONS

In the present work, we have successfully investigated viability of utilizing the tested electrospun polystyrene membranes in clean water production. Summarized data showed that these membranes may act as active components in existing desalination technologies and assist in the generation of fresh water. The process conditions the DCMD bench scale system was optimized is such a way that high salt rejections up to 99% were achieved and at the same time membrane wetting was avoided. The calculated salt rejection values reached as high as 98% and 99% for high and low feed concentrations, respectively. Overall, a significant change was noted when reducing the feed's salt concentration to almost the half showing higher permeate fluxes of 15.95 LMH and 11.68 LMH for PTFE and PS membranes, respectively. The results were comparable with that of commercial membranes.

Furthermore, long-term performance of a pilot DCMD system was investigated in this study for polyethylene membranes and has shown high energetic performance at different salinity levels of the synthetic brine. High flux recovery ratios of 86%, 94%, and 95% were depicted at increasing fouling concentrations of 15, 25, and 45 ppm, respectively. However, after 40 h of direct membrane exposure with the feed, the humic acid foulant particles on the membrane surface started to form cake layers causing a decline in the permeate flux. Towards the end of the entire DCMD operation of 100 h, the fouling pattern became evenly spread within the grains of the membrane, reducing its pore size and therefore leading to pore wetting.

As a basis of this work, and based on the effective process conditions used for testing polyethylene membranes, the electrospun polystyrene were then used in the DCMD

pilot unit to further investigate its desalination performance at larger scale. Supported by the experimental findings, an optimized iterative method was used to minimize the error between the initial estimate of surface membrane temperature and the actual values, allowing them to predict the temperature accurately in each experiment. The prediction model used in this study was effective in predicting the permeate flux as results have shown good agreement between the experimental results and the optimization model with an error between 8-13 %. Theoretical modelling data points showed that at higher temperature difference between the feed and permeate sides, the greater was the vapor pressure difference, resulting in an increased permeate flux, until a threshold is reached, and the flux stops improving. This lead to a reduction in thermal and evaporation efficiencies by 4% and 5%, respectively. Further investigations on how heat loss minimization should be carried out experimentally for consideration in larger scale applications.

To address the current research gap, the outcomes of this study align with the latest innovative wastewater technologies and play a significant role in investigating the impact of synthetic brine on synthesized polystyrene and commercial polyethylene membranes using a high-tech pilot-scale DCMD unit, emphasizing the effects of varying brine concentrations on its energetic performance and the long-term impact of membrane fouling. Such insights are difficult to achieve through conventional bench-scale DCMD setups. The results obtained from this work can contribute to creating a good basis for future studies on the scalability of PS membranes for potential membrane-based desalination technologies in the industry. The findings come in line with recent innovative wastewater technologies and are largely accountable for the optimization of industrial MD processes during the treatment of industrial wastewater. The incorporation of novel types

of PS-based membranes could potentially enhance the performance of existing membrane-based technologies and pave the way for the development of more energy efficient and cost-effective membrane distillation processes, which are of paramount importance for addressing the global water scarcity issue.

CHAPTER 6: FUTURE WORK

In light of the increasing demand of freshwater, the treatment of wastewater has gained significant attention over the past decade. Wastewater is considered a key resource with high potential, rather than just a waste product. The recovery of such valuable resources from various forms of wastewater, such as saline wastewater and produced water generated from the oil and gas industry, not only decreases operational costs but also contributes to achieving zero-discharge goals in different industries. Membrane-based processes are promising and sustainable solutions for treating wastewater due to its high effectiveness in freshwater generation. It is important to point out that, compared to other conventional membrane processes, the DCMD process has the potential to consume much less energy, making it an attractive option for industrial wastewater treatment. Yet, fouling remains the major challenge in DCMD, especially at pilot-scale.

Similar to the work covered in this thesis, the majority of MD studies have tested the performance of the membranes using either a single component feed or a synthetically prepared feed made-up of multiple components. Although simulated feed may be of high concentration, it does not involve the actual unknown contaminants existing in real industrial wastewater. In fact, if a single contaminant is used, the interactions among ions and complex molecules that are present in actual wastewater as well as their interactions with the membrane surface could be neglected. In this case, the likelihood of membrane fouling and anti-scaling investigations would not reflect real industrial conditions. Hence, future studies should aim to reproduce the findings in a pilot unit using the real complex nature of industrial wastewater in order to fully achieve accurate and reliable performance data.

Therefore, future research should be conducted using more realistic operating conditions to investigate prevention strategies against fouling. This can be done by tailoring the morphology and porous structure of membranes. An interesting topic for future work would be to prepare multilayer superhydrophobic membranes consisting of PS/PE by electrospinning. Polystyrene fibers can be electrospun onto polyethylene (as the support layer) and its effect on the energy performance in DCMD can be investigated. Results can then be compared with that obtained from this study and provide a good starting point for further analysis and discussion.

Furthermore, future research should shed the light on the effect of the addition of nanoparticles (such as reduced graphene oxide) on the membrane's wettability and effect on its mechanical strength. These combined parameters should be compromised in such a way that high desalination performance is maintained. Future work should consider the potential impact of nanoparticles on the on mass and heat transfer properties in pilot scale, as this effect was not thoroughly explored in the literature. The outcomes of this research indicate significant implications for pilot DCMD technologies in the global petrochemical industry, particularly in gulf desalination plants, as it contributes to the production of fresh water. Yet, there is much work to be done in developing a membrane that is mechanically and structurally as good as commercial membranes fit for use in DCMD. However, through the implementation of further research and proper innovative strategies, the chances of increasing the technological readiness of DCMD systems, from lab to industry level, can be achieved.

REFERENCES

1. Piesse, M. Global Water Supply and Demand Trends Point Towards Rising Water Insecurity. **2020**.
2. Ibrahim, T.H.; Sabri, M.A.; Khamis, M.I. Application of multiwalled carbon nanotubes and its magnetite derivative for emulsified oil removal from produced water. *Environ. Technol.* **2019**, *40*, 3337–3350.
3. Clay, L.; Pichtel, J. Treatment of Simulated Oil and Gas Produced Water via Pilot-Scale Rhizofiltration and Constructed Wetlands. *Int. J. Environ. Res.* **2019**, *13*, 185–198.
4. Mohammed, T.; Abbas, E.; Ahmed, T. Turbidity and oil removal from oilfield produced water, middle oil company by electrocoagulation technique. In Proceedings of the MATEC Web of Conferences; EDP Sciences, 2018; Vol. 162, p. 5010.
5. Li, L.; Al-Muntasheri, G.A.; Liang, F. A review of crosslinked fracturing fluids prepared with produced water. *Petroleum* **2016**, *2*, 313–323.
6. Faksness, L.G.; Grini, P.G.; Daling, P.S. Partitioning of semi-soluble organic compounds between the water phase and oil droplets in produced water. *Mar. Pollut. Bull.* **2004**, *48*, 731–742, doi:10.1016/j.marpolbul.2003.10.018.
7. Frid, C. Bioaccumulation in Marine Organisms. Effect of Contaminants from Oil Well Produced Water. *Org. Geochem.* **2003**, *34*, 149, doi:10.1016/s0146-6380(02)00213-9.
8. Tibbetts, P.J.C.; Buchanan, I.T.; Gawel, L.J.; Large, R. A Comprehensive Determination of Produced Water Composition. *Prod. Water* **1992**, 97–112,

doi:10.1007/978-1-4615-2902-6_9.

9. Fathima, A.; Almohsin, A.; Michael, F.M.; Bataweel, M.; Alsharaeh, E.H. Polymer nanocomposites for water shutoff application-A review. *Mater. Res. Express* **2018**, *6*, 32001.

10. Esmaeilirad, N.; Carlson, K.; Ozbek, P.O. Influence of softening sequencing on electrocoagulation treatment of produced water. *J. Hazard. Mater.* **2015**, *283*, 721–729.

11. Sappington, E.N.; Rifai, H.S. Low-frequency electromagnetic treatment of oilfield produced water for reuse in agriculture: effect on water quality, germination, and plant growth. *Environ. Sci. Pollut. Res.* **2018**, *25*, 34380–34391.

12. PENTAIR *Water Desalination Report: Advanced Filtration Technology For Reverse Osmosis Pretreatment*; 2017;

13. Choon, K.; Thu, K.; Kim, Y.; Chakraborty, A.; Amy, G. Adsorption desalination : An emerging low-cost thermal desalination method. *DES* **2013**, *308*, 161–179, doi:10.1016/j.desal.2012.07.030.

14. Cyganowski, J.; Lutz, H. Chapter 8. Post-processing. In *Ultrafiltration for Bioprocessing*; 2015; pp. 131–149.

15. Kim, B.; Kwak, R.; Kwon, H.J.; Pham, V.S.; Kim, M.; Al-Anzi, B.; Lim, G.; Han, J. Purification of high salinity brine by multi-stage ion concentration polarization desalination. *Sci. Rep.* **2016**, *6*, doi:10.1038/srep31850.

16. Abdelrazeq, H.; Khraisheh, M.; Ashraf, H.M.; Ebrahimi, P.; Kunju, A. Sustainable innovation in membrane technologies for produced water treatment: Challenges and limitations. *Sustain.* **2021**, *13*, doi:10.3390/su13126759.

17. Xu, J.; Singh, Y.B.; Amy, G.L.; Ghaffour, N. Effect of operating parameters and membrane characteristics on air gap membrane distillation performance for the treatment of highly saline water. *J. Memb. Sci.* **2016**, *512*, 73–82, doi:10.1016/j.memsci.2016.04.010.

18. Reza Shirzad Kebria, M.; Rahimpour, A. Membrane Distillation: Basics, Advances, and Applications. In *Advances in Membrane Technologies*; 2020; pp. 1–16.

19. Al-Obaidani, S.; Curcio, E.; Macedonio, F.; Di Profio, G.; Al-Hinai, H.; Drioli, E. Potential of membrane distillation in seawater desalination: Thermal efficiency, sensitivity study and cost estimation. *J. Memb. Sci.* **2008**, *323*, 85–98, doi:10.1016/j.memsci.2008.06.006.

20. Liang, B.; Pan, K.; Li, L.; Giannelis, E.P.; Cao, B. High performance hydrophilic pervaporation composite membranes for water desalination. *Desalination* **2014**, *347*, 199–206, doi:10.1016/j.desal.2014.05.021.

21. Cho, H.; Choi, Y.; Lee, S. Effect of pretreatment and operating conditions on the performance of membrane distillation for the treatment of shale gas wastewater. *Desalination* **2018**, *437*, 195–209, doi:10.1016/j.desal.2018.03.009.

22. Khayet, M.; Wang, R. Mixed Matrix Polytetrafluoroethylene/Polysulfone Electrospun Nanofibrous Membranes for Water Desalination by Membrane Distillation. *ACS Appl. Mater. Interfaces* **2018**, *10*, 24275–24287, doi:10.1021/acsami.8b06792.

23. Chew, N.G.P.; Zhao, S.; Malde, C.; Wang, R. Polyvinylidene fluoride membrane modification via oxidant-induced dopamine polymerization for sustainable direct-contact membrane distillation. *J. Memb. Sci.* **2018**, *563*, 31–42,

doi:10.1016/j.memsci.2018.05.035.

24. Ke, H.; Feldman, E.; Guzman, P.; Cole, J.; Wei, Q.; Chu, B.; Alkhudhiri, A.; Alrasheed, R.; Hsiao, B.S. Electrospun polystyrene nanofibrous membranes for direct contact membrane distillation. *J. Memb. Sci.* **2016**, *515*, 86–97, doi:10.1016/j.memsci.2016.05.052.

25. Abdelrazeq, H.; Khraisheh, M.; Al Momani, F.; McLeskey, J.T.; Hassan, M.K.; Gad-el-Hak, M.; Tafreshi, H.V. Performance of electrospun polystyrene membranes in synthetic produced industrial water using direct-contact membrane distillation. *Desalination* **2020**, *493*, 114663, doi:10.1016/j.desal.2020.114663.

26. Esteves, R.J.A.; Gornick, V.; Alqurwani, D.S.; Koenig-Lovejoy, J.; Abdelrazeq, H.; Khraisheh, M.; Forzano, A. V.; Gad-el-Hak, M.; Tafreshi, H.V.; McLeskey, J.T. Activated carbon-doped polystyrene fibers for direct contact membrane desalination. *Emergent Mater.* **2020**, doi:10.1007/s42247-020-00107-z.

27. Abdullah, A.; Al-Qahatani, A.; Alquraish, M.; Bailey, C.; El-Shazly, A.; El-Mofty, S. Modeling and simulation of fabricated graphene nanoplates/polystyrene nanofibrous membrane for dcmd. *Polymers (Basel).* **2021**, *13*, doi:10.3390/polym13172987.

28. Ke, H.; Feldman, E.; Guzman, P.; Cole, J.; Wei, Q.; Chu, B.; Alkhudhiri, A.; Alrasheed, R.; Hsiao, B.S. Electrospun polystyrene nanofibrous membranes for direct contact membrane distillation. *J. Memb. Sci.* **2016**, *515*, 86–97, doi:10.1016/J.MEMSCI.2016.05.052.

29. Hashemifard, S.A.; Abdoli, A.; Khosravi, A.; Matsuura, T.; Abbasi, M. Predicting and evaluating the performance of DCMD : The effect of non-ideal morphology and

thermal conductivity of porous nanocomposite. *Chem. Eng. Res. Des.* **2023**, *192*, 638–652, doi:10.1016/j.cherd.2023.03.005.

30. Rahimnia, R.; Pakizeh, M. Preparation and characterization of PPO/PS porous membrane for desalination via direct contact membrane distillation (DCMD). *J. Memb. Sci.* **2023**, *669*, 121297, doi:10.1016/j.memsci.2022.121297.
31. Khoshnevisan, S.; Bazgir, S. Treatment of dye wastewater by direct contact membrane distillation using superhydrophobic nanofibrous high-impact polystyrene membranes. *Int. J. Environ. Sci. Technol.* **2021**, *18*, 1513–1528, doi:10.1007/s13762-020-02894-8.
32. Shirazi, M.M.A.; Bazgir, S.; Meshkani, F. A novel dual-layer, gas-assisted electrospun, nanofibrous SAN4-HIPS membrane for industrial textile wastewater treatment by direct contact membrane distillation (DCMD). *J. Water Process Eng.* **2020**, *36*, 101315, doi:10.1016/j.jwpe.2020.101315.
33. Sadeghzadeh, A.; Bazgir, S.; Shirazi, M.M.A. Fabrication and characterization of a novel hydrophobic polystyrene membrane using electroblowing technique for desalination by direct contact membrane distillation. *Sep. Purif. Technol.* **2020**, *239*, 116498, doi:10.1016/j.seppur.2019.116498.
34. Li, X.; Wang, C.; Yang, Y.; Wang, X.; Zhu, M.; Hsiao, B.S. Dual-biomimetic superhydrophobic electrospun polystyrene nanofibrous membranes for membrane distillation. *ACS Appl. Mater. Interfaces* **2014**, *6*, 2423–2430, doi:10.1021/am4048128.
35. Ahmed, F.; Johnson, D.; Hashaikeh, R.; Hilal, N. Barriers to Innovation in Water Treatment. *Water (Switzerland)* **2023**, *15*, doi:10.3390/w15040773.

36. UNICEF *Progress on Drinking Water , Sanitation and Hygiene*; 2017;

37. Kargari, A.; Shirazi, M.J.A. Direct contact membrane distillation for seawater desalination AU - Shirazi, Mohammad Mahdi A. *Desalin. Water Treat.* **2012**, *49*, 368–375, doi:10.1080/19443994.2012.719466.

38. Echchelh, A.; Hess, T.; Sakrabani, R. Reusing oil and gas produced water for irrigation of food crops in drylands. *Agric. Water Manag.* **2018**, *206*, 124–134, doi:10.1016/j.agwat.2018.05.006.

39. Arzate, S.; Pfister, S.; Oberschelp, C.; Sánchez-Pérez, J.A. Environmental impacts of an advanced oxidation process as tertiary treatment in a wastewater treatment plant. *Sci. Total Environ.* **2019**, *694*, doi:10.1016/j.scitotenv.2019.07.378.

40. Qatar Electricity & Water Co. *Annual Report 2019*; 2019;

41. Akyon, B.; Lipus, D.; Bibby, K. Glutaraldehyde inhibits biological treatment of organic additives in hydraulic fracturing produced water. *Sci. Total Environ.* **2019**, *666*, 1161–1168, doi:10.1016/j.scitotenv.2019.02.056.

42. Lutzu, G.A.; Dunford, N.T. Algal treatment of wastewater generated during oil and gas production using hydraulic fracturing technology. *Environ. Technol. (United Kingdom)* **2019**, *40*, 1027–1034, doi:10.1080/09593330.2017.1415983.

43. Akhbarizadeh, R.; Moore, F.; Mowla, D.; Keshavarzi, B. Improved waste-sourced biocomposite for simultaneous removal of crude oil and heavy metals from synthetic and real oilfield-produced water. *Environ. Sci. Pollut. Res.* **2018**, *25*, 31407–31420, doi:10.1007/s11356-018-3136-2.

44. El-Bourawi, M.S.; Ding, Z.; Ma, R.; Khayet, M. A framework for better understanding membrane distillation separation process. *J. Memb. Sci.* **2006**, *285*,

4–29, doi:10.1016/j.memsci.2006.08.002.

45. Mondal, S.; Wickramasinghe, S.R. Produced water treatment by nanofiltration and reverse osmosis membranes. *J. Memb. Sci.* **2008**, *322*, 162–170, doi:10.1016/j.memsci.2008.05.039.

46. Liao, Y.; Wang, R.; Tian, M.; Qiu, C.; Fane, A.G. Fabrication of polyvinylidene fluoride (PVDF) nanofiber membranes by electro-spinning for direct contact membrane distillation. *J. Memb. Sci.* **2013**, *425–426*, 30–39, doi:10.1016/j.memsci.2012.09.023.

47. Lokare, O.R.; Tavakkoli, S.; Wadekar, S.; Khanna, V.; Vidic, R.D. Fouling in direct contact membrane distillation of produced water from unconventional gas extraction. *J. Memb. Sci.* **2017**, *524*, 493–501, doi:10.1016/j.memsci.2016.11.072.

48. Kim, J.; Kwon, H.; Lee, S.; Lee, S.; Hong, S. Membrane distillation (MD) integrated with crystallization (MDC) for shale gas produced water (SGPW) treatment. *Desalination* **2017**, *403*, 172–178, doi:10.1016/j.desal.2016.07.045.

49. Xiong, B.; Zydney, A.L.; Kumar, M. Fouling of microfiltration membranes by flowback and produced waters from the Marcellus shale gas play. *Water Res.* **2016**, *99*, 162–170, doi:10.1016/j.watres.2016.04.049.

50. Zhang, Z.; Du, X.; Carlson, K.H.; Robbins, C.A.; Tong, T. Effective treatment of shale oil and gas produced water by membrane distillation coupled with precipitative softening and walnut shell filtration. *Desalination* **2019**, *454*, 82–90, doi:10.1016/j.desal.2018.12.011.

51. Miladi, R.; Frikha, N.; Kheiri, A.; Gabsi, S. Energetic performance analysis of seawater desalination with a solar membrane distillation. *Energy Convers. Manag.*

2019, *185*, 143–154, doi:10.1016/j.enconman.2019.02.011.

52. Lawson, K.W.; Lloyd, D.R. Membrane distillation. *J. Memb. Sci.* **1997**, *124*, 1–25, doi:10.1016/S0376-7388(96)00236-0.

53. Alkhudhiri, A.; Darwish, N.; Hilal, N. Membrane distillation: A comprehensive review. *Desalination* **2012**, *287*, 2–18, doi:10.1016/j.desal.2011.08.027.

54. Khayet, M. Membranes and theoretical modeling of membrane distillation : A review. *Adv. Colloid Interface Sci.* **2011**, *164*, 56–88, doi:10.1016/j.cis.2010.09.005.

55. Kiss, A.A.; Kattan Readi, O.M. An industrial perspective on membrane distillation processes. *J. Chem. Technol. Biotechnol.* **2018**, *93*, 2047–2055, doi:10.1002/jctb.5674.

56. Sallakh Niknejad, A.; Bazgir, S.; Kargari, A. Novel Triple-Layer HIPS/SBR/PP Nanofibrous Membranes for Robust DCMD Desalination. *Ind. Eng. Chem. Res.* **2021**, *60*, 2911–2920, doi:10.1021/acs.iecr.0c05737.

57. Wang, Z.; Wu, A.; Ciacchi, L.C.; Wei, G. Recent Advances in Nanoporous Membranes for Water Purification. *Nanomaterials* **2018**, *8*, 1–19, doi:10.3390/nano8020065.

58. Dervin, S.; Dionysiou, D.D.; Pillai, S.C. 2D nanostructures for water purification: Graphene and beyond. *Nanoscale* **2016**, *8*, 15115–15131, doi:10.1039/c6nr04508a.

59. Lee, A.; Elam, J.W.; Darling, S.B. Membrane materials for water purification: Design, development, and application. *Environ. Sci. Water Res. Technol.* **2016**, *2*, 17–42, doi:10.1039/c5ew00159e.

60. Werber, J.R.; Osuji, C.O.; Elimelech, M. Materials for next-generation desalination and water purification membranes. *Nat. Rev. Mater.* **2016**, *1*,

doi:10.1038/natrevmats.2016.18.

61. Ahmed, F.E.; Lalia, B.S.; Hashaikeh, R. A review on electrospinning for membrane fabrication : Challenges and applications. *Desalination* **2014**, *356*, 15–30, doi:10.1016/j.desal.2014.09.033.

62. Ullah, R.; Khraisheh, M.; Esteves, R.J.; McLeskey, J.T.; AlGhouti, M.; Gad-el-Hak, M.; Vahedi Tafreshi, H. Energy efficiency of direct contact membrane distillation. *Desalination* **2018**, *433*, 56–67, doi:10.1016/j.desal.2018.01.025.

63. Wang, P.; Chung, T.S. Recent advances in membrane distillation processes: Membrane development, configuration design and application exploring. *J. Memb. Sci.* **2015**, *474*, 39–56, doi:10.1016/j.memsci.2014.09.016.

64. Cong, H.; Chuai, D.; Chul, Y.; Kyong, H.; Duc, L. A novel electrospun, hydrophobic, and elastomeric styrene-butadiene-styrene membrane for membrane distillation applications. *J. Memb. Sci.* **2018**, *549*, 420–427, doi:10.1016/j.memsci.2017.12.024.

65. Wang, K.; Hou, D.; Wang, J.; Wang, Z.; Tian, B.; Liang, P. Applied Surface Science Hydrophilic surface coating on hydrophobic PTFE membrane for robust anti-oil-fouling membrane distillation. *Appl. Surf. Sci.* **2018**, *450*, 57–65, doi:10.1016/j.apsusc.2018.04.180.

66. Lee, E.J.; An, A.K.; Hadi, P.; Lee, S.; Woo, Y.C.; Shon, H.K. Advanced multi-nozzle electrospun functionalized titanium dioxide/polyvinylidene fluoride-co-hexafluoropropylene (TiO2/PVDF-HFP) composite membranes for direct contact membrane distillation. *J. Memb. Sci.* **2017**, *524*, 712–720, doi:10.1016/j.memsci.2016.11.069.

67. Lalia, B.S.; Guillen-Burrieza, E.; Arafat, H. a.; Hashaikeh, R. Fabrication and characterization of polyvinylidenefluoride-co-hexafluoropropylene (PVDF-HFP) electrospun membranes for direct contact membrane distillation. *J. Memb. Sci.* **2013**, *428*, 104–115, doi:10.1016/j.memsci.2012.10.061.

68. Lalia, B.S.; Guillen, E.; Arafat, H.A.; Hashaikeh, R. Nanocrystalline cellulose reinforced PVDF-HFP membranes for membrane distillation application. *Desalination* **2014**, *332*, 134–141, doi:10.1016/j.desal.2013.10.030.

69. Essalhi, M.; Khayet, M. Self-sustained webs of polyvinylidene fluoride electrospun nanofibers at different electrospinning times: 1. Desalination by direct contact membrane distillation. *J. Memb. Sci.* **2013**, *433*, 167–179, doi:10.1016/j.memsci.2013.01.023.

70. Lee, J.; Kim, Y.; Kim, W.; Francis, L.; Amy, G.; Ghaffour, N. Performance modeling of direct contact membrane distillation (DCMD) seawater desalination process using a commercial composite membrane. *J. Memb. Sci.* **2015**, *478*, 85–95, doi:10.1016/j.memsci.2014.12.053.

71. Tsyurupa, M.P.; Davankov, V.A. Porous structure of hypercrosslinked polystyrene: State-of-the-art mini-review. *React. Funct. Polym.* **2006**, *66*, 768–779, doi:10.1016/j.reactfunctpolym.2005.11.004.

72. Jalloul, G.; Hashem, M.H.; Tehrani-Bagha, A.R.; Ahmad, M.N.; Abu Tarboush, B.J. Unsupported electrospun membrane for water desalination using direct contact membrane distillation. *J. Appl. Polym. Sci.* **2021**, *138*, doi:10.1002/app.49861.

73. Essalhi, M.; Khayet, M. Self-sustained webs of polyvinylidene fluoride electrospun nanofibers at different electrospinning times: 1. Desalination by direct contact

membrane distillation. *J. Memb. Sci.* **2013**, *433*, 167–179, doi:10.1016/j.memsci.2013.01.023.

74. Hou, D.; Lin, D.; Ding, C.; Wang, D.; Wang, J. Fabrication and characterization of electrospun superhydrophobic PVDF-HFP/SiNPs hybrid membrane for membrane distillation. *Sep. Purif. Technol.* **2017**, *189*, 82–89, doi:10.1016/j.seppur.2017.07.082.

75. Ren, L.F.; Xia, F.; Chen, V.; Shao, J.; Chen, R.; He, Y. TiO2-FTCS modified superhydrophobic PVDF electrospun nanofibrous membrane for desalination by direct contact membrane distillation. *Desalination* **2017**, *423*, 1–11, doi:10.1016/j.desal.2017.09.004.

76. Deka, B.J.; Lee, E.J.; Guo, J.; Kharraz, J.; An, A.K. Electrospun Nanofiber Membranes Incorporating PDMS-Aerogel Superhydrophobic Coating with Enhanced Flux and Improved Antiwettability in Membrane Distillation. *Environ. Sci. Technol.* **2019**, *53*, 4948–4958, doi:10.1021/acs.est.8b07254.

77. Guillen-Burrieza, E.; Mavukkandy, M.O.; Bilad, M.R.; Arafat, H.A. Understanding wetting phenomena in membrane distillation and how operational parameters can affect it. *J. Memb. Sci.* **2016**, *515*, 163–174, doi:10.1016/J.MEMSCI.2016.05.051.

78. Kiefer, F.; Präbst, A.; Rodewald, K.S.; Sattelmayer, T. Membrane scaling in Vacuum Membrane Distillation - Part 1: In-situ observation of crystal growth and membrane wetting. *J. Memb. Sci.* **2019**, *590*, 117294, doi:10.1016/J.MEMSCI.2019.117294.

79. Liu, C.; Zhu, L.; Chen, L. Effect of salt and metal accumulation on performance of membrane distillation system and microbial community succession in membrane

biofilms. *Water Res.* **2020**, *177*, 115805, doi:10.1016/J.WATRES.2020.115805.

80. Rezaei, M.; Warsinger, D.M.; Lienhard V, J.H.; Duke, M.C.; Matsuura, T.; Samhaber, W.M. Wetting phenomena in membrane distillation: Mechanisms, reversal, and prevention. *Water Res.* **2018**, *139*, 329–352, doi:10.1016/J.WATRES.2018.03.058.

81. Wang, Z.; Chen, Y.; Sun, X.; Duddu, R.; Lin, S. Mechanism of pore wetting in membrane distillation with alcohol vs. surfactant. *J. Memb. Sci.* **2018**, *559*, 183–195, doi:10.1016/J.MEMSCI.2018.04.045.

82. Yao, M.; Tijing, L.D.; Naidu, G.; Kim, S.H.; Matsuyama, H.; Fane, A.G.; Shon, H.K. A review of membrane wettability for the treatment of saline water deploying membrane distillation. *Desalination* **2020**, *479*, 114312, doi:10.1016/J.DESAL.2020.114312.

83. Choudhury, M.R.; Anwar, N.; Jassby, D.; Rahaman, M.S. Fouling and wetting in the membrane distillation driven wastewater reclamation process – A review. *Adv. Colloid Interface Sci.* **2019**, *269*, 370–399, doi:10.1016/J.CIS.2019.04.008.

84. Abu-Zeid, M.A.E.R.; Zhang, Y.; Dong, H.; Zhang, L.; Chen, H.L.; Hou, L. A comprehensive review of vacuum membrane distillation technique. *Desalination* **2015**, *356*, 1–14, doi:10.1016/J.DESAL.2014.10.033.

85. Jacob, P.; Laborie, S.; Cabassud, C. Visualizing and evaluating wetting in membrane distillation: New methodology and indicators based on Detection of Dissolved Tracer Intrusion (DDTI). *Desalination* **2018**, *443*, 307–322, doi:10.1016/J.DESAL.2018.06.006.

86. Gryta, M. The study of performance of polyethylene chlorinetrifluoroethylene

membranes used for brine desalination by membrane distillation. *Desalination* **2016**, *398*, 52–63, doi:10.1016/J.DESAL.2016.07.021.

87. Gryta, M.; Barancewicz, M. Influence of morphology of PVDF capillary membranes on the performance of direct contact membrane distillation. *J. Memb. Sci.* **2010**, *358*, 158–167, doi:10.1016/J.MEMSCI.2010.04.044.

88. Guillen-Burrieza, E.; Ruiz-Aguirre, A.; Zaragoza, G.; Arafat, H.A. Membrane fouling and cleaning in long term plant-scale membrane distillation operations. *J. Memb. Sci.* **2014**, *468*, 360–372, doi:10.1016/J.MEMSCI.2014.05.064.

89. Yan, K.K.; Jiao, L.; Lin, S.; Ji, X.; Lu, Y.; Zhang, L. Superhydrophobic electrospun nanofiber membrane coated by carbon nanotubes network for membrane distillation. *Desalination* **2018**, *437*, 26–33, doi:10.1016/J.DESAL.2018.02.020.

90. Taylor, C.R.; Ahmadiannamini, P.; Hiibel, S.R. Identifying pore wetting thresholds of surfactants in direct contact membrane distillation. *Sep. Purif. Technol.* **2019**, *217*, 17–23, doi:10.1016/J.SEPPUR.2019.01.061.

91. Chen, Y.; Wang, Z.; Jennings, G.K.; Lin, S. Probing Pore Wetting in Membrane Distillation Using Impedance: Early Detection and Mechanism of Surfactant-Induced Wetting. *Environ. Sci. Technol. Lett.* **2017**, *4*, 505–510, doi:10.1021/ACS.ESTLETT.7B00372/SUPPL_FILE/EZ7B00372_SI_001.PDF.

92. Ahmed, F.E.; Lalia, B.S.; Hashaikeh, R. Membrane-based detection of wetting phenomenon in direct contact membrane distillation. *J. Memb. Sci.* **2017**, *535*, 89–93, doi:10.1016/J.MEMSCI.2017.04.035.

93. Francis, L.; Hilal, N. Electrohydrodynamic atomization of CNT on PTFE membrane for scaling resistant membranes in membrane distillation. *npj Clean Water* **2023**, *6*,

doi:10.1038/s41545-023-00229-x.

94. Al-Salmi, M.; Laqbaqbi, M.; Al-Obaidani, S.; Al-Maamari, R.S.; Khayet, M.; Al-Abri, M. Application of membrane distillation for the treatment of oil field produced water. *Desalination* **2020**, *494*, 114678, doi:10.1016/j.desal.2020.114678.

95. Pawar, R.; Zhang, Z.; Vidic, R.D. Laboratory and pilot-scale studies of membrane distillation for desalination of produced water from Permian Basin. *Desalination* **2022**, *537*, 115853, doi:10.1016/j.desal.2022.115853.

96. Woo, Y.C.; Tijing, L.D.; Park, M.J.; Yao, M.; Choi, J.S.; Lee, S.; Kim, S.H.; An, K.J.; Shon, H.K. Electrospun dual-layer nonwoven membrane for desalination by air gap membrane distillation. *Desalination* **2017**, *403*, 187–198, doi:10.1016/j.desal.2015.09.009.

97. Chen, Y.; Lu, K.J.; Japip, S.; Chung, T.S. Can Composite Janus Membranes with an Ultrathin Dense Hydrophilic Layer Resist Wetting in Membrane Distillation? *Environ. Sci. Technol.* **2020**, *54*, 12713–12722, doi:10.1021/acs.est.0c04242.

98. Li, W.P.; Paing, A.T.; Chow, C.A.; Qua, M.S.; Mottaiyan, K.; Lu, K.; Dhalla, A.; Chung, T.S.; Gudipati, C. Scale Up and Validation of Novel Tri-Bore PVDF Hollow Fiber Membranes for Membrane Distillation Application in Desalination and Industrial Wastewater Recycling. *Membranes (Basel).* **2022**, *12*, doi:10.3390/membranes12060573.

99. Ebrahimi, F.; Orooji, Y.; Razmjou, A. Applying membrane distillation for the recovery of nitrate from saline water using pvdf membranes modified as superhydrophobic membranes. *Polymers (Basel).* **2020**, *12*, 1–14, doi:10.3390/polym12122774.

100. Ali, E.; Orfi, J.; Najib, A. Developing and validating a dynamic model of water production by direct-contact membrane distillation. *PLoS One* **2020**, *15*, 1–24, doi:10.1371/journal.pone.0230207.

101. Huang, F.Y.C.; Arning, A. Performance comparison between polyvinylidene fluoride and polytetrafluoroethylene hollow fiber membranes for direct contact membrane distillation. *Membranes (Basel).* **2019**, *9*, doi:10.3390/membranes9040052.

102. Park, Y.; Lee, S. Analysis of thermal energy efficiency for hollow fiber membranes in direct contact membrane distillation. *Environ. Eng. Res.* **2019**, *24*, 347–353, doi:10.4491/EER.2018.253.

103. Kim, A.S.; Kim, H.J.; Moon, D.S. A fast and scalable mesh generation method of densely packed hollow fibers for membrane separations: Application to direct contact membrane distillation. *J. Comput. Phys.* **2021**, *427*, 110042, doi:10.1016/j.jcp.2020.110042.

104. Dow, N.; Gray, S.; Li, J.; Zhang, J.; Ostarcevic, E.; Liubinas, A.; Atherton, P.; Roeszler, G.; Gibbs, A.; Duke, M. Pilot trial of membrane distillation driven by low grade waste heat : Membrane fouling and energy assessment. *Desalination* **2016**, 1–13, doi:10.1016/j.desal.2016.01.023.

105. Yang, Z.; Zhou, Y.; Feng, Z.; Rui, X.; Zhang, T.; Zhang, Z. A review on reverse osmosis and nanofiltration membranes for water purification. *Polymers (Basel).* **2019**, *11*, 1–22, doi:10.3390/polym11081252.

106. Woo, Y.C.; Kim, Y.; Shim, W.; Tijing, L.D.; Yao, M.; Nghiem, L.D.; Choi, J.; Kim, S.; Kyong, H. Graphene/PVDF flat-sheet membrane for the treatment of RO brine

from coal seam gas produced water by air gap membrane distillation. *J. Memb. Sci.* **2016**, *16*, doi:10.1016/j.memsci.2016.04.014.

107. Seman, M.N.A.; Khayet, M.; Ali, Z.I. Bin; Hilal, N. Reduction of nanofiltration membrane fouling by UV-initiated graft polymerization technique. *J. Memb. Sci.* **2010**, *355*, 133–141, doi:10.1016/j.memsci.2010.03.014.

108. Tao, G.; Viswanath, B.; Kekre, K.; Lee, L.Y.; Ng, H.Y.; Ong, S.L.; Seah, H. RO brine treatment and recovery by biological activated carbon and capacitive deionization process. *Water Sci. Technol.* | **2011**, 77–82, doi:10.2166/wst.2011.604.

109. Chen, L.; Wang, C.; Liu, S.; Hu, Q.; Zhu, L.; Cao, C. Investigation of the long-term desalination performance of membrane capacitive deionization at the presence of organic foulants. *Chemosphere* **2017**, doi:10.1016/j.chemosphere.2017.11.130.

110. Yu, J.; Qin, J.; Kekre, K.A.; Viswanath, B.; Tao, G.; Seah, H. Impact of operating conditions on performance of capacitive deionisation for reverse osmosis brine recovery Jing Yu , Jianjun Qin , Kiran A . Kekre , Balakrishnan Viswanath , Guihe Tao. *J. Water Reuse Desalin.* | **2014**, 59–64, doi:10.2166/wrd.2013.008.

111. Horseman, T.; Su, C.; Christie, K.S.S.; Lin, S. Highly effective scaling mitigation in membrane distillation using a superhydrophobic membrane with gas purging. *Environ. Sci. Technol. Lett.* **2019**, *6*, 423–429, doi:10.1021/acs.estlett.9b00354.

112. Mansi, A.E.; El-Marsafy, S.M.; Elhenawy, Y.; Bassyouni, M. Assessing the potential and limitations of membrane-based technologies for the treatment of oilfield produced water. *Alexandria Eng. J.* **2022**, *68*, 787–815, doi:10.1016/j.aej.2022.12.013.

113. Boubakri, A.; Hafiane, A.; Bouguecha, S.A.T. Application of response surface

methodology for modeling and optimization of membrane distillation desalination process. *J. Ind. Eng. Chem.* **2014**, *20*, 3163–3169, doi:10.1016/j.jiec.2013.11.060.

114. Rattner, A.S.; Nagavarapu, A.K.; Garimella, S.; Fuller, T.F. Modeling of a flat plate membrane-distillation system for liquid desiccant regeneration in air-conditioning applications. *Int. J. Heat Mass Transf.* **2011**, *54*, 3650–3660, doi:10.1016/j.ijheatmasstransfer.2011.02.064.

115. Elrasheedy, A.; Rabie, M.; El-Shazly, A.; Bassyouni, M.; Abdel-Hamid, S.M.S.; El Kady, M.F. Numerical investigation of fabricated mwcnts/polystyrene nanofibrous membrane for dcmd. *Polymers (Basel).* **2021**, *13*, 1–11, doi:10.3390/polym13010160.

116. Eleiwi, F.; Ghaffour, N.; Alsaadi, A.S.; Francis, L.; Laleg-Kirati, T.M. Dynamic modeling and experimental validation for direct contact membrane distillation (DCMD) process. *Desalination* **2016**, *384*, 1–11, doi:10.1016/j.desal.2016.01.004.

117. Qasim, M.; Samad, I.U.; Darwish, N.A.; Hilal, N. Comprehensive review of membrane design and synthesis for membrane distillation. *Desalination* **2021**, *518*, 115168, doi:10.1016/j.desal.2021.115168.

118. Deshmukh, A.; Boo, C.; Karanikola, V.; Lin, S.; Straub, A.P.; Tong, T.; Warsinger, D.M.; Elimelech, M. Membrane distillation at the water-energy nexus: Limits, opportunities, and challenges. *Energy Environ. Sci.* **2018**, *11*, 1177–1196, doi:10.1039/c8ee00291f.

119. Laurijssen, J.; Faaij, A.; Worrell, E. Energy conversion strategies in the European paper industry - A case study in three countries. *Appl. Energy* **2012**, *98*, 102–113, doi:10.1016/j.apenergy.2012.03.001.

120. Neelis, M.; Ramirez-Ramirez, A.; Patel, M.; Farla, J.; Boonekamp, P.; Blok, K. Energy efficiency developments in the Dutch energy-intensive manufacturing industry, 1980-2003. *Energy Policy* **2007**, *35*, 6112–6131, doi:10.1016/j.enpol.2007.06.014.

121. González, D.; Amigo, J.; Suárez, F. Membrane distillation: Perspectives for sustainable and improved desalination. *Renew. Sustain. Energy Rev.* **2017**, *80*, 238–259, doi:10.1016/j.rser.2017.05.078.

122. Beltrán, J.; Koo-Oshima, S. Water desalination for agricultural applications. *Fao* **2006**.

123. Barron, O.; Ali, R.; Hodgson, G.; Smith, D.; Qureshi, E.; McFarlane, D.; Campos, E.; Zarzo, D. Feasibility assessment of desalination application in Australian traditional agriculture. *Desalination* 2015, *364*.

124. Shannon, M.A.; Bohn, P.W.; Elimelech, M.; Georgiadis, J.G.; Marĩas, B.J.; Mayes, A.M. Science and technology for water purification in the coming decades. *Nature* 2008, *452*.

125. Feitelson, E.; Rosenthal, G. Desalination, space and power: The ramifications of Israel's changing water geography. *Geoforum* **2012**, *43*, 272–284, doi:10.1016/j.geoforum.2011.08.011.

126. Memon, S.; Kim, Y.D.; Soomro, S.; Soomro, M.I.; Kim, W.S. A new approach for freshwater production and energy recovery from an oil field. *J. Water Process Eng.* **2020**, *34*, 101145, doi:10.1016/j.jwpe.2020.101145.

127. Elimelech, M.; Phillip, W.A. The future of seawater desalination: Energy, technology, and the environment. *Science (80-.).* 2011, *333*.

128. March, H.; Saurí, D.; Rico-Amorós, A.M. The end of scarcity? Water desalination as the new cornucopia for Mediterranean Spain. *J. Hydrol.* **2014**, *519*, 2642–2651, doi:10.1016/j.jhydrol.2014.04.023.

129. Criscuoli, A.; Capuano, A.; Andreucci, M.; Drioli, E. Low-temperature direct contact membrane distillation for the treatment of aqueous solutions containing urea. *Membranes (Basel).* **2020**, *10*, 1–12, doi:10.3390/membranes10080176.

130. Cohen-Tanugi, D.; McGovern, R.K.; Dave, S.H.; Lienhard, J.H.; Grossman, J.C. Quantifying the potential of ultra-permeable membranes for water desalination. *Energy Environ. Sci.* **2014**, *7*, 1134–1141, doi:10.1039/c3ee43221a.

131. Li, J.; Lai, C.; Zhang, H.; Xiao, L.; Zhao, J.; Wang, F.; Zhang, C.; Xia, L.; Miao, H.; Yuan, J. A combined phosphoric acid fuel cell and direct contact membrane distillation hybrid system for electricity generation and seawater desalination. *Energy Convers. Manag.* **2022**, *267*, 115916, doi:10.1016/j.enconman.2022.115916.

132. Shafieian, A.; Khiadani, M. A novel solar-driven direct contact membrane-based water desalination system. *Energy Convers. Manag.* **2019**, *199*, doi:10.1016/j.enconman.2019.112055.

133. Soomro, M.I.; Kim, W.S. Parabolic-trough plant integrated with direct-contact membrane distillation system: Concept, simulation, performance, and economic evaluation. *Sol. Energy* **2018**, *173*, 348–361, doi:10.1016/j.solener.2018.07.086.

134. Zhao, Q.; Zhang, H.; Hu, Z. Hybridizing photovoltaic cell with direct contact membrane distillation for electricity and freshwater cogeneration: Concept and performance evaluation. *Desalination* **2020**, *496*, 114701,

doi:10.1016/j.desal.2020.114701.

135. Minier-matar, J.; Hussain, A.; Janson, A.; Benyahia, F.; Adham, S. Field evaluation of membrane distillation technologies for desalination of highly saline brines. *DES* **2014**, *351*, 101–108, doi:10.1016/j.desal.2014.07.027.

136. Yao, M.; Woo, Y.C.; Tijing, L.D.; Shim, W.G.; Choi, J.S.; Kim, S.H.; Shon, H.K. Effect of heat-press conditions on electrospun membranes for desalination by direct contact membrane distillation. *Desalination* **2016**, *378*, 80–91, doi:10.1016/j.desal.2015.09.025.

137. Chou, S.; Torres, J.; Li, X.; Fane, A.G.; Fang, W.; Tang, C.Y.; Chaitra, G.; Hu, X.; Shi, L.; Wang, R. Nature gives the best solution for desalination: Aquaporin-based hollow fiber composite membrane with superior performance. *J. Memb. Sci.* **2015**, *494*, 68–77, doi:10.1016/j.memsci.2015.07.040.

138. Field, R.W.; Pearce, G.K. Critical, sustainable and threshold fluxes for membrane filtration with water industry applications. *Adv. Colloid Interface Sci.* **2011**, *164*, 38–44, doi:10.1016/j.cis.2010.12.008.

139. Field, R.W.; Wu, D.; Howell, J.A.; Gupta, B.B. Critical flux concept for microfiltration fouling. *J. Memb. Sci.* **1995**, *100*, 259–272, doi:10.1016/0376-7388(94)00265-Z.

140. Miller, D.J.; Kasemset, S.; Paul, D.R.; Freeman, B.D. Comparison of membrane fouling at constant flux and constant transmembrane pressure conditions. *J. Memb. Sci.* **2014**, *454*, 505–515, doi:10.1016/j.memsci.2013.12.027.

141. Phattaranawik, J.; Jiraratananon, R.; Fane, A.G. Effect of pore size distribution and air flux on mass transport in direct contact membrane distillation. *J. Memb. Sci.*

2003, *215*, 75–85, doi:10.1016/S0376-7388(02)00603-8.

142. Khayet, M.; Mengual, J.I.; Matsuura, T. Porous hydrophobic/hydrophilic composite membranes: Application in desalination using direct contact membrane distillation. *J. Memb. Sci.* **2005**, *252*, 101–113, doi:10.1016/j.memsci.2004.11.022.

143. Khayet, M.; Matsuura, T.; Mengual, J.I.; Qtaishat, M. Design of novel direct contact membrane distillation membranes. *Desalination* **2006**, *192*, 105–111, doi:10.1016/j.desal.2005.06.047.

144. Li, G.P.; Zhang, L.Z. Investigation of a solar energy driven and hollow fiber membrane-based humidification-dehumidification desalination system. *Appl. Energy* **2016**, *177*, 393–408, doi:10.1016/j.apenergy.2016.05.113.

145. Luo, A.; Lior, N. Critical review of membrane distillation performance criteria. *Desalin. Water Treat.* **2016**, *57*, 20093–20140, doi:10.1080/19443994.2016.1152637.

146. Manawi, Y.M.; Khraisheh, M.; Kayvani, A.; Benyahia, F.; Adham, S. Effect of operational parameters on distillate fl ux in direct contact membrane distillation (DCMD): Comparison between experimental and model predicted performance. *Desalination* **2014**, *336*, 110–120.

147. Vigneswaran, S.; Kwon, D. Effect of Ionic Strength and Permeate Flux on Membrane Fouling: Analysis of Forces acting on Particle Deposit and Cake Formation. *KSCE J. Civ. Eng.* **2015**, *19*, 1604–1611, doi:10.1007/s12205-014-0079-0.

148. Fane, A.G.; Schofield, R.W.; Fell, C.J.D. The efficient use of energy in membrane distillation. *Desalination* **1987**, *64*, 231–243, doi:10.1016/0011-9164(87)90099-3.

149. Ali, M.I.; Summers, E.K.; Arafat, H.A.; Lienhard V, J.H. Effects of membrane properties on water production cost in small scale membrane distillation systems. *Desalination* **2012**, *306*, 60–71, doi:10.1016/j.desal.2012.07.043.

150. Lee, J.; Kim, W.; Choi, J.; Gha, N.; Kim, Y. Dynamic solar-powered multi-stage direct contact membrane distillation system : Concept design , modeling and simulation. *Desalination* **2018**, *435*, 278–292, doi:10.1016/j.desal.2017.04.008.

151. Kayvani Fard, A.; Manawi, Y.M.; Rhadfi, T.; Mahmoud, K.A.; Khraisheh, M.; Benyahia, F. Synoptic analysis of direct contact membrane distillation performance in Qatar: A case study. *Desalination* **2015**, *360*, 97–107, doi:10.1016/j.desal.2015.01.016.

152. Wu, H.Y.; Wang, R.; Field, R.W. Direct contact membrane distillation: An experimental and analytical investigation of the effect of membrane thickness upon transmembrane flux. *J. Memb. Sci.* **2014**, *470*, 257–265, doi:10.1016/j.memsci.2014.06.002.

153. Li, X.; Deng, L.; Yu, X.; Wang, M.; Wang, X.; García-Payo, C.; Khayet, M. A novel profiled core-shell nanofibrous membrane for wastewater treatment by direct contact membrane distillation. *J. Mater. Chem. A* **2016**, *4*, 14453–14463, doi:10.1039/c6ta05492g.

154. Meng, S.; Ye, Y.; Mansouri, J.; Chen, V. Fouling and crystallisation behaviour of superhydrophobic nano-composite PVDF membranes in direct contact membrane distillation. *J. Memb. Sci.* **2014**, *463*, 102–112, doi:10.1016/j.memsci.2014.03.027.

155. Alklaibi, A.M.; Lior, N. Membrane-distillation desalination: status and potential. *Desalination* **2004**, *171*, 111–131, doi:10.1016/j.desal.2004.03.024.

156. Jiang, S.; Li, Y.; Ladewig, B.P. Science of the Total Environment A review of reverse osmosis membrane fouling and control strategies. *Sci. Total Environ.* **2017**, *595*, 567–583, doi:10.1016/j.scitotenv.2017.03.235.

157. Liu, E.; Lee, L.Y.; Ong, S.L.; Ng, H.Y. Treatment of industrial brine using Capacitive Deionization (CDI) towards zero liquid discharge – Challenges and optimization. *Water Res.* **2020**, *183*, doi:10.1016/j.watres.2020.116059.

158. Xiao, Z.; Zheng, R.; Liu, Y.; He, H.; Yuan, X.; Ji, Y.; Li, D.; Yin, H.; Zhang, Y.; Li, X.; et al. Slippery for scaling resistance in membrane distillation: a novel porous micropillared superhydrophobic surface. *Water Res.* **2019**, *155*, 152–161, doi:10.1016/j.watres.2019.01.036.

159. Julian, H.; Julian, H.; Ye, Y.; Li, H.; Chen, V. Scaling Mitigation in Submerged Vacuum Membrane Distillation and Crystallization (VMDC) with Periodic Air-backwash Scaling mitigation in submerged vacuum membrane distillation and crystallization (VMDC) with periodic air-backwash. *J. Memb. Sci.* **2017**, *547*, 19–33, doi:10.1016/j.memsci.2017.10.035.

160. Xiao, Z.; Li, Z.; Guo, H.; Liu, Y.; Wang, Y.; Yin, H. Scaling mitigation in membrane distillation : From superhydrophobic to slippery. *Desalination* **2019**, *466*, 36–43, doi:10.1016/j.desal.2019.05.006.

161. Nthunya, L.N.; Gutierrez, L.; Khumalo, N.; Derese, S.; Mamba, B.B.; Verliefde, A.R.; Mhlanga, S.D. Superhydrophobic PVDF nanofibre membranes coated with an organic fouling resistant hydrophilic active layer for direct-contact membrane distillation. *Colloids Surfaces A Physicochem. Eng. Asp.* **2019**, *575*, 363–372, doi:10.1016/j.colsurfa.2019.05.031.

162. Abdelatty, R.; Khan, A.; Yusuf, M.; Alashraf, A.; Shakoor, R.A. Effect of silicon nitride and graphene nanoplatelets on the properties of aluminum metal matrix composites. *Materials (Basel).* **2021**, *14*, doi:10.3390/ma14081898.

163. Alsawaftah, N.; Abuwatfa, W.; Darwish, N.; Husseini, G. A Comprehensive Review on Membrane Fouling: Mathematical Modelling, Prediction, Diagnosis, and Mitigation. *water* **2021**, *13*, 1–37.

164. Gryta, M.; Markowska, A.; Karakulski, K. The influence of polypropylene degradation on the membrane wettability during membrane distillation. *J. ofMembrane Sci. J.* **2009**, *326*, 493–502, doi:10.1016/j.memsci.2008.10.022.

165. Chen, L.; Xu, P.; Wang, H. Interplay of the factors affecting water flux and salt rejection in membrane distillation: A state-of-the-art critical review. *Water (Switzerland)* **2020**, *12*, doi:10.3390/w12102841.

166. Zuo, J.; Bonyadi, S.; Chung, T.S. Exploring the potential of commercial polyethylene membranes for desalination by membrane distillation. *J. Memb. Sci.* **2016**, *497*, 239–247, doi:10.1016/j.memsci.2015.09.038.

167. McGaughey, A.L.; Gustafson, R.D.; Childress, A.E. Effect of long-term operation on membrane surface characteristics and performance in membrane distillation. *J. Memb. Sci.* **2017**, *543*, 143–150, doi:10.1016/j.memsci.2017.08.040.

168. Mansour, S.; Giwa, A.; Hasan, S.W. Novel graphene nanoplatelets-coated polyethylene membrane for the treatment of reject brine by pilot-scale direct contact membrane distillation: An optimization study. *Desalination* **2018**, *441*, 9–20, doi:10.1016/j.desal.2018.04.026.

169. Ding, Z.; Liu, L.; Liu, Z.; Ma, R. Fouling resistance in concentrating TCM extract

by direct contact membrane distillation. *J. Memb. Sci.* **2010**, *362*, 317–325, doi:10.1016/j.memsci.2010.06.040.

170. Khayet, M.; Mengual, J.I. Effect of salt concentration during the treatment of humic acid solutions by membrane distillation. *Desalination* **2004**, *168*, 373–381, doi:10.1016/J.DESAL.2004.07.023.

171. Shen, X.; Liu, J.; Feng, X.; Zhao, Y.; Chen, L. Preliminary investigation on hemocompatibility of poly (vinylidene fluoride) membrane grafted with acryloylmorpholine via ATRP. *J. Biomed. Mater. Res. A* **2015**, *103*, 683–692, doi:10.1002/jbm.a.35213.

172. Cho, D.; Kwon, G. Influence of humic acid on the long-term performance of direct contact membrane distillation. *Energy Environ.* **2019**, *30*, 109–120, doi:10.1177/0958305X18787279.

173. Miao, R.; Wu, Y.; Wang, P.; Wu, G.; Wang, L.; Li, X.; Wang, J.; Lv, Y.; Liu, T. New insights into the humic acid fouling mechanism of ultrafiltration membranes for different Ca2+ dosage ranges: results from micro- and macro-level analyses. *Water Sci. Technol.* **2018**, *77*, 2265–2273, doi:10.2166/wst.2018.141.

174. Shen, X.; Xie, T.; Wang, J.; Wang, F. Improved fouling resistance of poly (vinylidene fluoride) membrane modified with poly (acryloyl morpholine) -based amphiphilic copolymer. *Colloid Polym Sci* **2017**, *295*, 1211–1221, doi:10.1007/s00396-017-4117-6.

175. Srisurichan, S.; Jiraratananon, R.; Fane, A.G. Mass transfer mechanisms and transport resistances in direct contact membrane distillation process. *J. Memb. Sci.* **2006**, *277*, 186–194, doi:10.1016/j.memsci.2005.10.028.

176. Shen, X.; Xie, T.; Wang, J.; Liu, P.; Wang, F. An anti-fouling poly(vinylidene fluoride) hybrid membrane blended with functionalized ZrO2 nanoparticles for efficient oil/water separation. *RSC Adv.* **2017**, *7*, 5262–5271, doi:10.1039/C6RA26651G.

177. Alkhouzaam, A.; Qiblawey, H. Novel polysulfone ultrafiltration membranes incorporating polydopamine functionalized graphene oxide with enhanced flux and fouling resistance. *J. Memb. Sci.* **2020**, 118900, doi:10.1016/j.memsci.2020.118900.

178. Qtaishat, M.; Matsuura, T.; Kruczek, B.; Khayet, M. Heat and mass transfer analysis in direct contact membrane distillation. *Desalination* **2008**, *219*, 272–292, doi:10.1016/j.desal.2007.05.019.

179. Meng, S.; Mansouri, J.; Ye, Y.; Chen, V. Effect of templating agents on the properties and membrane distillation performance of TiO2-coated PVDF membranes. *J. Memb. Sci.* **2014**, *450*, 48–59, doi:10.1016/J.MEMSCI.2013.08.036.

180. Kim, Y.D.; Thu, K.; Ghaffour, N.; Choon Ng, K. Performance investigation of a solar-assisted direct contact membrane distillation system. *J. Memb. Sci.* **2013**, *427*, 345–364, doi:10.1016/J.MEMSCI.2012.10.008.

181. Adnan, S.; Hoang, M.; Wang, H.; Xie, Z. Commercial PTFE membranes for membrane distillation application: Effect of microstructure and support material. *Desalination* **2012**, *284*, 297–308, doi:10.1016/j.desal.2011.09.015.

182. Lee, J.G.; Kim, W.S.; Choi, J.S.; Ghaffour, N.; Kim, Y.D. Dynamic solar-powered multi-stage direct contact membrane distillation system: Concept design, modeling and simulation. *Desalination* **2018**, *435*, 278–292, doi:10.1016/J.DESAL.2017.04.008.

183. Floros, I.N.; Kouvelos, E.P.; Pilatos, G.I.; Hadjigeorgiou, E.P.; Gotzias, A.D.; Favvas, E.P.; Sapalidis, A.A. Enhancement of flux performance in PTFE membranes for direct contact membrane distillation. *Polymers (Basel).* **2020**, *12*, 1–13, doi:10.3390/polym12020345.

184. Li, J.; Ren, L.F.; Shao, J.; Tu, Y.; Ma, Z.; Lin, Y.; He, Y. Fabrication of triple layer composite membrane and its application in membrane distillation (MD): Effect of hydrophobic-hydrophilic membrane structure on MD performance. *Sep. Purif. Technol.* **2020**, *234*, 116087, doi:10.1016/J.SEPPUR.2019.116087.

185. Swaminathan, J.; Chung, H.W.; Warsinger, D.M.; AlMarzooqi, F.A.; Arafat, H.A.; Lienhard, J.H. Energy efficiency of permeate gap and novel conductive gap membrane distillation. *J. Memb. Sci.* **2016**, *502*, 171–178, doi:10.1016/J.MEMSCI.2015.12.017.

186. Abdelrazeq, H.; Khraisheh, M.; Hassan, M.K. Long-Term Treatment of Highly Saline Brine in a Direct Contact Membrane Distillation (DCMD) Pilot Unit Using Polyethylene Membranes. *Membranes (Basel).* **2022**, *12*, 424, doi:10.3390/membranes12040424.

187. Gryta, M. Effectiveness of water desalination by membrane distillation process. *Membranes (Basel).* **2012**, *2*, 415–429, doi:10.3390/membranes2030415.

188. U. Lawal, D.; E. Khalifa, A. Flux Prediction in Direct Contact Membrane Distillation. *Int. J. Mater. Mech. Manuf.* **2014**, *2*, 302–308, doi:10.7763/ijmmm.2014.v2.147.

189. Ni, W.; Li, Y.; Zhao, J.; Zhang, G.; Du, X.; Dong, Y. Simulation study on direct contact membrane distillation modules for high-concentration nacl solution.

Membranes (Basel). **2020**, *10*, 1–18, doi:10.3390/membranes10080179.

190. Olatunji, S.O.; Camacho, L.M. Heat and mass transport in modeling membrane distillation configurations: A review. *Front. Energy Res.* **2018**, *6*, 1–18, doi:10.3389/fenrg.2018.00130.

191. Fane, A.G. (Tony. A grand challenge for membrane desalination: More water, less carbon. *Desalination* **2018**, *426*, 155–163, doi:10.1016/j.desal.2017.11.002.

192. Simionescu, L.N.; Gherghina, Ștefan C.; Sheikha, Z.; Tawil, H. Does water, waste, and energy consumption influence firm performance? Panel data evidence from S &P 500 information technology sector. *Int. J. Environ. Res. Public Health* **2020**, *17*, 1–31, doi:10.3390/ijerph17145206.

193. Duong, H.C.; Cooper, P.; Nelemans, B.; Cath, T.Y.; Nghiem, L.D. Evaluating energy consumption of air gap membrane distillation for seawater desalination at pilot scale level. *Sep. Purif. Technol.* **2016**, *166*, 55–62, doi:10.1016/j.seppur.2016.04.014.

194. Lin, S.; Yip, N.Y.; Elimelech, M. Direct contact membrane distillation with heat recovery : Thermodynamic insights from module scale modeling. *J. Memb. Sci.* **2014**, *453*, 498–515, doi:10.1016/j.memsci.2013.11.016.

195. Duong, H.C. Membrane distillation for strategic desalination applications, University of Wollongong, 2017.

196. Laurijssen, J.; Faaij, A.; Worrell, E. Benchmarking energy use in the paper industry: A benchmarking study on process unit level. *Energy Effic.* **2013**, *6*, 49–63, doi:10.1007/s12053-012-9163-9.

197. Criscuoli, A.; Concetta, M.; Drioli, E. Evaluation of energy requirements in

membrane distillation. *Chem. Eng. Process.* **2008**, *47*, 1098–1105, doi:10.1016/j.cep.2007.03.006.

198. Gordon, A. Evaluation of hollow fiber - based direct contact and vacuum membrane distillation systems using aspen process simulation. *J. Memb. Sci.* **2014**, *464*, 127–139.

199. Lawrence, A.; Thollander, P.; Andrei, M.; Karlsson, M. Specific energy consumption/use (SEC) in energy management for improving energy efficiency in industry: Meaning, usage and differences. *Energies* **2019**, *12*, doi:10.3390/en12020247.

200. Suhr, M.; Klein, G.; Kourti, I.; Rodrigo Gonzalo, M.; Giner Santonja, G.; Roudier, S.; Delgado Sancho, L. *Best Available Techniques (BAT) Reference Document for the Production of Pulp, Paper and Board*; 2015; ISBN 9789279481673.

201. Jantaporn, W.; Ali, A.; Aimar, P. Specific energy requirement of direct contact membrane distillation. *Chem. Eng. Res. Des.* **2017**, *128*, 15–26, doi:10.1016/j.cherd.2017.09.031.

202. Abdel-Karim, A.; Leaper, S.; Alberto, M.; Vijayaraghavan, A.; Fan, X.; Holmes, S.M.; Souaya, E.R.; Badawy, M.I.; Gorgojo, P. High flux and fouling resistant flat sheet polyethersulfone membranes incorporated with graphene oxide for ultrafiltration applications. *Chem. Eng. J.* **2018**, *334*, 789–799, doi:10.1016/j.cej.2017.10.069.

203. Rauf, A.; Li, H.; Ullah, S.; Meng, L.; Wang, B.; Wang, M. Statistical study about the influence of particle precipitation on mesosphere summer echoes in polar latitudes during July 2013. *Earth, Planets Sp.* **2018**, *70*, doi:10.1186/s40623-018-

0885-6.